International Scientific-Technical and Production Journal

The Paton WELDING JOURNAL

May
2005
5

English translation of the monthly «Avtomaticheskaya Svarka» (Automatic Welding) journal published in Russian since 1948

Founders: *E.O. Paton Electric Welding Institute of the NAS of Ukraine*
International Association «Welding»

Publisher: *International Association «Welding»*

Address:
E.O. Paton Electric Welding Institute,
International Association «Welding»,
11, Bozhenko str., 03680, Kyiv, Ukraine
Tel.: (38044) 287 67 57
Fax: (38044) 528 04 86
E-mail: journal@paton.kiev.ua
http://www.nas.gov.ua/pwj

State Registration Certificate
KV 4790 of 09.01.2001

Subscriptions:
$324, 12 issues per year,
postage and packaging included.
Back issues available.

CONTENTS

SCIENTIFIC AND TECHNICAL

INDUSTRIAL

BRIEF INFORMATION

NEWS

OUTLOOK FOR APPLICATION OF LASER-LIGHT TECHNOLOGIES

G.M. ALEKSEEV[1], **U. DILTHEY**[2], **A.V. GUMENYUK**[2], **G.A. TURICHIN**[3], **V.A. LOPOTA**[3], **S.S. SHILOV**[1],
A.G. GRIGORIANTS[4], **I.N. SHIGANOV**[4], **A.I. MISYUROV**[4], **V.I. MASYCHEV**[5] and **V.K. SYSOEV**[5]
[1]Open Joint Stock Company «NIITavtoprom», Russia
[2]ISF-Welding Institute, Aachen University, Germany
[3]Institute for Laser Technology of St-Petersburg State Technical University, Russia
[4]N.E. Bauman Moscow State Technical University, Russia
[5]Federal State Unified Enterprise «S.A. Lavochkin Research and Production Company», Russia

Trends in development of laser welding, including hybrid processes, are considered. It is shown that application of laser-light equipment holds promise in terms of reduced power consumption and widened technological capabilities. The fields of potential efficient application of laser-light technologies are noted.

Keywords: laser technologies, laser welding, hybrid methods, laser-light technology, power expenditures, modelling, operational capabilities

High monochromaticity, coherency and low divergence of the laser beam allowed development of an advanced type of highly concentrated heat source. The laser beam opened up new capabilities in theory and practice of welding processes. Today it is the only welding energy source that provides power density of over 10^6 W / cm^2 under atmospheric conditions.

Local thermal heating of materials with a concentrated laser beam is commercially applied almost everywhere now all over the world. Focusing of the high-power coherent laser beams on the surface of materials results in such phase transformations in the condensed media as melting, evaporation and second-kind transitions. They make the physical basis for a number of technological processes, such as cutting, welding, heat treatment, alloying, etc. At present the world sales of laser equipment for materials processing amount to US $ 1 billion a year [1].

Laser welding and cladding are among the most important technological processes. Welding can be performed practically on any material (metals, composite and organic materials, etc.) under any conditions (on earth, in ocean and in space). Results of the special study conducted by the American Welding Society and Edison Welding Institute in 1999–2000 on quantitative estimation of the contribution of welding to the main enabling industries prove that more than half of the gross national product of industrialised countries is formed using welding and related technologies.

Requirements to welding as a process based on thermal heating of materials are increasing every year. Such traditional methods as gas, electric arc welding and others are more and more often replaced by laser methods, characterised by precision and versatility, and having a number of other technological advantages. For example, laser technologies have high productivity, allow avoidance of welding defects and improvement of performance of a product. Laser processing of materials results in minimum burnout of alloying elements. The process is environmentally clean, and it can be automated.

Laser technologies help customers to address a number of problems, such as rise in productivity, reduction in manufacturing costs, increase in operational strength, and improvement of quality and outward appearance of products. Laser sources are different types of gas and solid-state lasers. In particular, they include high-power CO_2-lasers (0.5–5.0 kW and higher) and solid-state Nd:YAG lasers with a wavelength of 10.6 and 1.06 μm, respectively. The recent world trend is to the use of mostly solid-state Nd:YAG lasers, which allow the light to be transmitted via a light guide, the welding head to be manipulated with by placing it on a robot, and welding of 3D structures to be performed (in aerospace engineering, ship building, motor industry, car-building industry, etc.).

Technical and service parameters of high-power laser systems are being continuously improved. However, the welding processes using lasers are still rather expensive. According to the data of the Center of Laser Technologies (Plymouth, USA), the cost of 1 W of the solid-state laser power is US $ 120–200. For a new generation of solid-state fibre lasers, which can successfully cut and weld even aluminium and copper (materials with a high reflection coefficient), the cost of 1 W of their power amounts to US $ 300. All this limits the application of high-power lasers in welding industry, and makes investigators look for new ways of reducing power consumption.

Analysis of the application of lasers shows that the main physical and technical limitation in a way of reducing the cost of unit energy of laser radiation is the efficiency of conversion of an electric pumping energy into a coherent radiation. The efficiency of modern high-power laser systems is 10–15 % for CO_2-lasers, and 1–3 % for Nd:YAG lasers. Reserves for increasing the efficiency have been exhausted to a considerable degree, as they are close to ultimate physical characteristics of active media.

Having certain advantages over the known classical welding methods, laser welding also has a number of drawbacks [2], such as rigid thermal cycles that may lead to decrease in operational strength of welded joints; probability of spattering at high welding speeds; hampered evolution of gas from a molten weld metal at high welding speeds and, accordingly, increased pore formation; hydrodynamic instability of the molten pool at high welding speeds; low value of the total efficiency; and high cost of welding of a running metre of the weld. Like any other welding method, the laser welding technology has its advantages and disadvantages, which determine the limits of its technological capabilities and effective technical-economic fields of its application.

The trend in the field of formation of a strong flow of the coherent energy is to increasing the radiation power, which is accompanied by rise in the electric power consumption. In turn, this leads to sophistication of laser welding equipment, deterioration of its reliability and reduction in technical-economical indices, which eventually prevents the full realisation of the fundamental capabilities of the laser technology. Further development of laser welding was embodied into hybrid methods, i.e. double-beam laser, laser-arc, laser-induction, laser-plasma and laser-light welding, which find an increasingly wide commercial application owing to their high technical and economical efficiency. Combination of different welding methods with laser welding into one technological welding process offers decreasing drawbacks of each method and widening technological possibilities. In particular, the laser-light combination allows programming of temperature at a treatment point on a workpiece following the set thermal cycle [3]. In particular, this enables butt welding of thin-sheet materials using no filler.

Based on analysis of peculiarities of the combined effect on metals using hybrid welding methods, the authors of study [4] made a conclusion of the existence of relationship between the hybrid heat sources (laser and arc), leading to violation of additivity of the thermal effect on a workpiece. The latter means that the combined heat source can provide a higher speed of metal treatment than each heat source taken separately, the effective power of each source being equivalent to the total power of the sources (at the absence of interaction between them). In other words, the combined use of heat sources in the hybrid welding methods makes it possible to achieve the same productivity of the process as in conventional laser welding, using much lower power of laser radiation. Besides, it should be noted that the use of the hybrid welding methods allows the productivity of metal processing to be raised through using a less expensive energy of the second heat source, rather than through using the expensive energy of laser radiation. This is one of the major advantages of the hybrid methods of metals joining and processing.

Therefore, the demand for laser-light equipment and technologies is determined by reduction in power expenditures, characteristic of laser-light processing, and, at the same time, by widening of technological capabilities.

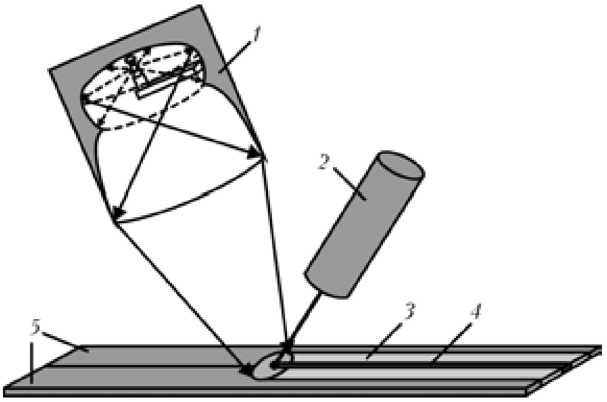

Figure 1. Schematic diagram of laser-light welding using Nd:YAG or CO_2-lasers in combination with high-power polychromatic energy sources: *1* — polychromatic energy source; *2* — Nd:YAG or CO_2-laser; *3* — zone of metal heating with light source; *4* — weld; *5* — workpieces

Reduction in power expenditures in laser-light processing. The substantial progress in development of energy-saving technologies can be achieved by using a new concept for thermal heating of materials. It is based on an integrated approach, i.e. using two heaters with different methods for generation of the beam energy and real-time activation of the surface at a treatment point.

It is suggested that, in addition to the coherent heat source (laser), the energy of a polychromatic gas-discharge light source, having a special optical system (Figure 1), should be used for heating of materials and their subsequent welding or cladding.

Absorbing ability of the surface treated by the laser beam depends upon the laser beam wavelength, temperature and optical properties of the surface [2]. Figure 2 shows dependence of the absorbing ability of steel and aluminium upon the laser beam wavelength at room temperature.

Absorbing ability of aluminium is about 2 % when using a CO_2-laser with a wavelength of 10.6 μm, and 5–10 % when using a solid-state laser with $\lambda = 1.06$ μm. Laser radiation is absorbed by metallic materials in the skin layer, and power is transferred through conductivity electrons deep into a metal. Temperature of the electron gas and crystalline lattice

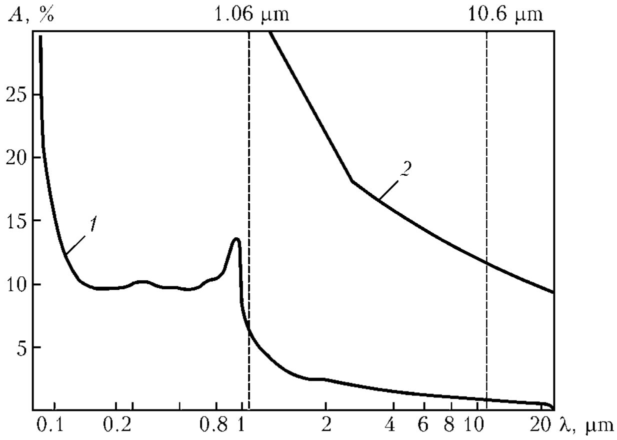

Figure 2. Dependence of absorbing ability *A* upon the laser beam wavelength for aluminium (*1*) and steel (*2*)

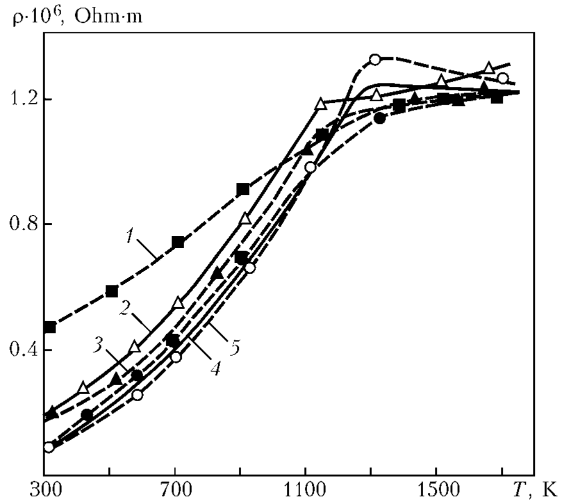

Figure 3. Temperature dependence of specific resistance for iron and steels: *1* — E3Kh138; *2* — St45; *3* — StU12; *4, 5* — Fe

is gradually levelled, and approximately after 10^{-9}–10^{-8} s the metal within the treatment zone can be assumed to have the same temperature.

Values of the reflection and absorption coefficients depending upon the incidence angle are known for polished metal surfaces at relatively low temperatures. According to the Hagen–Rubens relationship, absorption coefficient A is determined by the value of the coefficient of electrical conductivity:

$$A \sim \sigma^{-1/2},$$

where σ is the specific electrical conductivity of metal, (Ohm·m)$^{-1}$.

As electrical conductivity of metals decreases with increase in temperature (Figure 3), the absorption coefficient increases accordingly. When metal is transformed from the solid state in the liquid one, the quantity of the conductivity electrons per metal atom, metal density and specific resistance (the current being kept constant) vary, this leading to growth of the absorption coefficient with increase in temperature at the metal heating point, according to the Hagen–Rubens law (Figure 4).

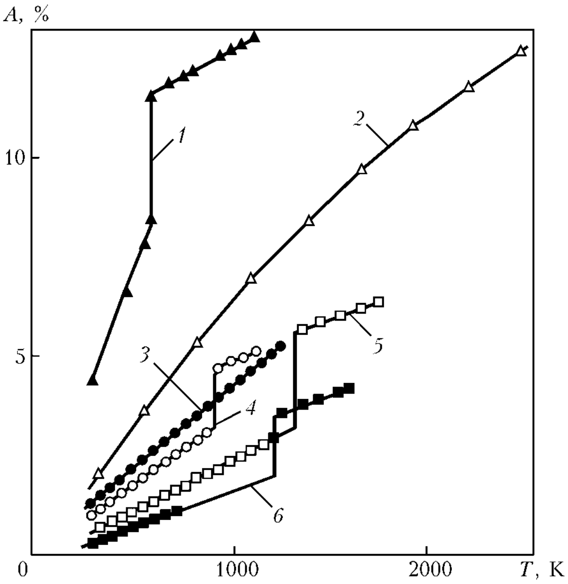

Figure 4. Temperature dependence of the coefficient of absorption of CO_2-laser radiation for pure metals: *1* — Pb; *2* — W; *3* — Cu; *4, 5* — Al; *6* — Ag

Low level of absorbing ability of the surface treated and its dependence upon the laser radiation wavelength are important drawbacks of the laser processing technology, as they lead to a substantial increase in a threshold value of the level of power density needed for processing of a material. However, the absorbing ability of metal can be considerably increased using special surface treatment by physical methods, which are performed simultaneously (in parallel) with laser welding and provide a great increase in the absorbing ability through changing properties of the surface.

The work was completed on the development of a mathematical model of laser-light welding to determine the efficiency of utilisation of the light energy during the welding process. This model intended for calculation of energy parameters of the hybrid laser + light process for welding thin-sheet metallic materials will allow the use of computer-aided design of the hybrid welding process by conducting a preliminary experiment on a computer instead of expensive and time-consuming field experiments, as well as calculation substantiation of intensive marketing in potential application fields of this process. The experimental work in this case is needed only for point verification of computer modelling of the weld pool and weld formation process.

Modelling of the combined effect on material by laser radiation and focused beam of high-power light radiator. With the combined effect of the coherent laser beam and focused beam of a high-power polychromatic light radiator on metal, a heat source is formed on the metal surface. Spatial distribution of the latter is determined by superposition of radiation flows from the laser and light radiator. To develop a mathematical model of light heating, a 2D square grid with a cell number of 30 × 30 and spacing equal to 0.1 of the focal radius of a spot from the light radiator was formed on the surface of a material. The source was set by distributing the intensity of incident radiation over the grid nodes. The earlier developed model of deep penetration [5] was used to describe the laser source (depending upon the power density of an incident radiation), or, in the case where the power density was insufficient for formation of a keyhole, an extra surface grid 5 × 5 with a spacing equal to the focal radius of the laser beam was used, and the laser source was set by the same method as the light one. The chosen diagram allowed modelling of the process of laser-light heating with a possibility of changing relative positions of the laser and light focal spots on a workpiece. The process of heating of a workpiece was considered in a quasi-stationary approximation, where the heat fields did not explicitly depend upon the time in a co-ordinate system moving together with the source.

Heating of the workpiece surface with a flow of the focused radiation of the high-power light radiator leads to formation of a distributed moving heat source on the metal surface. Distribution of the heat flow from this source into a material is determined by local values of the radiation flow power density and local values of the radiation absorption coefficient, which depend upon the surface temperature through the value of surface impedance. Therefore, the problem of heating of a material with the light heat source is non-linear, as power of the heat source depends upon the surface temperature.

Consider first the problem in its linear statement. For this, use the known expression for the Green function of a 3D problem of thermal conductivity in a moving co-ordinate system. Allowing for temperature non-linearity of the absorption coefficient, this expression is an integral equation which can be solved by using the following algorithm: only the temperature of the surface was determined at the first stage. When calculating integral by summation using the 2D grid, the algebraic non-linear equation for each cell was solved by the simple iteration method. Besides, the local temperature at each cell on the surface was determined, and a local value of the absorbed radiation power of the light radiator was estimated with its help. Then the heat field from the light heat source was calculated using the known value of distribution of the absorbed power. The heat field thus determined was summed up with the heat field of the laser source, the kind of which was determined, as noted above, from the value of the laser radiation power density.

Thus found surface distribution of temperature and heat flow allowed solving of the heat problem and determination of the penetration depth. For this purpose, the equation of thermal conductivity written in the co-ordinate system that moves together with the laser beam was solved using the explicit method on a 3D adaptive grid, the spacing of which in a direction of axis Z (normal to the workpiece surface) was determined on the basis of the preliminary analytical solution of the problem of heating of a material with the spot source having a corresponding power, providing that not less than 30 cells of the grid could be accommodated at depth of the weld pool. The obtained numerical solutions were joined at the grid boundary with similar solutions of the problem of distribution of heat from the distributed heat source. Continuity of temperature and its space derivatives were selected to be the joining conditions. The use of analytical solutions for regions located at a distance from the heat source made it possible to allow for the design of a welded joint by adding the efficient reflected sources providing adiabaticity of the workpiece surfaces.

The described algorithm was realised in the form of PC-oriented software written in the Pascal language in visual programming system DELPHI 6 and optimised for access time and size of the used memory. It ensures the time of modelling of one welding mode equal to no more than a few minutes using modern personal computers. The interactive interface and data banks on materials properties and parameters of the process equipment, connected to the system, permit prediction of size and shape of the weld pool, calculation of thermal cycles at any point of the weld and HAZ, selection of parameters of the laser and light radiator, as well as their relative position. The used calculation method guarantees the accuracy of calculations within 5–7 % of a relative error.

Fields of potential application of laser-light equipment and technology. Important indicator of the equipment developed is the possibility of programming temperature at a treatment point on a workpiece following the optimal thermal cycle [6–8] in butt welding of the thin-sheet materials over the 3-axis (volumetric) weld path. For example, software ULSAB for making of an ultra light steel auto body allows using quenching high-strength and super high-strength steels, which can provide an up to 30 % reduction in weight of the body. These steels have good shock resistance and high performance. Software ULSAB recommends that laser welding should be used for joining components of the body. Allowing for rigidity of a thermal cycle, laser welding leads to formation of quenching structures in a welded joint.

Welding thermal cycles exert a substantial effect on weldability of metals. Decrease in the rigidity of a thermal cycle, which in certain cases may have a favourable effect on weldability, can be achieved by simultaneously applying a laser welding thermal cycle and less rigid thermal cycles of light treatment [9–12], using them in a mode of preliminary, concurrent and subsequent heating, following the assigned programmable thermal cycle to provide an optimal metal structure in the welded joint in real time.

Software ULSAB was developed by the leading American and European automobile companies, steel manufacturers and research centres. It is intended to demonstrate the efficient utilisation of steel in the construction of cars with a much lower weight.

Laser-light processing finds wide application for deposition of metal powders with special properties (DMD process), as well as improvement of wear resistance of fast-wearing surfaces of parts of oil and gas producing drill rigs, e.g. drill pipe nipples. Coated nipples are used to join service pipelines of the offshore drill rigs. The high-intensity processing methods using the coherent beam, providing high-quality parts by welding, cladding, heat treatment, etc., hold high promise for aerospace engineering, where the guaranteed high quality is a mandatory requirement.

At the same time, providing of the guaranteed high quality of parts with improved performance requires utilisation of materials with special properties (composite, high-strength, high-alloyed, etc.). Welding, cladding and heat treatment of these materials cause decrease in safety factor for their operational strength (capability of relaxing stresses, crack resistance of welded joints, etc.), which requires the use of programmed optimal thermal cycles within the treatment zone.

For example, the process of formation of pores during welding of aluminium alloys belongs to complex physical-chemical phenomena, and its evolution is caused not only by properties of the initial metal, but also by the welding parameters [2]. One of the main causes of pore formation in welding of aluminium and its alloys is hydrogen, which gets into the weld pool metal from the base and filler metals. Because of high affinity of molten metal for oxygen and fall in solubility taking place during solidification of aluminium, it is necessary to take measures to prevent any inflow of hydrogen into the weld zone. Mol-

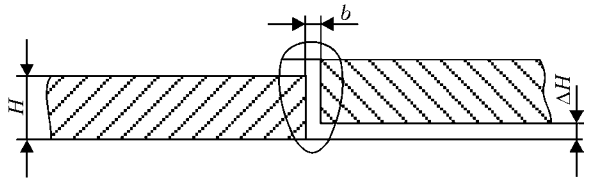

Figure 5. Schematic of a butt joint with gap and weld edge displacement

Table 1. Requirements to gap size and edge displacement in laser welded joints

Metal thickness, mm	*Welding speed, mm/s*	*Maximum permissible gap size b, mm*	*Maximum permissible edge displacement Δf, mm*
0.8–1.5	5.5--22.2	0.12	0.1
0.8–1.5	22.2–33.3	0.10	0.1

ten aluminium alloys at a temperature of 660 °C can solve about 0.7 cm^3 / 100 g of hydrogen, while at 658 °C, as soon as it has solidified, only 0.036. A distinctive feature of laser welding is a low heat input. Therefore, hydrogen has too little time for reverse diffusion, which leads to formation of hydrogen pores. At the same time, porosity can be reduced by using the welding methods where the heat input is higher, the weld pool is larger and solidification time is longer (which permits evacuation of a larger amount of hydrogen). Therefore, as a result of increased heat input, hybrid laser-light welding allows the thermal cycle to be made softer and pore formation to be reduced.

Requirements to the accuracy of the fit-up geometry and, therefore, costs can be greatly reduced through increasing the volume of the weld pool and decreasing the value of the weld shape factor. This can be achieved by using the light heat source simultaneously with the laser beam, i.e. the hybrid technology of laser-light welding [5, 11]. By forming the weld pool in the thermal conductivity mode, the light source provides a substantial decrease in the weld shape factor and closes local gaps as a result of thermal expansion of the weld edges heated by the light beam periphery.

High values of the coefficient of concentration of the laser welding energy source determine minimal volumes of the molten weld pool, and the deep penetration mode provides a high value of the weld shape factor [2]. The above factors impose higher requirements on accuracy of the geometry of the fit-up of workpieces for welding. For example, in butt welding of structural steel with thickness H without a filler (Fi-gure 5), the requirements imposed on joint gap b and edge displacement ΔH in laser welding are very stringent according to TR 1.4.1569--86 «Laser Welding of Structural Steels» (Table 1). Failure to meet requirements for the geometry of fit-up of workpieces for laser welding may lead to thinning (weakening) of the weld, loss in structural strength of the welded joint or lack of penetration of the weld root.

Therefore, utilisation of the coherent and polychromatic flows of the radiant energy is promising and more cost effective, compared with utilisation of the laser beam alone. At the same time, all advantages of the laser beam are retained in this case.

The laser-light machine (LLM) developed to address the above problems is a compact modular stationary equipment installed in a workshop. It can be programmed and flexibly built into robotic manufacturing systems. Also, it can be additionally fitted with a powder feeder, if necessary to perform cladding using metal powder. LLM (Figure 6) includes a mass produced solid-state Nd:YAG laser, light module, light guide or mirror-hinged assembly, and modular control and cooling units.

Application of LLM allows:

- reduction in costs of products through reducing manufacturing expenses, making the materials treatment process cheaper through energy saving, decreasing power expenditures, saving of consumed raw materials, high cost effectiveness of light energy, and increasing efficiency;
- rise in productivity as a result of the synergic effect;
- improvement of quality of the products and widening of operational capabilities through programming the heating temperature at a set treatment point.

Operational advantages of the offered technology include:

- decrease in requirements to joint gaps in thin-sheet workpieces (0.5–1.0 mm), compared with laser welding;
- widening of ranges of materials for joining and processing, as well as increase in the quantity of operations performed (welding, cladding and heat treatment of welded joints);
- possibility of using the LLM radiator in the automated mode or placing LLM on industrial robots;
- decrease in gas saturation of the weld metal;

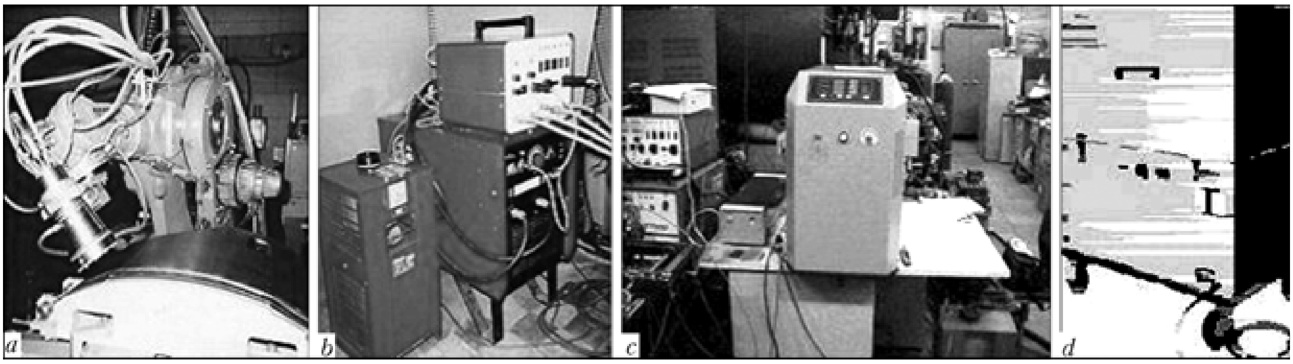

Figure 6. LLM set for robotic welding system: *a*, *b* — robotised light module of LLM; *c*, *d* — laser module of LLM

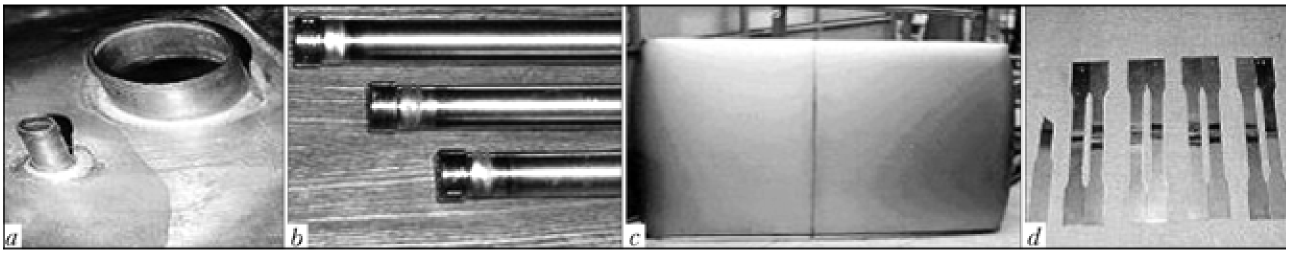

Figure 7. Examples of application of laser-light technologies for welding, cladding and brazing: *a* — auto petrol tanks made by the laser-light technology with no damage of the anticorrosion coatings in the heating zone; *b* — casings of ionised radiation sources; *c* — auto body components (car roof); *d* — testing of mechanical properties of welded joints

Table 2. Indicators of widening of operational capabilities of laser equipment fitted with light module

Indicator	*LLM*	*Laser equipment*
Purpose	Welding, cladding, heat treatment	
Range of programming heating temperature following a set thermal cycle, °C	200--1200	No
Efficiency, %	Up to 25–30	Nd:YAG laser: 1--3
Mean failure-free operation time, h	1000	1000
Service life, years	5	5
Duty cycle, %	85	85
Cost (1 W of radiant energy), US $ / W	40–75	120–200
Deposition of special heat-resistant coatings following a set thermal cycle	Possible	No
Deposition of wear-resistant and special coatings following a set thermal cycle	Same	Same
Local heat treatment following a set thermal cycle	»	»
Processing of materials following a set thermal cycle	»	»

- high consistency, environmental cleanness and safety.

Open Joint Stock Company «NIITavtoprom» performed for Open Joint Stock Company «AvtoVAZ» the experimental work on optimisation of the technology for laser-light welding of thin-sheet butt joints in body components 0.8–1.2 mm thick, and for Federal State Unified Company «Mayak» — same for casings of ionised radiation sources (at the Research and Training Centre of «NIITavtoprom», in collaboration with associates of the laser equipment and technology faculty of the N.E. Bauman Moscow State Technical University and a team of developers of the laser-light devices from the Czech Company «Svar») (Figure 7). The calculations made by specialists of the Laser Technology Institute of St-Petersburg State Technical University, N.E. Bauman Moscow State Technical University and «NIITavtoprom» show (Table 2) that the laser-light welding technology provides widening of operational capabilities of laser equipment and retains general trends of synergic control. Welding speed with the laser as a result of its fitting with the light module grows by 50 % and more on thickness of up to 1 mm. The laser-light processing using solid-state lamp-pumped lasers provides a 3–4 times reduction in power expenditures [6].

The laser-light machines are a result of the research intended to find ways of widening operational capabilities of lasers.

At the first stage of the research, we have chosen and investigated the solid-state lamp-pumped laser, which is being dynamically developed and is in high demand in the world market. The combination of two sources of the radiant energy provides not only the efficient heating of a workpiece material to assigned temperatures and simultaneous penetration of the material with the coherent beam of a comparatively low power, but also the welding process of an increased productivity and efficiency.

Acknowledgement. The authors express gratitude to V.S. Drizhov, L.N. Majorov, V.M. Fyodorov, I.S. Chepyzhev, V.P. Sokolov and S.V. Shakhov for their active participation in activities of the Research and Training Centre.

1. (2002) World market of lasers: 2002 review and prediction for 2003. In: *Inform. Bull. of Laser Association «Laser-Inform»*, 258(**3**).
2. Grigoriants, A.G., Shiganov, I.N., Chirkov, A.M. (2004) *Hybrid technologies of laser welding*. Moscow: N.E. Bauman MGTU.
3. Alekseev, G.M., Shilov, S.S. (2003) Laser-light technologies and equipment for welding and brazing of thin-sheet materials. *Instrument, Tekhnologiya, Oborudovanie*, **5**, 13, 17.
4. Seyffarth, P., Krivtsun, I.V. (2002) *Laser-arc processes and their applications in welding and material treatment*. Vol. 1. London: Taylor & Francis.
5. Lopota, V.A., Sukhov, Yu.T., Turichin, G.A. (1997) Model of laser welding with deep penetration for technological application. *Izvestiya AN SSSR. Series Physics*, 61(**8**), 1613–1618.
6. Alekseev, G.M., Shilov, S.S. (2003) Development of technology and manufacture of equipment for production of welded-stamped billets of materials with different thickness, chemical composition and properties. In: *Report of OAO «NIITavtoprom» on State Contract No.*10.802.11.0018 of 21 Febr. 2003.
7. Alekseev, G.M. et al. (2000) *Welding Int.*, 14(**3**), 246–248.
8. Alekseev, G.M., Butov, V.N. (1999) Light-beam welding equipment. *Svarochn. Proizvodstvo*, **9**, 33–35.
9. Alekseev, G.M. (2003) Possibilities of laser-light welding. In: *Inform. Bull. of Laser Association «Laser-Inform»*, 274(**19**).
10. Alekseev, G.M. et al. (2002) Laser-light technologies and equipment — a new trend in welding and brazing of parts. In: *Abstr. of 39th AAI Int. Sci.-Techn. Conf. on Priorities of Development of National Automobile-and-Tractor Industry and Training of Engineers and Researchers* (Moscow, Sept. 25–26, 2002). Moscow: MGTU MAMI.
11. Alekseev, G.M., Borisov, M.T., Butov, V.N. (1999) Development and making of robotic system for light-beam brazing and welding of parts of «Moskvich» car bodies. In: *Coll. pap. of ASM-Holding 6th Int. Conf.*
12. Alekseev, G.M. (2002) Laser-light technologies and equipment — a new trend in welding and brazing of parts. *ITO-Novosti*, **6**, 6.

HIGH-TEMPERATURE GAS CORROSION OF NICKEL ALLOY TURBINE BLADES DURING OPERATION

K.A. YUSHCHENKO, V.S. SAVCHENKO, L.V. CHERVYAKOVA and **A.V. ZVYAGINTSEVA**
E.O. Paton Electric Welding Institute, NASU, Kiev, Ukraine

The character of gas corrosion of power plant blades made from nickel alloy Inconel 738 has been studied. It is shown that redistribution of alloying elements occurs in a narrow zone adjoining the crack surface. Evaluation of microhardness showed the loss of strength taking place in this zone.

Keywords: heat-resistant nickel alloys, gas corrosion, microhardness, grain boundary, diffusion, local crack

Gas turbine blades subjected to long-time service at high temperatures and complex loading undergo structural changes caused by temperature, service conditions, corrosive environment and other factors [1]. In a number of cases the complex impact by the above factors on material of the blades leads to an accelerated fracture of the material as a result of localisation of processes in certain zones [2]. This article describes studies of the character of gas corrosion of power plant blades made from nickel alloy In738, having the following chemical composition, wt.%: 0.17C, 8.5Co, 16.1Cr, 1.8Mo, 3.4Al, 3.4Ti, 2.6W, 1.8Ta, 0.8Nb, and Ni — base.

The blades studied were in operation for about 15,000 h. The network of cracks in the middle part of an airfoil in a range of maximal temperatures of metal was revealed by visual examination of the blade surfaces. As shown by metallography, fracture (up to 0.6 mm) occurred along the austenite grain boundaries (Figure 1, *a*). In addition, redundant phases (Figure 1, *b*) with an extra depth of 0.6–0.8 mm precipitated ahead of a crack along the grain boundaries. Therefore, the total depth of structural changes was approximately 1.2–1.4 mm.

It was suggested that intergranular precipitates and subsequent fracture were caused by gas corrosion. Microhardness of different structural zones in a crack formation region was evaluated under a load of 0.1 N. The studies showed the loss of strength taking place in a narrow zone adjoining the crack surface (Figure 2). Thus, microhardness of the matrix was *HV* 550, compared with microhradness of the narrow zone near the crack equal to *HV* 290. Standard solution annealing (austenising) of metal failed to provide dissolution of the redundant phases formed along the grain boundaries ahead of the crack front. This confirms a high thermodynamic stability of the precipitates and hypothesis of a selective oxidation of grain boundaries of metal during operation.

Chemical composition of structural zones of metal in a crack region was examined using the Comebax analyser, which allows quantitative evaluation of the content of a number of elements, including oxygen. Thus, it was found that the content of elements with limited diffusion mobility (niobium, tungsten, nickel and molybdenum) across the section being analysed remained almost unchanged (Figure 3). At the same time, a decreased content of aluminium, titanium and chromium was detected in a narrow zone with lower hardness. Moreover, the above zone had increased oxygen content.

The studies performed suggest the following mechanism of corrosion fracture (Figure 4). Initially, despite the presence of protective coatings, a limited

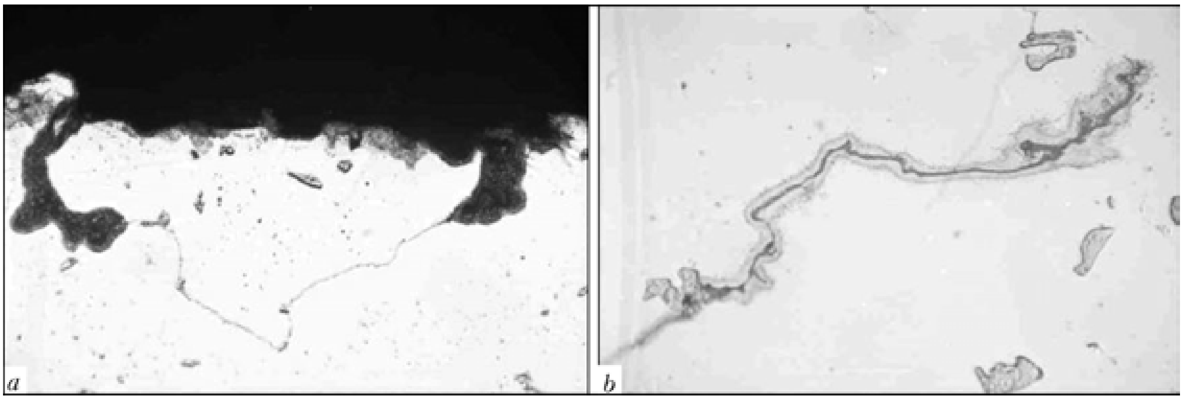

Figure 1. Microstructure of the used In738 airfoil (×200): *a* — beginning of corrosion fracture; *b* — degradation of grain boundaries

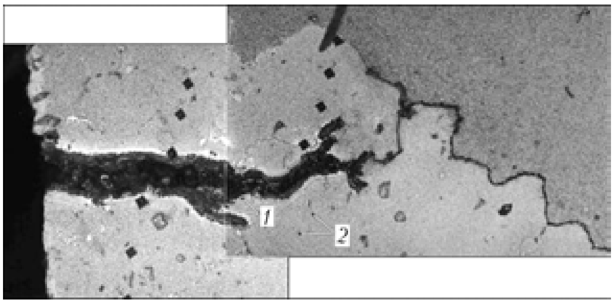

Figure 2. Microhardness of structural components of the In738 airfoil after gas corrosion during operation: *1* — diamond pyramid indentations in the boundary zone; *2* — indentations on grain body (×200)

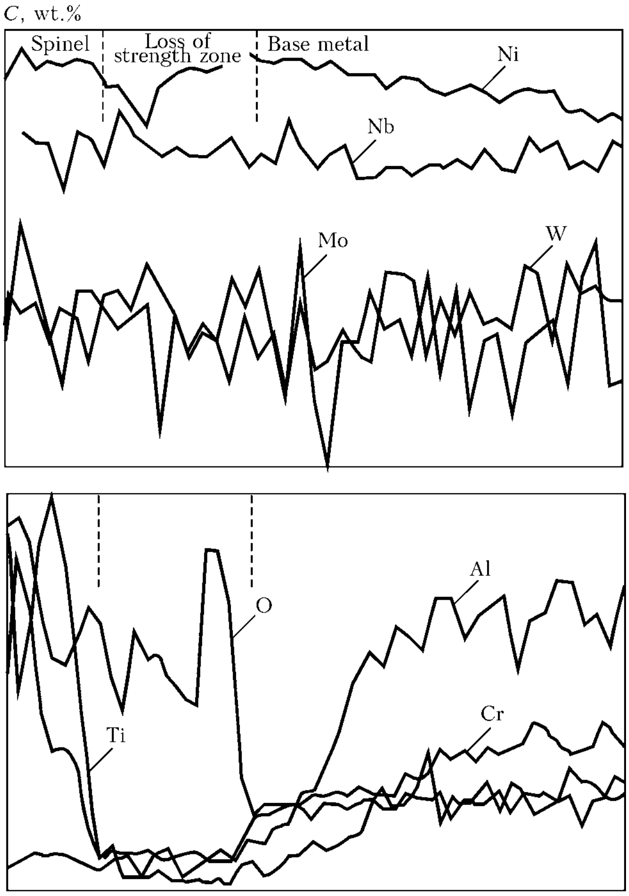

Figure 3. Qualitative distribution of chemical elements in the boundary zone of an airfoil region subjected to gas corrosion

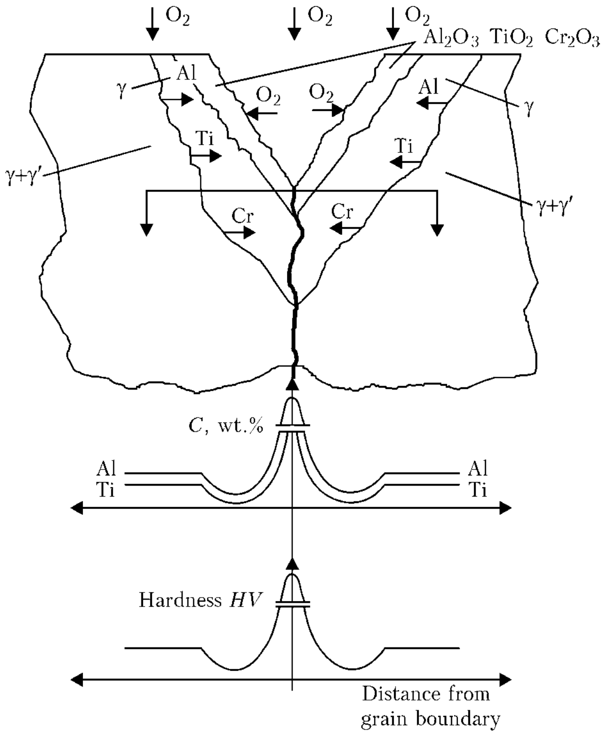

Figure 4. Schematic of evolution of corrosion fracture on surface of the In738 airfoil after long-time operation

diffusion of oxygen takes place along the grain boundaries of the cast metal of blades under certain conditions. Elastic or local plastic strains promote realisation of the diffusion process. Being an active element, oxygen combines with aluminium, titanium and chromium to form oxides of the type of spinel along the grain boundaries. Solid solution of metal of the zones adjoining the boundary becomes depleted in these elements. As aluminium and titanium are the elements that promote formation of the strengthening γ'-phase, decrease in the content of these elements in local zones leads to dissolution of the γ'-phase and loss of strength of the metal, which is proved by metallography and measurements of microhardness. This results in formation of a weakened boundary zone, where a local crack is initiated under the effect of operational loads. The process is periodically repeated, leading to formation of a macrocrack. The high-temperature corrosion attack on the surface of blades substantially diminishs owing to the presence of effective protective coatings, thus allowing the service life of power plant equipment to be extended several times.

It should be noted in conclusion that parts made from heat-resistant nickel alloys strengthened by the γ'-phase are prone to high-temperature intercrystalline corrosion fracture during operation. The basic mechanism of the latter is interaction of an oxygen gas with aluminium and titanium, which, on the one hand, have high affinity for oxygen and, on the other hand, are metal strengtheners, leading to formation of the strengthening γ'-phase. Formation of oxides of the above elements primarily along the grain boundaries results in their depletion of the sub-surface layers and loss of strength of the metal, which favours local propagation of a crack along the grain boundaries. The process is repeated many times, leading eventually to macrofracture.

1. Gryaznov, B.A., Gorodetsky, S.S., Nalimov, Yu.S. et al. (1992) *Fatigue of heat-resistant alloys and gas turbine engine blades*. Kiev: Naukova Dumka.
2. Keiji, S., Zukio, T. (1991) Cracking by elevated temperature embrittlement in the HAZ of alloy 800H. *Transact. of Jap. Weld. Soc.*, 22(**1**), 10–15.

METAL STRUCTURE IN THE FUSION ZONE AND HAZ OF WELDED JOINTS ON HIGH-CHROMIUM HEAT-RESISTANT STEELS

V.Yu. SKULSKY
E.O. Paton Electric Welding Institute, NASU, Kiev, Ukraine

It is shown that a coarse-crystalline structure may form in the region between the weld and HAZ in fusion welding of high-chromium martensitic steels of P91 type. This structure is a fusion zone, wherein the base metal grains undergo a different degree of melting,. Segregation and diffusion redistribution of carbon may lead to formation of a relatively decarburized ferritic phase (δ-ferrite) within the fusion zone. Moreover, this zone is characterized by formation of coarse grains of primary austenite. It is shown that metal in the HAZ in the tempering region located behind the phase recrystallization region loses its strength.

Keywords: arc welding, high-chromium steels, welded joints, microstructure, weld, fusion zone, carbon, segregation, δ-ferrite, grain size, HAZ, tempering zone

New high-temperature steels with a higher chromium content began to be applied in fabrication of critical elements of thermal power plant equipment (pipes, thick-walled fittings, manifolds) over the last two decades [1–4]. The advantages of the new materials compared to the earlier used steels for similar applications (higher level of long-term strength, corrosion resistance, possibility of transition to super critical steam temperatures right up to T = 580–610 °C with the respective increase of electric plant efficiency to 43–45 % and reducing harmful evolutions of CO and NO_x) are quite broadly covered in publications of their manufacturers and in a number of research works. Nonetheless, some phenomena and features of property variation found in practical application of new materials are still insufficiently studied, or insufficiently well-covered in publications.

The group of new generation pipe steels include complex-alloyed steels with 9 wt.% Cr — P91 (X10CrMoVNb91), E911, NF616. Having a close content of carbon, chromium, molybdenum and nickel, which are the elements, determining the type of phase transformations and final structure formation, such materials are characterized by the same stability of austenite under the conditions of overcooling and susceptibility to formation of a single-phase martensitic structure in a broad range of cooling rates. Without discussing the features of finely-dispersed phase precipitation during tempering, due to the differences in the content of carbide-forming element additions (E911 and NF616 steels additionally contain tungsten), it may be assumed that such steels should have the same regularities of the processes of welded joint structure formation. This allows considering them, taking one steel of this group as a example.

This paper presents the results of studying the features of structure formation in welded joints of steels with 9 wt.% Cr in the case of P91 steel. Phenomena are considered which are related to structure formation in the region of the fusion zone (FZ) and HAZ.

Experiments were performed using commercial-grade pipe steel from two different manufacturers with the composition corresponding to the following specification, wt.%:

- steel 1 — 0.1C; 0.34Si; 0.47Mn; 0.003S; 0.018P; 8.5Cr; 0.28Ni; 0.93Mo; 0.2V; 0.072Nb; 0.06N;
- steel 2 — 0.085C; 0.33Si; 0.43Mn; 0.015S; 0.013P; 8.85Cr; 0.12Ni; 1.0Mo; 0.25V; 0.069Nb (N — not determined).

Welded joint structure was simulated by deposition of individual beads on the surface of plates of the studied steels. For this purpose mechanized submerged-arc welding with highly basic flux CFT9 was performed using test flux-cored wire PP9, providing the deposited metal composition similar to that of steel P91, and high-alloyed (austenitic) wire Sv-04Kh19N9T.

Chromel-alumel thermocouples were used for temperature measurement and recording of thermal cycles in the HAZ metal. The thermocouples were connected to KSP4 potentiometers calibrated for operation with this type of thermocouples. Sections for microstructural studies were cut out across the longitudinal axis of the weld. The microstructure was revealed by chemical etching in a 15 % alcohol solution of nitric acid. Microhardness was measured in PMTZ instrument with 20 g load, and 5 kg load was used when measuring the Vickers hardness. X-ray microprobe analysis was conducted in Camebax system. Neophot-32 light microscope was used for metallographic examination.

Structure in the weld and FZ region. As was noted above, steel P91 belongs to martensitic class of materials. This steel is welded using consumables providing weld metal alloying that is practically identical to that of the steel, and, hence, martensitic structure of weld metal with the hardness of about HV50-430–470. Martensite forming in as-normalized steel and in the welds after welding belongs to the category of lath (acicular) martensite [5]. Such a final structure is secondary relative to the primary structure formed at solidification before the start of polymorphous transformations. The primary structure enables analyzing with a certain degree of validity the mechanism or conditions of formation of the studied zones of welded joints. As the secondary structure in hardening steel welded joints, etched out during microsection preparation, usually obscures the primary structure, a separate detection of the primary structure without the secondary one is performed. The work considers the primary structure of weld metal, revealed by a specially selected reagent.

In welding of P91 steel, the welds solidify with formation of primary columnar crystals (primary solidification elements), of predominantly celullar and celullar-dendritic structure with different sizes of their cross-section and extent (Figure 1, *a*). HAZ metal (dark region in Figure 1, *a*) has a specific surface relief after chemical etching, formed by closely located pits, curved grooves and microprotrusions similar to microscopic net. Such a variable resistance of the metal to the etchant is related to chemical microinhomogeneity (or insufficient degree of homogenizing), formed under the impact of the thermodeformational cycle in this region. Let us call it a net structure. In the region of the zone of transition from the steel being welded to the weld, the metal structure differs from that of HAZ metal or weld metal (Figure 1, *b*). A metal interlayer forms between the base metal (BM) and the weld, being similar to the cast structure of the weld, but having the crystal shape close to the equiaxed or coarse cellular structure with shorter axes (Figure 1, *a*--*d*, *g*). This coarse-crystalline region can, sometimes, also have individual regions with a net structure (Figure 1, *a*). Metal in this region is of a lighter colour than the weld metal adjacent to the HAZ.

Metal with a net structure can be unambiguously regarded as BM, which has been heated up to high temperatures and has not reached a high degree of homogenizing during micro-disperse phase dissolution, as it is believed that in the HAZ metal of steels with very active carbide-forming elements the time can be insufficient for a complete dissolution of the carbide phases at fast temperature rise and drop characteristic for the usual thermal cycle of welding [6].

On the other hand, it is somewhat difficult to explain the origin of the zone with the coarse-crystalline structure. Based on the morphological features this metal can be regarded as the weld metal, i.e. metal, which melted and solidified. However, a certain «equiaxity» suggests that this metal could form at overheating of the HAZ metal up to the complete dissolution of the dispersed phases and maximum uniformity in distribution of the alloying and impurity elements in the grain body. Under such conditions the grain grows up to considerable dimensions. However, the irregular shape of the grains, characteristic for the cast structure, does not allow fully guaranteeing it.

In welding publications the zone of transition from the weld metal to BM (HAZ metal proper) which did not melt during welding, is the FZ, where the metal was heated up to temperatures between solidus and liquidus [7]. According to [8–10], regions of completely molten BM, which did not mix with the filler metal during the welding cycle, can also form here («unmixed zone» [8]). In welded joints of steels with phase transformations it is not always possible to reveal and identify the characteristic features of metal of exactly such a structure. As was noted above, it often remains obscured by the secondary structure. There is also a transition zone between the main part of weld metal and FZ, where melt alloying changes gradually from the composition of the steel being welded to the weld composition, primarily as a result of different contributions of molten welding wire and BM during mixing. With identical alloying of the filler material and the steel welded the section of a variable composition may not be structurally revealed. This zone, however, is always present in reality, because of certain differences in the composition of steel and welding consumables (for instance, by impurity content).

Some of the significant factors, influencing structure formation in FZ, are the degree of overheating of the metal being welded in the zone of contact with the melt and the hydrodynamic situation, forming at the pool walls. BM is heated by the heat evolving from the welding arc column, and may be additionally preheated by the molten and overheated metal of the weld pool [11], where the average temperature of the melt is equal to approximately 1770 °C [12, 13], as well as the latent heat evolved by the weld at solidification [9]. Wetting of surface-melted BM grains by the molten metal of the weld leads to formation of a solid metal–melt contact zone, where the solid metal and the liquid have a certain adhesion strength, due to the impact of the surface interphase tension forces. In addition, the temperature of the liquid contacting the metal surface is lower than that of the ambient melt, which increases its viscosity [14]. The velocity of such liquid motion at the pool wall is practically zero, because of the impact of the interphase tension forces and increased viscosity. As a result of tangential friction stresses [14], the adjacent melt flows apply forces to BM through a layer, which is in direct contact with BM grains, these forces trying to move or separate the surface layer of BM grains. The latter becomes possible in the case of weakening of the bond between the grains, primarily on the interphases due to development of grain-boundary melting. Time stresses and shear deformations of the metal in the HAZ, which are due to bulk changes of the metal at welding heating, apparently have an important role in separation of BM grains at the fusion line, and formation of cracks and delaminations [15].

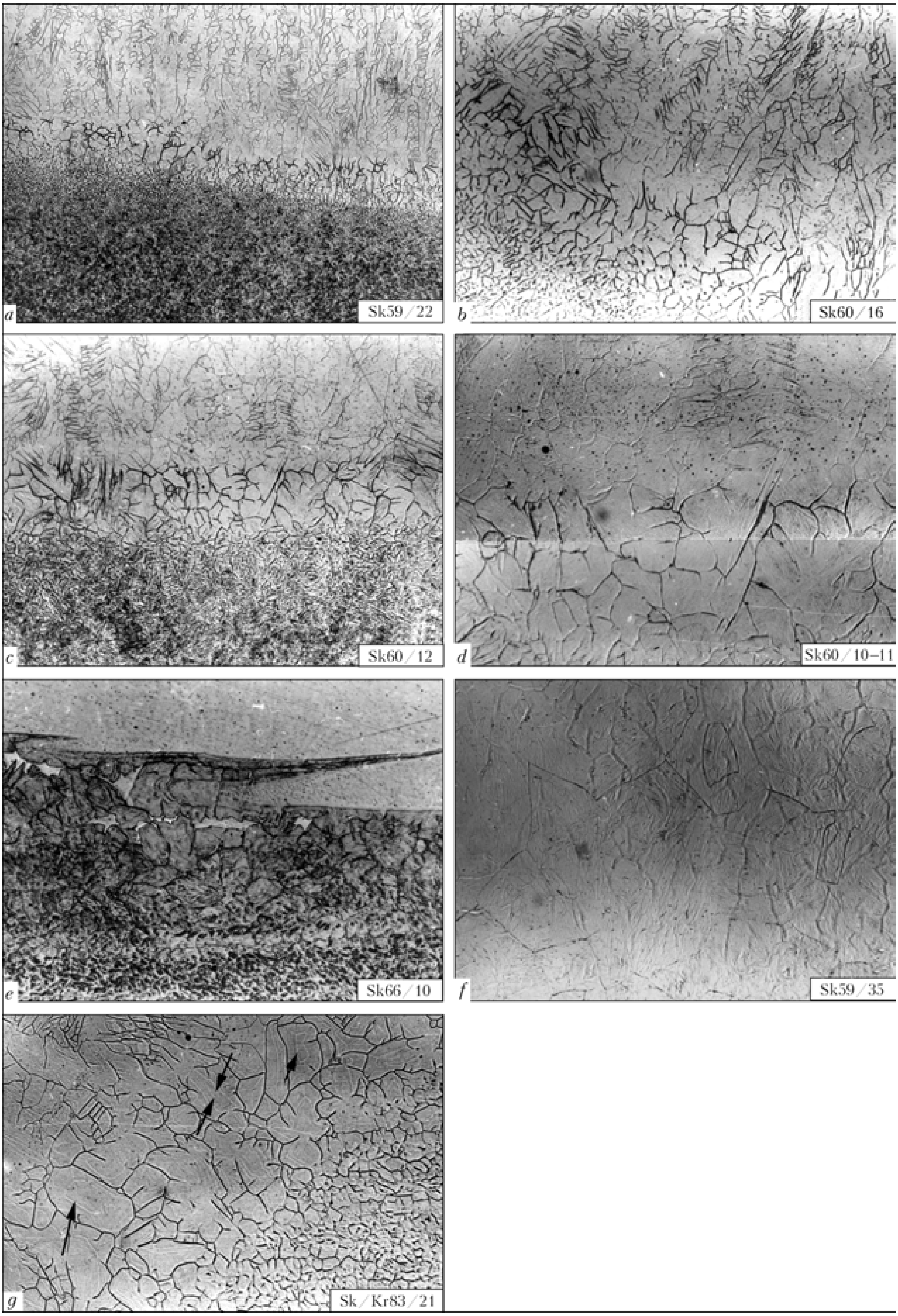

Figure 1. Microstructure of welded joint of steel P91 (steel 2) in FZ region: *a* — ×125; *b* — ×200; *c* — ×250; *d* — ×630; *e* — ×500; *f* — ×800; *g* — ×320

Causes for surface melting of grain boundaries in the overheating zone can be lowering of the effective solidus temperature, in connection with dissolution of excess phases and grain-boundary accumulation of impurity and alloying elements, present in the composition of these two phases; dissolution of phases, boundary enrichment by carbon and running of the reverse peritectic reaction $A \rightarrow \delta + L(C)$, i.e. austenite decomposition into δ-ferrite (decarburized) and carbon-enriched liquid (possibility of such a reaction running is suggested in [16–18]).

As is seen from Figure 1, *e*, turbulent flows of the liquid separate from the pool walls the layers of grains adhering to each other («grain conglomerates» [19]), which, as they are «drawn» into the higher temperature areas become thinner, because of surface melting, and form specific whisker-shaped branches. These can also be individual regions of «broken away» BM, not completely molten, or molten, but not having had time to mix with the pool melt. Such a structure is easily revealed, when weld metal is produced to have greater corrosion resistance in the etching solution than the steel being welded (in this case, in deposition of highly alloyed metal of 18Cr–10Ni type).

Thus, in the studied FZ section BM was heated minimum up to temperatures not lower than effective solidus T_S, which was accompanied by grain boundary melting. It is quite probable that an even greater overheating could lead to a higher degree of grain melting — complete or partial with preservation of remaining fragments of unmolten grains.

In the central region of the deposited weld in the zone of the active spot, and, therefore, of maximum dynamic impact of the arc on the melt, the FZ coarse-crystalline structure has minimum width, pool bottom surface becomes relatively smooth without whisker formation. In the peripheral zones the pool walls become wavy, shelves and whiskers of delaminated metal form, and FZ becomes wider. This confirms the assumption, that the hydrodynamic forces and the heat imparted by the melt to the pool wall metal initially heated by thermal radiation of the arc, have the determinant influence on formation of FZ structure. The molten metal is ousted by the arc in the direction opposite to that of welding, so that the considered processes of structural changes under the impact of melt flows develop to a greater extent behind the welding arc. The width of the considered zone becomes smaller in the subsurface regions, this being, obviously, related to a lower temperature of BM initial heating, surface heat removal and lower effectiveness of its overheating by small volumes of rolling-over melt flows. In mechanized submerged-arc welding with flux-cored wire (I_w = 350–370 A, U_a = = 37–39 V, v_w = 19 m/h) FZ width was 0.05–0.10 mm in the lower part of one of the weld sections (in the active spot area), on the side surface of the weld pool wall the maximum width of this zone reached 0.30–0.45 mm, and at the steel surface it decreased to 0.10–0.15 mm (Figure 2).

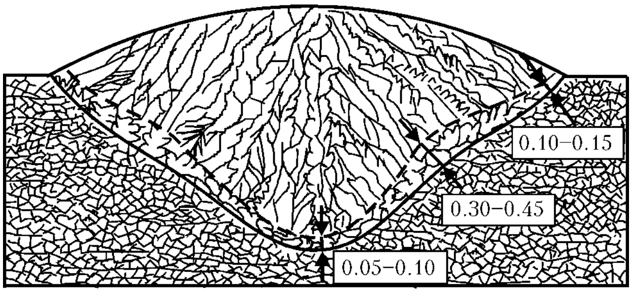

Figure 2. Nature of variation of the width of FZ with a coarse-crystalline structure in the section of a sample with a bead deposited by submerged-arc process

Metallographic investigations allow revealing the characteristic features of formation of a coarse-crystalline metal structure in the FZ.

Figure 1, *d* shows an enlarged fragment of a microstructure in Figure 1, *c*, which includes a section of FZ and weld metal. The latter contains a noticeable amount of non-metallic inclusions, formed as a result of proceeding of metallurgical reactions with participation of welding consumables. No such inclusions are present in FZ or in BM. Thus, the considered coarse-crystalline FZ region has the metal structure formed without mixing with the welding consumables. Fragments of secondary boundaries etched out in this zone, i.e. austenite grain boundaries (Figure 1, *f*) have correct geometrical shape and are randomly oriented relative to the twisting thicker boundaries of large-cellular crystals. Such a situation is the most typical for the cast metal. As is known, primary boundaries form at intergrowing of the solidification elements with segregational redistribution of impurity and alloying elements ahead of the solidification front that is characteristic for this process, and the resultant development of chemical microinhomogeneity in the growing solid phase. The degree of chemical inhomogeneity is maximum in the zones of intergrowing of the primary solidification elements [12, 20, 21]. It accounts for the difference in the corrosion resistance of different microregions of the primary crystalline formations to the impact of a specific etchant liquid. This results in a rather easy and more precise etching out of the primary boundaries. When the solidification is over, the final formation of grains in the solid phase proceeds with the characteristic for this process re-arrangement of the atoms layout in the region of the primary crystal intergrowing and shifting (migration) of new boundaries to another position relative to the primary boundaries [21, 22]. In the presence of other phases in the metal, such a boundary takes up the position of the interphase. Similar observations of an arbitrary arrangement of secondary boundaries of austenite grains relative to solidification ones in the grain melting region in the FZ are also reported, for instance, in [9, 23].

Thus, it may be assumed that a certain part of the metal in the considered microregion, having passed the stages of overheating, maximum homogenizing of the solid solution and surface melting of the interphases, went into the state of an even greater melting

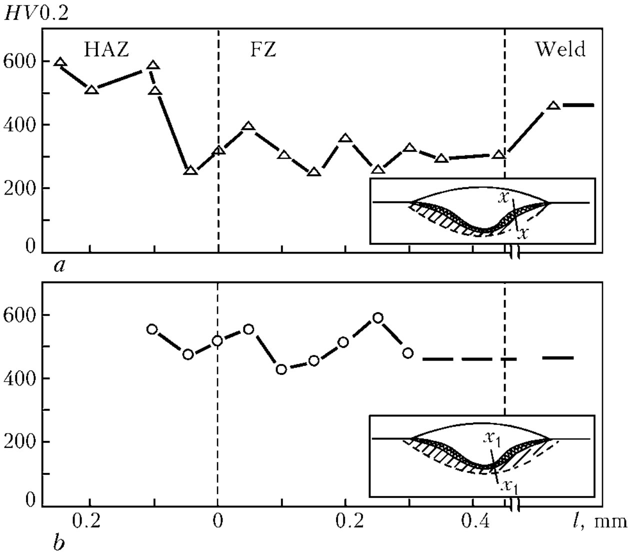

Figure 3. Change of metal microhardness in two regions across FZ in the section of the bead deposited on steel P91 by mechanized flux-cored wire submerged-arc welding: *a* — x–x section with maximum FZ width; *b* — x_1–x_2 section in the weld root region

of the grains, corresponding to heating up to temperatures between effective solidus T_S and liquidus T_L. The metal of this zone, consisting of the remains of the grains surrounded by their own melt, does not participate in mixing with the deposited filler metal. On the other hand, a certain part of the grains located closer to BM, can only go through the stages of homogenizing and dynamic recrystallization [24, 25], accompanied by their coarsening, if this has enough time to proceed during the short time of their stay in the region of temperatures above that of stable dispersed phase dissolution.

Light-coloured boundaries of inner substructure elements are sometimes visible in the grains of the considered coarse-crystalline zone (shown by arrows in Figure 1, *g*). It may be assumed that, on the one hand, these boundaries are the outlines of the remains of the grains, which did not melt at development of intergranular melting. On the other hand, they may be the contours of fine grains formed at heating and intergrowing through coalescence into one coarse grain of irregular shape. However, presence of fine boundaries of austenite grains, randomly located relative to the «coarse» boundaries of the grains of this zone, suggests that the latter type of the boundaries can be of segregational origin.

The above-said suggests that the observed coarsening of FZ structure can be based on two mechanisms.

1. In the section adjacent to BM, homogenizing (in complex-alloyed steels the most stable carbide compounds can dissolve at heating above 1260 °C [26]) and grain growth proceed under the conditions of continuous deformation as a result of initial recrystallization and subsequent secondary recrystallization, including the bulk recrystallization (although, it is believed [24] that the motive force of collective recrystallization can be by several orders of magnitude lower than that of the initial one) or coalescence. Overheating of oriented in a certain way intergranular boundaries [27] (with excess of just the free energy and without allowing for the probability of eutectic phase appearance) can lead to boundary surface melting.

2. The processes of grain coarsening and deformation, and their surface melting proceed in the zone of greater overheating located closer to the pool melt. Fine grains (which did not have enough time to grow) melt to a greater degree or completely, and are absorbed as the formed liquid by the adjacent surface-melted or recrystallizing grains.

FZ width is determined by the completeness of the above process development. It is controlled by the degree of BM initial heating by the heat evolving from the welding arc, then additional overheating by the heat, evolving from the weld pool melt (at its cooling before the solidification start and latent heat of melting), and the rate of heat transfer from this zone into colder regions of steel being welded. Convective flows to a greater degree determine the melt structure at the weld pool walls and the width of the variable composition region.

Investigations showed that the metal with the considered coarse-crystalline structure in FZ can have a lower microhardness, compared to that of the HAZ metal and the main part of weld metal (Figure 3, *a*).

A lower metal hardness in FZ can be attributed to carbon transition into the melt from the regions of overheated BM grains contacting the liquid metal [12, 19, 28]. Lowering of carbon content in FZ will be even greater at melting of BM grains and its subsequent sergeration at melt solidification (carbon is known to belong to readily segregating elements, and by the degree of its segregation takes the third place after sulphur and phosphorus [12, 28]).

For the selected welding conditions and the corresponding weld geometry, the considered lowering of microhardness in FZ was found at the weld pool side walls, where more favourable conditions were established for metal overheating, its surface melting and development of chemical microinhomogneity as a result of segregation [27]. The latter is indicated by microhardness measurements in the cell center (*HV*0.2-272–344) and on its boundary (*HV*0.2-306–445) in FZ region at approximately 0.4 mm distance from BM with a net structure. On the other hand, in the central (root) zone of weld section, where the dynamic action of the arc resulted in more effective ousting of the mobile layers of the heated metal, and just the most strongly adhering to each other BM grains were preserved in the overheated state, development of chemical inhomogeneity and corresponding hardness drop did not reach such a level (Figure 3, *b*). With the weld geometry obtained in welding with the above parameters, in the central (root) region, the width of HAZ metal, revealed as a dark strip, is smaller than that from the weld pool sides. In this case, this is indicative of a larger temperature gradient under the weld, and smaller at its side walls, i.e. under the conditions of a more abrupt temperature

Table 1. Microhardness *HV*0.2 of metal in different regions at bead deposition on P91 plate by flux-cored wire submerged-arc process (I_w = 350–370 A, U_a = 37–39 V, v_w = 19 m / h) after bead deposition and sample tempering (760 °C, 20 min)

Condition	*FZ*		*HAZ*	*BM*
	Martensite grains	*Light grains*		
As-deposited	378–415 406	194--258 217	415–600 593	220
As-tempered	288–324 304	202--248 222	306	194--253 220

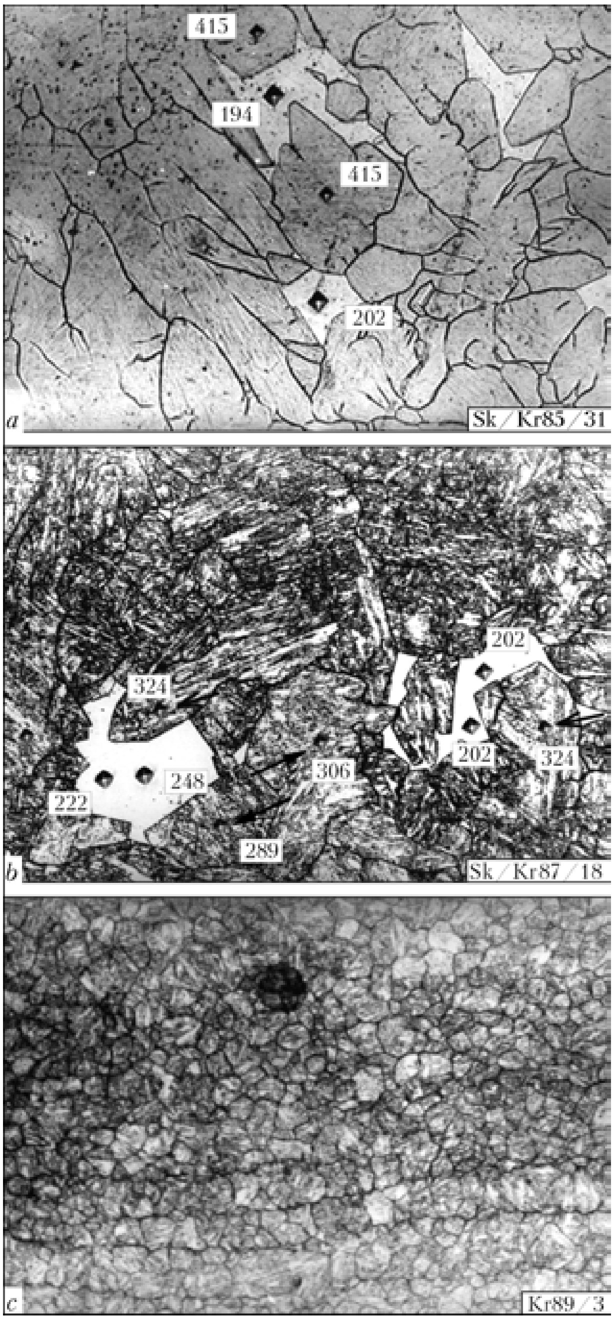

Figure 4. Metal microstructure in FZ (*a*, *b*) and HAZ near the weld (*c*) in deposition of a bead on P91 steel by flux-cored wire submerged-arc process: *a* — as-deposited condition; *b*, *c* — after tempering (T = 760 °C, τ = 40 min) (numbers shows microhardness values *HV*0.2) (×400)

change, the phase changes and chemical inhomogeneity due to overheating, may not have enough time to develop.

Individual light grains, the contours of which are usually marked by rectangular boundaries, are found in FZ sections removed from the root zone and closer to the steel surface (Figure 4, *a*). Such grains have minimum microhardness, compared to the adjacent darker regions of the metal of FZ, weld and HAZ (Table 1). By the degree of alloying (Table 2), the light regions grains almost do not differ from the metal of the adjacent regions, although in some cases increase of niobium content by an order of magnitude was found in them. The latter is, probably, related to penetration of particles of carbides or nitrides of this element into the studied zone at local microprobe analysis.

Tempering does not lead to formation of finely-dispersed phases in the light grains, characteristic of tempering structures of hardening steels (Figure 4, *b*). It is evident that greater alloying element and carbon redistribution could have occurred between the light regions and the adjacent regions of FZ metal than in the surrounding metal, thus making the light grain metal closer in its composition to δ-ferrite of a lower hardness. It is more probable that carbon depletion of the light regions has the main role in the drop of hardness (as well as strength). A center of development of the initial chemical microinhomogeneity could be formation of δ-ferrite, proceeding by the above reaction associated with surface melting and development of diffusion processes. At the cooling stage this inhomogeneity could be partially eliminated as a result of redistribution of the alloying and impurity elements in the metal at homogenizing temperatures [27].

From the viewpoint of technology, the obtained grain size is an important consequence of the considered processes. In FZ with the coarse-crystalline structure and the adjacent zone of HAZ metal, the grains readily etchable in as-tempered condition (Figure 4, *b, c*) had the seventh and approximately ninth-tenth number on average (according to GOST 5639--82).

Table 2. Results of X-ray microprobe analysis of structural components of the metal in FZ at mechanized deposition of a bead on P91 steel using austenitic wire Sv-04Kh19N9T (as-deposited condition)

Object of analysis	*Weight fraction of elements, %*						
	Si	*Cr*	*Mo*	*Nb*	*Ni*	*Mn*	*Ti*
Martensite grain	0.590	10.204	1.256	0.043	0.170	0.051	0.028
Light grain	0.589	10.108	1.312	0.320	0.246	0.081	0

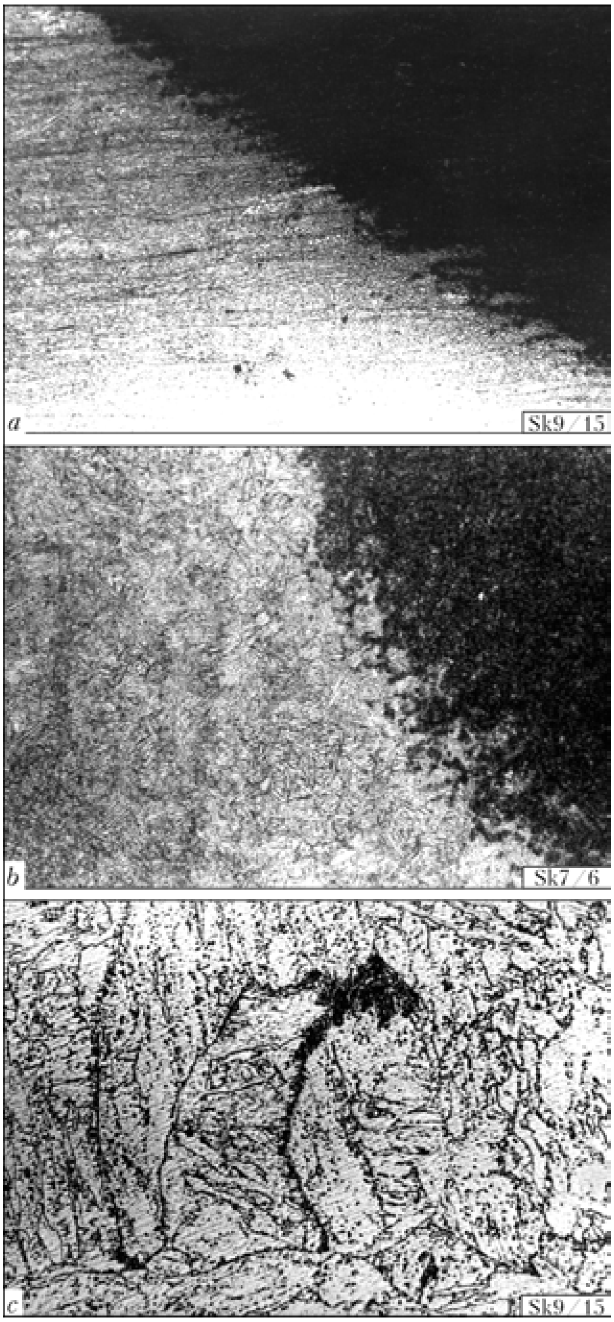

Figure 5. Microstructure in the region of transition from the higher etchability zone to BM: *a*, *c* — steel 1; *b* — steel 2 (*a*, *b* — ×100; *c* — ×1600)

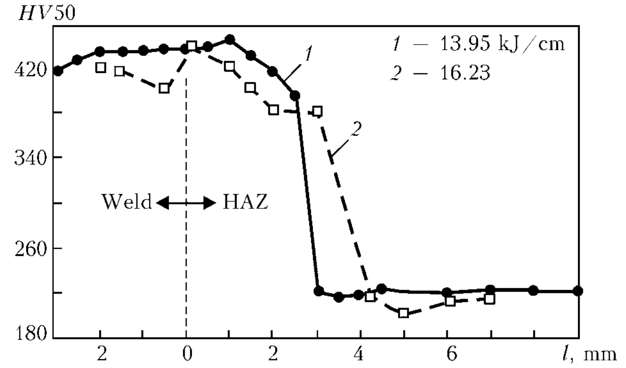

Figure 6. Nature of hardness variation at transition to BM (steel P91) from a bead deposited by flux-cored wire submerged-arc process (preheating to 200 °C) in as-deposited condition at different values of the heat input q/v

Metal structure in the HAZ. A feature of welded joints of martensitic steel with 9 wt.% Cr is the HAZ metal blackening under the conditions of chemical etching. The weld and FZ in this case preserve the light colour. The degree of blackening becomes stronger the farther from the weld, and an abrupt transition from the higher etchability zone to a light BM is found. This boundary has microprotrusions on the microlevel (Figure 5). In the case of steel 1 these protrusions are directed predominantly along the boundaries between the deformation layers of the metal (Figure 5, *a*), in steel 2 (produced, obviously, with application of a different processing sequence) they have an arbitrary orientation (Figure 5, *b*). Individual dark microzones, oriented along the grain boundaries, can be found in the considered near-boundary region of BM (Figure 5, *c*). Metal hardness also changes relatively abruptly, when going through the boundary of the higher etchability zone to BM (Figure 6).

To determine the temperature, to which the metal was heated in the region of the boundary of transition from the higher etchability zone to BM, the thermal cycles of welding were recorded at different distances from the weld, and the thus established distribution of maximum heating temperatures in the HAZ metal and distance from the weld to this boundary were correlated (Figure 7). In the region of the boundary between the weld and BM, the temperature was con-

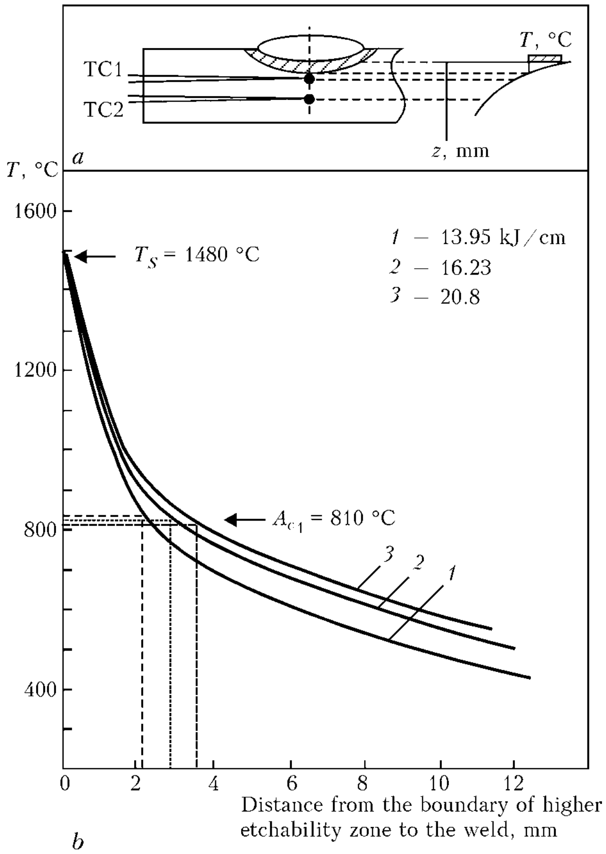

Figure 7. Schematic of measurement (*a*) and variation of maximum heating temperature (*b*) in the HAZ metal at mechanized flux-cored wire submerged-arc deposition of a bead on steel P91 (preheating to 200 °C) with temperature determination in the region of the boundary of higher etchability zone at different heat input values q/v; TC — thermocouple

sidered to be equal to that of solidus (T_S = 1480 °C) of the studied steel. Change of welding mode is accompanied by the change of the rate of metal cooling in the HAZ, which is expressed by different slope of temperature distribution curves in the presented graphs. The values of sought temperatures are approximately on the level of 826, 830 and 840 °C. Average value (832 °C) is close to A_{c_1} temperature of steel with 9 wt.% Cr (805--810 °C). It should be noted that in welding a fast heating and temperature drop in the HAZ metal does not allow sufficient time for proceeding of the reactions of carbide phase dissolution and $\alpha \to \gamma$ transformation in a region heated up to the temperature, corresponding to equilibrium point A_{c_1}. Under the conditions of a fast temperature change, these processes have time to become active only at a higher temperature. The boundary isotherm, separating the region of phase recrystallization, shifts towards higher temperatures, compared to equilibrium A_{c_1}.

Thus, the «effective»* temperature A_{c_1}, corresponding to the start of $\alpha \to \gamma$ transformation, can be conditionally regarded as the temperature boundary in the place of transition from the higher etchability zone to BM. As shown above (see Figure 5), the transformation initiates primarily on the grain boundaries and propagates further into the grain bulk. The surface melting process starts along the same boundaries in FZ, which may be accompanied by formation of individual interlayers of δ-ferrite.

Structure formation in the higher etchability zone after the start of the polymorphous tansformation is associated with a gradual dissolution of dispersed precipitations and diffusion-controlled homogenizing of γ-solid solution, the degree of which depends on heating temperature and duration of its impact on a specific microregion. Near the weld, homogenizing reaches the maximum level, similar to the FZ. Such a metal with a relatively uniform distribution of the alloying and impurity elements in the grain bulk has a higher resistance to the action of chemical reagents, and retains its light colour after etching. At the boundary of the higher etchabiltiy zone with BM, a pronounced chemical microinhomogeneity of the grains is observed, which is due to the low temperature and duration of their heating, insufficient for fast dissolution of the carbide and carbonitride phases, and uniform redistribution of the chemical elements through the grain bulk. Corresponding micro-non-uniformity of chemical resistance of closely located microregions provides a particular «microdispersed» relief of the surface and maximum degree of blackening at etching.

In the zone, where welding is accompanied by phase recrystallization similar to that in the weld, metal hardening with martensite formation proceeds, and the metal has a high hardness (see Figure 6).

No noticeable structural changes occur beyond the higher etchability zone. However, metal staying at temperatures between that of phase recrystallization and temperature of steel tempering under the shop conditions (775–780 °C [3, 29]) leads to additional final tempering of metal in this zone. It is noted [30] that carbide phase coagulation and weakening of the dispersion hardening effect are observed here. The corresponding softening of the solid solution is observed by a certain lowering of hardness (for instance, in Figure 6 this is more pronounced for the case of welding with q / v = 16.23 kJ / cm).

At testing of welded joint samples in as-welded condition by short-time tension the fracture runs through the final tempering zone (of lower strength). Tempering of the as-welded joint does not increase the strength of the considered region, and the samples tested to rupture also fail in this zone. Under creep conditions, fracture may initiate also in the softened zone in such welded joints. According to [30, 31] the cracks developing in this zone are called cracks of the IV type.

In conclusion it may be noted that a zone of a coarse-crystalline structure with morphological characteristics of the cast metal, forms between the weld and BM in the primary structure of welded joints on martensitic heat-resistant steels with 9 wt.% Cr, made with welding consumables providing weld metal alloying similar to that of BM. It was suggested that this zone is the FZ, in which part of BM grains overheated up to temperatures between the effective solidus and liquidus, experiences melting according to the reached melting temperature, and subsequent solidification without mixing with the deposited welding consumables.

BM overheating and lowering of the temperature gradient in the near-weld region promotes widening of the coarse-crystalline FZ, as well as formation of δ-ferrite grains in it. These grains form as a result of intergranular surface melting and diffusion, and segregational displacement of carbon into the adjacent microregions of austenite and molten metal.

No significant growth of the austenite grain was noted in the HAZ metal, this being, probably, related to the presence of heat-stable carbide and nitride phases in BM. Coarser grains form in the coarse-crystalline FZ.

A dark region etched out near the weld in the microsections is a zone of phase recrystallization limited on the outer side by an isotherm, corresponding to non-equilibrium (effective) temperature A_{c_1}. As a result of normalizing, the metal in this zone acquires a martensite structure and high hardness (approximately up to HV 470), which decreases in the incomplete recrystallization zone and drops abruptly on the boundary with untransformed BM to the level of BM

---

*In this case, «effective» means temperature, sufficient for proceeding of the diffusion processes and start of transformation under conditions of fast heating. This temperature should shift towards higher temperatures, compared to equilibrium point A_{c_1}.

hardness (~HV 220--230). The metal adjacent to the phase recrystallization zone, which is heated above the temperature of steel tempering in the plant, experiences final tempering, which may result in this microregion having a lower hardness, compared to the initial hardness of steel, and minimum strength in the welded joint.

1. Bendick, W., Haarmann, K., Rigg, M. et al. (1996) Assessment of creep rupture strength of new steels for advanced power plant piping and tubing. In: *Proc. of 9th Int. Symp. on Creep Resistant Metallic Materials* (Hradec and Moravici, Czech Rep., Sept. 23–26, 1996). Mannesmann.
2. Hoyser, G. (1997) Filler materials for welding in power engineering. *Avtomatich. Svarka*, **9**, 40–44, 47.
3. Zschau, M., Niederhoff, K. (1994) Construction of piping systems of the new steel P91 including hot induction bends. *VGB Kraftwerkstechnik*, 74(**2**), 142–149.
4. Skulsky, V.Yu., Tsaryuk, A.K. (2004) Problems of selection of weldable steel for high-temperature components of TPS power units (Review). *The Paton Welding J.*, **3**, 2–6.
5. Krauss, G., Marder, A.R. (1971) The morphology of martensite in iron alloys. *Metallurg. Transact.*, 2(**9**), 2343–2357.
6. Lundin, C.D., Khan, K.K. (1996) Fundamental studies of the metallurgical causes and mitigation of reheat cracking in 1.25Cr–0.25Mo and 2.25Cr–1Mo steels. *WRC Bull.*, **2**, 117.
7. (1974) *Dictionary-reference book on welding*. Ed. by K.K. Khrenov. Kiev: Naukova Dumka.
8. Savage, W.F., Nippes, E.F., Szekeres, E.A. (1976) A study of weld interface phenomena in a low-alloy steel. *Welding J.*, **9**, 260–268.
9. Makarov, E.L. (1981) *Cold cracks in welding of alloy steels*. Moscow: Mashinostroenie.
10. Skulsky, V.Yu., Yushchenko, K.A., Dzykovich, I.Ya. et al. (1997) Structure and properties of fusion zone of welded joint of steel 02Kh8N22S6 (EP794). *Avtomatich. Svarka*, **11**, 14–17.
11. (1953) *Automatic electric arc welding*. Ed. by E.O. Paton. Moscow-Kiev: Mashgiz.
12. Petrov, G.L., Tumarev, A.S. (1977) *Theory of welding processes*. Moscow: Vysshaya Shkola.
13. (1978) *Welding in machine building*. Refer. Book. Ed. by N.A. Olshansky. Vol. 1. Moscow: Mashinostroenie.
14. Bashta, T.M., Rudnev, S.S., Nekrasov, B.B. et al. (1982) *Hydraulics, hydraulic machines and drives*. Moscow: Mashinostroenie.
15. Kasatkin, B.S., Prokhorov, V.M., Chertov, I.M. (1987) *Stresses and strains in welding*. Kyiv: Vyshcha Shkola.
16. Lashko, N.F., Lashko-Avakyan, S.V. (1954) *Metals science of welding*. Moscow: Mashgiz.
17. Laha, K., Latha, S., Bhanu, K. et al. (2001) Comparison of creep behaviour of 2.25Cr–1Mo / 9Cr--1Mo dissimilar weld joint with its base and weld metals. *Mat. Sci. and Tech.*, 17(**10**), 1265–1272.
18. Fedoseev, B.A., Gejnish, Z.V., Lamzin, A.G. et al. (1984) About the mechanism of formation of austenitic grain boundaries in fusion zone during welding of low-carbon, low- and medium-alloy steels. *Avtomatich. Svarka*, **1**, 20–25.
19. Gotalsky, Yu.N. (1981) *Welding of dissimilar steels*. Kyiv: Tekhnika.
20. Lippold, J.C., Savage, W.F. (1979) Solidification of austenitic stainless steel weldments. Part I-A: Proposed Mechanism. *Welding J.*, **12**, 362–474.
21. Arata, Y., Matsuda, F., Katayama, S. (1976) Solidification crack susceptibility in weld metals of fully austenitic stainless steels. Part 1: Fundamental investigation on solidification behavior of fully austenitic and duplex microstructures and effect of ferrite on microsegregation. *Transact. of JWRI*, 5(**2**), 135–151.
22. Matsuda, F., Nakagawa, H., Ogata, S. et al. (1978) Fractographic investigation on solidification crack in the varestraint test of fully austenitic stainless steel. *Ibid.*, 7(**1**), 59–70.
23. Makara, A.M., Sarzhevsky, V.A., Mosendz, N.A. et al. (1973) On primary and secondary boundaries in weld metal and near-the-weld zone of medium-alloy steel welded joints. *Avtomatich. Svarka*, **4**, 1–4.
24. Gorelik, S.S. (1978) *Recrystallization of metals and alloys*. Moscow: Metallurgiya.
25. Likhachyov, V.A., Myshlyaev, M.M., Senkov, O.N. (1987) On the role of structure transformations in superplasticity. *Fizika Metallov i Metalloved.*, 63(**6**), 1045–1060.
26. Ustinovshchikov, Yu.N., Kovensky, I.M. (1976) Mechanism of formation of special carbides in steels alloyed by Cr, Mo, V. *Ibid.*, 41(**1**), 99–111.
27. Prokhorov, N.N. (1976) *Physical processes in metals during welding*. Vol. 2: Internal stresses, strains and phase transformations. Moscow: Metallurgiya.
28. Petrov, G.L., Zemzin, V.N., Gonserovsky, F.G. (1963) *Welding of heat-resistant stainless steels*. Moscow: Mashgiz.
29. Gnirb, G. (2001) Welding and heat treatment of joints made of dissimilar materials. *Welding in the World*, **45**, 23--40.
30. Bergquist, E.-L. (1999) Consumables and welding modified 9Cr–1Mo steel. *Svetsaren*, 54(**1 / 2**), 22–25.
31. Nishimura, N., Iwamoto, K., Yamauchi, M. et al. (1999) Creep life management of thick-wall high temperature component welds in fossil power boilers. *IIW Doc. XI-702–99*.

WELDABILITY OF HIGH-ALLOYED HEAT-HARDENABLE NICKEL-BASE ALLOYS
(REVIEW)

A.B. MALY[1], **Yu.V. BUTENKO**[1] and **V.F. KHORUNOV**[2]
[1]State Enterprise «Zorya-Mashproekt», Nikolaev, Ukraine
[2]E.O. Paton Electric Welding Institute, NASU, Kiev, Ukraine

Causes of hot cracking of the weld metal in fusion welding of high-alloyed heat-hardenable nickel-base alloys have been analysed. It is shown that recommendations available in literature on elimination of cracks are applicable only for alloys with a low content of the γ'-phase. Ways of solving this problem for alloys with a high content of aluminium and titanium are indicated.

Keywords: arc welding, heat-hardenable nickel alloys, γ'-phase, hot cracks, chemical composition, relaxation resistance, heat treatment, filler wire, strength

Upgrading of gas turbine plants (GTP) provides for increase in temperature of the working medium, rise in their capacity and extension of service life. Reliability of industrial GTP is determined not only by their design characteristics. Properties of the materials utilised are of no less importance. On this base, homogeneous non-heat-hardenable nickel-base alloys of the EI 435 type were replaced by heterogeneous heat-hardenable alloys characterised by higher heat resistance, which is achieved mostly as a result of alloying with aluminium and titanium. Because of their chemical compositions, parts of almost all heat-hardenable alloys are made only by casting, which allows formation of a developed internal cavity in blades and nozzle vanes to provide their efficient cooling. The most common heat-hardenable alloys used in industrial gas turbine construction are alloys of the types of EI 698, ChS 104, EP 99, EP 202, etc. Their structure consists of γ-solution, γ'-phase of the $Ni_3(Al, Ti)$ type, the content of which may amount to about 50–60 vol.%, carbides (MeC, Me_6C, etc.), carbonitrides (Ti(C, N) and borides (Me_3B_2, etc.) [1–4].

Construction of gas turbines is impossible without welding, which is the most cost-effective method for joining of components that does not lead to increase in their mass. In this case, it is necessary to perform the following operations: welding of casting defects, electron beam welding (EBW) of shafts to rotors, welding of blades into packs, strengthening of airfoil tips using wear-resistant alloys, etc. Welding of homogeneous alloys involves no special problems. However, most heat-hardenable alloys belong to structural materials that are unweldable or have limited weldability, as they are characterised by sensitivity to crack formation in the weld and weld zone (WZ) during welding, heat treatment and high-temperature operation (Figure 1). Microcracks formed at any of these stages go on growing under operational loading. Also, it is a challenge to provide the weld metal close in composition to the base one, as it is sensitive to hot cracking because of high heat resistance [2–7]. All the above-said is true for fusion welding, which is characterised by a concentrated heating leading to high temperature gradients within the HAZ.

Cracking can be avoided to a substantial degree by using vacuum brazing with high-temperature brazing filler alloys, or welding without melting of the base metal, e.g. diffusion bonding. These joining methods have three main drawbacks, such as low process productivity, impossibility to produce welded joints of a variable geometry, and necessity to employ complex equipment. At present, fusion welding is the most common and cost effective joining method. TIG welding in argon atmosphere is widely applied to join high alloys. In this connection, of special interest are the methods that increase crack resistance and provide welded joints with strength equal to that of the base metal.

It is a known fact that hot cracking in welding (it is this type of fracture that is characteristic of nickel-base alloys) is caused by tensile stresses formed as a result of non-uniform heating and cooling of the metal welded, as well as by rigid fixation of workpieces. Hot crack resistance for all metals and alloys is determined by the brittle temperature range, ductility within this range and rate of growth of plastic strains. Hot cracking is affected by the degree of con-

Figure 1. Characteristic appearance of a hot crack that was formed in WZ and propagated into the weld metal (×100)

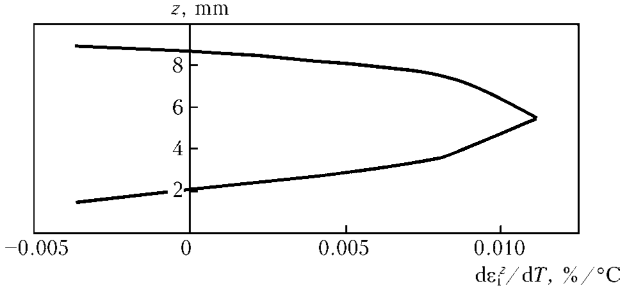

Figure 2. Distribution of strain rate $d\varepsilon_i^z / dT$ through thickness of a plate in one-pass EBW at heat input q / v = 6270 J / cm [9]; ε_i — internal strain along axis z

tamination of alloy with low-melting point impurities, penetration shape, grain size of the base metal, etc. But the basic effect is exerted by chemical composition of the base metal, deterioration of weldability being in direct relationship with its γ-phase content [6–8]. As reported in [7, 9, 10], thermal-physical peculiarities of nickel-base alloys (low thermal conductivity and high heat resistance) influence an increase in growth of tensile stresses, which in turn depends upon the heat input into the base metal and thickness of the plates welded (Figure 2).

In addition to the above-said, study [3] notes also the relaxation resistance. The relaxation process is determined by transformation of a crystalline body from the non-equilibrium to equilibrium state, which is achieved through decreasing the level of stresses with time in a loaded rigid body having constant linear dimensions. Relaxation of stresses is related to transformation of elastic strain into the non-elastic one. Only the stresses that are in excess of the elasticity limit are relaxed. The relaxation resistance of heat-resistant nickel alloys grows with growth of the content of elements that strengthen solid solution, such as cobalt, molybdenum, tungsten and niobium, but mostly with the combined strengthening of solid solution and precipitation of the finely dispersed γ-phase of the $Ni_3(Al, Ti)$ type, or Ni_3Nb phase. Increase in the relaxation resistance and level of stresses is accompanied by decrease in hot crack resistance of alloy in the weld and WZ. The γ-phase content (vol.%) of different nickel alloys [3] is given below in an increasing order of welding stresses, relaxation resistance and hot crack sensitivity:

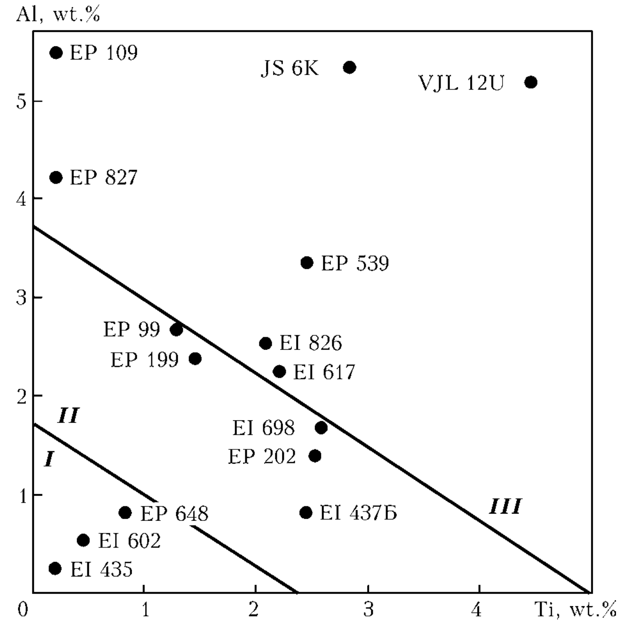

Figure 3. Dependence of sensitivity of nickel alloys to cracking in heat treatment of welded joints upon the aluminium and titanium content (I–III — see explanations in the text)

EI 437B	up to 10
EP 708	13–15
EP 693	13–15
EP 199	16–18
EI 698	14–17
EP 99	18–22

Alloys EI 435, EI 602 and EI 868 contain no γ-phase.

Study [11] considers the issue of formation of cracks in welded joints during heat treatment. This type of fracture is associated with the total effect of residual welding and volumetric stresses formed with precipitation of the γ-phase from solid solution, as well as thermal stresses. The content of aluminium and titanium is a key factor that determines the sensitivity to formation of such cracks. In analogy with study [2], the diagram was plotted to evaluate sensitivity of domestic alloys to formation of cracks in welded joints during welding and heat treatment (Figure 3) (not all the alloys indicated in the original are shown in the Figure).

Nickel alloys can be subdivided into three groups on the basis of this indicator. Group *I* includes homogeneous and slightly ageing alloys with a γ-phase content of not more than 3–5 vol.%, which are resistant to cracking in welding and heat treatment. Group *II* includes precipitation-hardening alloys with a γ-phase content of not more than 18–20 vol.%, which are characterised by a moderate crack sensitivity. It can be decreased through optimisation of the welding technology and using the following heat treatment procedure: quenching, welding, quenching, ageing. For alloys with an increased content of aluminium and titanium, which are close to the upper bound of this group (EP 99, EP 199, EI 698, etc.), it is necessary to use overageing (900–950 °C, 5–10 h) prior to welding. Group *III* includes heat-resistant nickel alloys with a γ-phase content of more than 20–25 vol.%. Alloys which are near the lower bound of this group (EI 617, EI 826, etc.) should be subjected to multistage overageing, while those with a γ-phase content of over 45 vol.% should be subjected to concurrent heating to more than 950–1000 °C.

The positive effect of overageing on weldability and hot crack resistance of precipitation-hardening alloys is also reported in studies [2–4, 12]. Overageing can be performed by stepwise ageing or austenising with slow cooling [12]. This causes precipitation of coarse particles of the γ-phase in an alloy, thus leading to decrease in heat resistance, relaxation resistance and increase in ductility of the base metal.

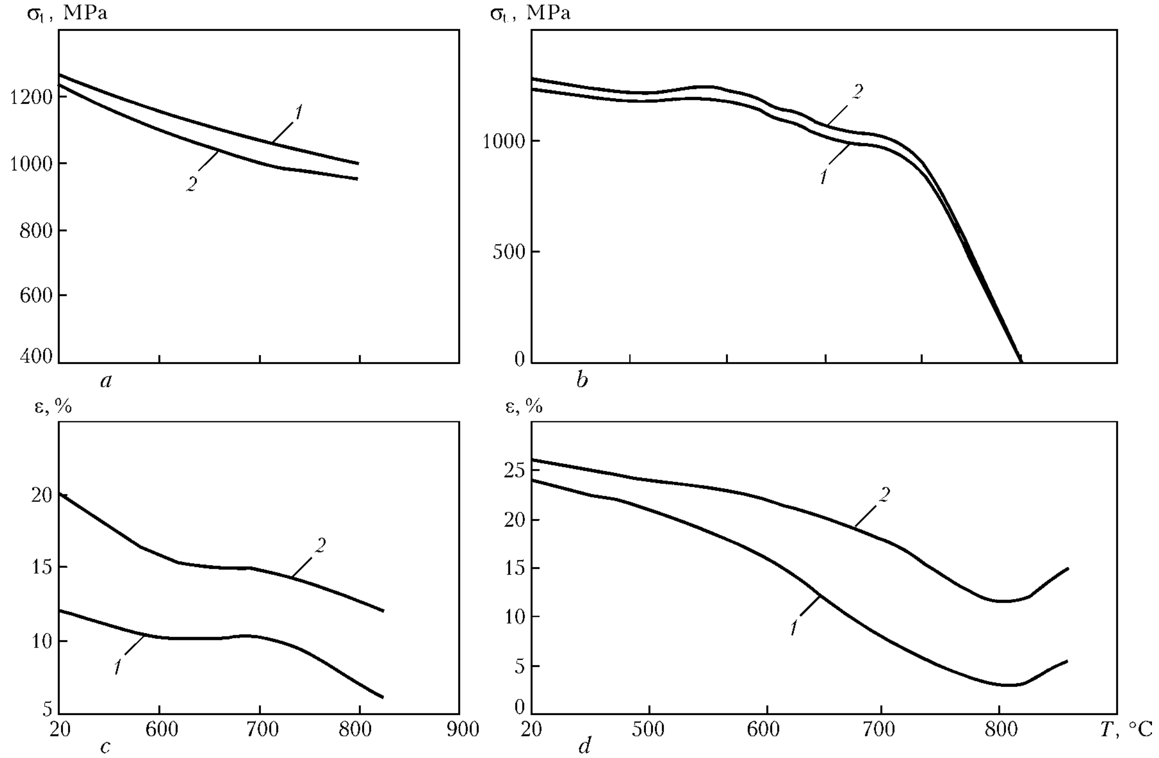

Figure 4. Temperature dependence of mechanical properties of alloys EP 957 (*a, c*) and EP 800 (*b, d*): *1, 2* — numbers of modes (see the Table) [13]; σ_t — tensile strength; ε — elongation

Demand for extending service life of GTP requires the search for new parameters of heat treatment for heat-resistant nickel alloys to raise their tensile strength, impact toughness and stability of structure of the alloys with no loss in their heat-resistant characteristics. Different modes of heat treatment with slow cooling after austenising and multistage ageing were tried out by authors of study [13] for three commercial nickel alloys (EP 957, EP 800 and EK 78). These modes are given in the Table. It is concluded in this study than an optimal proportion of strength and ductile characteristics over a wide temperature range can be provided during the process of two-stage cooling after austenising: at the first stage — at a rate of 1.5–5.0 °C / min, and at the second stage — in air (Figure 4). This leads to formation of grains with a serrated boundary, which is associated with precipitation of the strengthening γ'-phase in the form of coarse grains decorated with fine carbides MeC, Me_6C and $Me_{23}C_6$. Austenising with slow cooling is followed by final ageing of the alloys.

As noted above, it is very difficult to provide welded joints with heat resistance at a level of that of the base metal, which is caused by high hot crack resistance of the weld metal. Using filler wires of the base metal enhances cracking of welded joints (Figure 5). Crack resistance of welded joints increases with aluminium and titanium excluded from the composition of filler wires, which is associated with increase in the relaxation ability of the welded joints and absence (or decrease) of the γ'-phase precipitated in the weld metal during reheating [14]. In this case strength of the welded joints does not exceed 0.85–0.90 of that of the base metal (Figure 6) [12].

According to studies [12, 14], the best combination of strength and corrosion resistance of welded joints is provided by wire EP 533, which, at the same time, is much inferior to wires EI 683, EP 648, EP 367, EP 595 and EK 22 (with decreased content of aluminium and titanium or without them) in hot crack resistance of the weld metal.

It should be noted that the problems of ensuring crack resistance and full strength of alloys with a γ'-phase content of their structure that is far from being too high (up to 29 vol.%) are covered in literature comprehensively and in detail. Alloys of group *III* (see Figure 3) characterised by high crack sensitivity are covered in less detail. Filler wire EP 533 containing 12 vol.% of the γ'-phase fails to provide full strength of welded joints in alloys of this group.

Alloys with a high total content of these elements (JS6U-VI, JS6K, JS26, ChS 70, ChS 88, ChS 104VI,

Modes used for heat treatment of alloys EP 957 and EP 900

Alloy	*Mode 1*	*Mode 2*
EP 957	1180 °Ñ, 3 h + 1050 °Ñ, 2 h + 950 °Ñ, 2 h + 850 °Ñ, 5 h (intermediate air cooling)	1180 °Ñ, 3 h (furnace cooling for 30–45 min to 1030 °C, then air cooling) + 850 °C, 15 h (air cooling)
EP 800	1150--1180 °Ñ, 5 h + 1050 °Ñ, 2 h + 1000 °Ñ, 2 h + + 900 °Ñ, 2 h + 850°Ñ, 2 h (intermediate air cooling)	1160 °C, 3 h (furnace cooling for 60–90 min to 950 °C, then air cooling) + 850 °C, 15 h (air cooling)

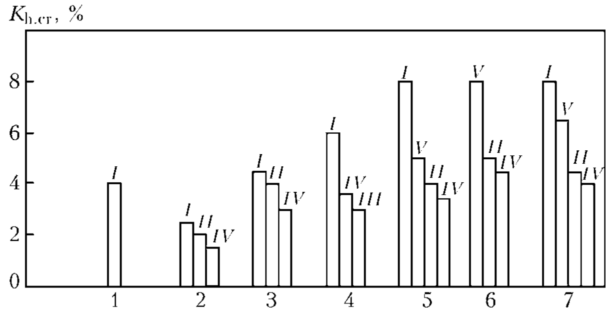

Figure 5. Resistance $K_{h.cr}$ of heat-resistant alloys KhN78T (1), KhN75MBTYu (2), KhN60VT (3), KhN50VMTYuB (4), KhN30VMT (5), KhN45MBTYuBR (6) and KhN65VMBYu (7) to hot cracking during welding using wires of base metal (*I*), Sv-06Kh15N60M15 (*II*), Sv-Kh11N60M23 (*III*), Sv-KhN64KBMYuVF (*IV*) and Sv-08Kh20N57M8V8T3R (*V*) [14]

IN-738LC, 713C, etc.), characterised by a substantial γ′-phase content (superalloys) of their structure, are considered unweldable, unless the special measures are taken. Thus, study [15] recommends to perform welding with heating to 600 °C (argon-arc welding) and to 900 °C (EBW) to produce crack-free welds. The authors of other study [16] state that the crack-free welds in alloy IN-738LC can be produced by EBW with heating to 1120 °C both with and without filler metal. It is shown in study [17] that the crack sensitivity of alloy 713C decreases with increase in heat input and decrease in the welding speed. Results given in the above-mentioned studies are of high importance. However, it should be borne in mind that they were obtained under ideal conditions, which are far from being identical to those taking place in performance of repair technology, where a case by case approach is required to repair each type of defects.

It can be concluded on the basis of the above-said that, despite a large amount of studies dedicated to investigation of weldability of high-alloyed heat-resistant nickel alloys, this problem cannot be considered solved. All the recommendations available in literature of the former USSR and CIS countries relate to metal with a rather low content of aluminium and titanium and, hence, the γ′-phase. Studies of the American investigators are dedicated to materials with a higher content of the γ′-phase [15–17], but they do not give recommendations suitable for practical applications either.

It is still to be determined whether the reserves for increasing ductility of alloys with a high γ′-phase content have been exhausted, and investigated what effect the heat input and filler metal with a fundamentally new alloying system may have on crack sensitivity of the welds.

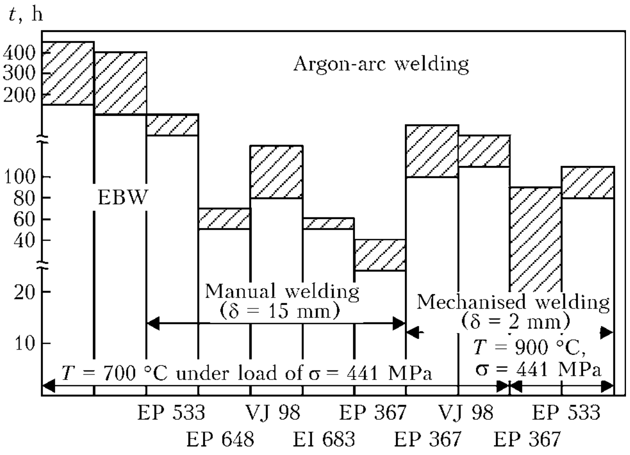

Figure 6. Time to fracture for joints in alloy EP 202 made by argon-arc welding using different types of filler wires and by EBW (dashed regions — spread of data [12])

1. Kolachyov, B.A., Livanov, V.A., Elagin, V.I. (1981) *Metals science and heat treatment of non-ferrous metals and alloys.* Moscow: Metallurgiya.
2. Sims, Ch., Hagel, V. (1976) *High-strength alloys.* Moscow: Metallurgiya.
3. Sorokin, L.I. (1999) Stresses and cracks in welding and heat treatment of high-strength nickel alloys. *Svarochn. Proizvodstvo*, **12**, 11–17.
4. Volchenko, V.N. (1991) Welding and materials to be welded. Moscow: Metallurgiya.
5. Sorokin, L.I. (1997) Optimization of repair technology for gas-turbine parts of heat-resistant alloys. *Svarochn. Proizvodstvo*, **1**, 19–23.
6. Zemzin, V.N. (1972) *High-temperature strength of welded joints.* Leningrad: Mashinostroenie.
7. Paton, B.E. (1974) *Technology for fusion welding of metals and alloys.* Moscow: Mashinostroenie.
8. Medovar, B.I. (1966) *Welding of high-strength austenitic steels and alloys.* Moscow: Mashinostroenie.
9. Ejdelshtejn, V.E., Yakushin, B.F., Makhnenko, V.I. et al. (1980) Analysis of thermal-deformation processes in heat-affected zone during welding of high-strength nickel alloys. *Avtomatich. Svarka*, **1**, 11–15.
10. Savchenko, V.S., Yushchenko, K.A., Makhnenko, V.I. et al. (1993) Effect of physical characteristics of cast nickel alloys on development of thermal-deformation processes in fusion welding. *Ibid.*, **11**, 6–9.
11. Sorokin, L.I., Tupikin, V.I. (1985) Classification of high-strength nickel alloys by their crack resistance in heat treatment of welded joints. *Ibid.*, **5**, 23–25.
12. Kvasnitsky, V.F. (1985) Welding and brazing of high-strength alloys in ship-building. *Ibid.*, **10**, 26–30.
13. Filatova, M.A. (1995) Effect of heat treatment on structure and properties of high-strength nickel alloys. *Metallovedenie i Term. Obrab. Metallov*, **6**, 12–15.
14. Sorokin, L.I., Bagdasarov, Yu.S., Tupikin, V.I. (1993) Comparative evaluation of filler wires for argon-arc welding of high-strength alloys. *Svarochn. Proizvodstvo*, **10**, 31–33.
15. Haafkens, M.H., Matthey, J.H.G. (1982) A new approach to the weldability of nickel-base as-cast and powder metallurgy superalloys. *Welding J.*, November, 25–30.
16. Jahnke, B. (1982) High-temperature electron beam welding of the nickel-base superalloy IN-738LC. *Ibid.*, 343–347.
17. Koren, A., Roman, M., Weisshaus, I. et al. (1982) Improving the weldability of Ni-base superalloys 713C. *Ibid.*, 348–351.

KINETICS OF ACCELERATION OF ELEMENTS OF MULTILAYER METAL STACK PLATES IN EXPLOSION WELDING

S.V. KUZMIN
Volgograd State Technical University, Volgograd, Russia

Main principles of the kinetics of acceleration of a multilayer stack plates in explosion welding are considered. The effect of initial welding conditions on the character of variations in the collision velocity at the second interlayer boundary has been evaluated by an example of a three-layer stack.

Keywords: explosion welding, high-speed collision, multilayer stack, laminated composite, welding conditions, acceleration kinetics

A reliable estimation of the values of parameters characterizing kinetics of the collision of layers of multilayer composite in explosion welding (in the first place the order of layer-by-layer collision velocities) is one of the most important problems in technological design. Complexity of this solution is specified by the absence of any more or less physically justified calculation methods and also by scarce experimental data. The available mathematical models [1–7] describe the process of collision of elements of the multilayer stack plates in explosion welding in a very crude approximation. Because of the assumptions these models have they exclude from consideration the important one, which is the initial stage of acceleration [6–8] at the second and subsequent boundaries of the stack being welded, which eventually leads to considerable errors in estimating multilayer collision velocities and, thus, to a complicity in implementing optimal properties of multilayer composites. It is possible to refine the available models on the basis of a detailed experimental study of the regularities of acceleration of the elements of the multilayer stack plates in explosion welding.

Objective and methods of studies. The aim of the work is to study the effect of the explosion welding conditions (thickness and mass of the colliding elements, velocity of the explosive detonation and acceleration phase of the flyer plate) on the character and kinetics of the acceleration of the elements of three-layer stacks on the second interlayer boundary of the welded composite using the method proposed in [9].

To achieve the set task a number of one-fact tests were carried out (Table) varying thickness of the welded allumium plates δ_i, detonation velocity D of the explosive and a flyer element acceleration phase characterized by a correlation h_1 / H (h_1 is the clearance on the first boundary of the stack; H is the height of the explosive charge) and quantitatively determining a relative value of a residual pressure p / p_0 (where p is the residual pressure of detonation products on the surface of the flyer plate at a chosen time τ; p_0 is the pressure acting on the surface of the flyer plate in the front of the detonation wave [10]):

$$p = \frac{64}{27} p_0 \left(\frac{H}{D\tau}\right)^3, \qquad (1)$$

$$p_0 = \frac{1}{4} \rho_0 D^2, \qquad (2)$$

where ρ_0 is the initial density of the employed explosive.

A degree of influence of this or other parameter was estimated by comparing durations of initial acceleration stages $\tau_{\rm i}$ of the stack of two welded plates with different values of one of the parameters varying in the preset parameter range while the rest of the parameters in every test series remained unchanged (Table). In all cases the calculated [10] and experimental acceleration curves for every boundary of collision as well as graphic dependences characterizing the dynamics in the motion velocity variation of the back side of the stack of two plates $v_{c_2} = f(\tau)$ at the initial acceleration rate were constructed.

Duration of the initial acceleration stage $\tau_{\rm i}$ was assumed as time for acceleration of a back side of the two-plate stack welded in flying up to flying velocity $v_{\rm f}$ calculated from the law of conservation of momentum for an isolated system [11]. This parameter was determined as follows.

1. Experimental curves of the stack acceleration were approximated by the empirical dependences of

Parameters of welding in the series of one-factor tests

No. of test series	*Thickness of layers δ, mm*	*Velocity of detonation D, m/s*	*h_1/H*
1	1.9 + 1.9 + 3.8	3420	0.017
	3.8 + 3.8 + 7.6	3420	0.017
2	3.8 + 3.8 + 7.6	3420	0.017
	3.8 + 3.8 + 7.6	3420	1.000
3	3.8 + 3.8 + 7.6	3600	0.014
	3.8 + 3.8 + 7.6	3600	1.000
4	3.8 + 3.8 + 7.6	2500	0.014
	3.8 + 3.8 + 7.6	2500	1.000
5	3.8 + 3.8 + 7.6	3600	1.000
	3.8 + 3.8 + 7.6	2500	1.000
6	3.8 + 3.8 + 7.6	3600	0.014
	3.8 + 3.8 + 7.6	2500	0.014

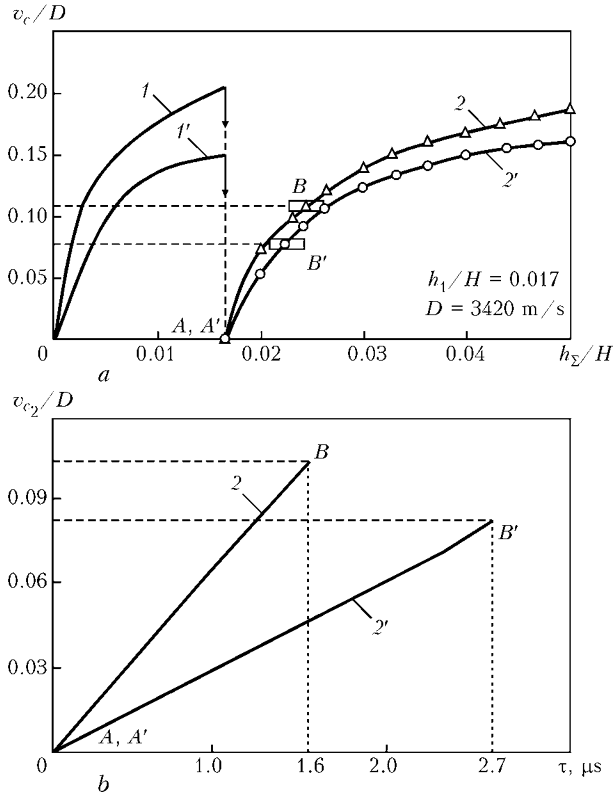

Figure 1. Curves of the acceleration of elements in three-layer aluminium stack plates (*a*) and a character of change v_{c_2} at the initial stage of acceleration (*b*) with different thickness of the plates being welded (test series 1): *1, 1′* — calculated curves [7] (acceleration of the flyer plate); *2, 2′* — experimental curves (acceleration of the two-layer plate stack welded in flight); *1, 2* — $\delta_1 + \delta_2$ = (1.9 + 1.9) mm; *1′, 2′* — $\delta_1 + \delta_2$ = (3.8 + 3.8) mm; points *A* and *A′* — start of two-layer stack motion from the rest (for two conditions of the experiment corresponding to curves *1, 1′* and *2, 2′*); *B* and *B′* — moment when the two-layer stack achieves the velocity calculated from the law of conservation of momentum; □ — velocity of the stack calculated from the law of conservation of momentum (4)

the exponential type relating $v_{c_2}(y)$ with the distance passed by a side surface of the stack y:

$$v_{c_2}(y) = A(1 - e^{-by}), \qquad (3)$$

where A and b are the experimental coefficients.

2. Flight velocity of the stack of two welded plates after their collision was calculated from the law of conservation of momentum for isolated system:

$$v_{\mathrm{f}} = \frac{m_1}{m_1 + m_2} v_{c_1}, \qquad (4)$$

where m_1 and m_2 is the unit mass of the flyer (first) and intermediate (second) plate in the three-layer stack to be welded, respectively; v_{c_1} is the collision velocity at the first intermediate boundary.

3. A distance $y = h_{\mathrm{s}}$ (h_{s} is the distance from the lower surface of the stack of two plates where it acquires velocity v_{f} calculated from the law of conservation of momentum) was determined by previously obtained empirical dependences or graphically.

4. The desired τ_{i} was then calculated:

$$\tau_{\mathrm{i}} = \int_0^{y = h_{\mathrm{s}}} \frac{\mathrm{d}y}{v_{c_2}(y)}. \qquad (5)$$

Let us consider in a more detail the effect of the indicated parameters on the character of the acceleration of multilayer stack plates and duration of its initial stage τ_{i}.

Effect of the mass of elements to be welded. The performed studies showed that the mass (thickness) of the plates to be welded considerably influences the duration of the initial acceleration stage, which grows together with the mass of the plates.

So, when welding aluminium stack plates with correlation of the thickness of layers (1.9 + 1.9 + + 3.8) mm (D = 3420 m/s, h_1/H = 0.017) (test series 1) a duration of the initial acceleration stage τ_{i} of stack plates was about 1.6 μs.

Doubled increase of the thickness of the elements to be welded (3.8 + 3.8 + 7.6) mm, other conditions being equal, led to a proportional growth of τ_{i} to about 2.7 μs (Figure 1). In this case a more massive stack accelerates less intensively, which is evidently related to a different sluggishness of the elements being welded.

Effect of the acceleration phase. Changes in the phase of acceleration of the flyer element, as it was previously indicated, qualitatively determines a relative value of the residual pressure of detonation products on the surface of the stack being welded p/p_0, also it essentially influences both duration of the initial stage of the stack plate acceleration and the character of the change v_{c_2} (Figure 2). In this case growth of relation h_1/H from 0.017 to 1.000 (test series 2) causes growth of the duration of the initial acceleration stage approximately from 2.7 to 6.5 μs.

Similar results were obtained under different welding conditions: in test series 3 (D = 3600 m/s) and 4 (D = 2500 m/s) where the duration of the initial stage was changed, respectively, from 1.8 to 4.6 and from 4.0 to 8.7 μs at h_1/H equal 0.014 and 1.000.

Such change in the sluggishness of the acceleration process may be attributed to a corresponding effect of the residual external pressure p of a system of correlating elements shown in Figure 3 where point A corresponds to a residual pressure acting on the surface of the upper (flyer) plate at the moment of the plate collision at h_1/H = 0.017 ($p \approx$ 2.8 GPa) while point A' at h_1/H = 1.000 ($p \approx$ 8.0 GPa).

Effect of detonation velocity. Detonation velocity D essentially affects duration of the initial stages of acceleration — in this case the higher are D values, the more intense acceleration of the stack is observed, which results a decrease of τ_{i}. So, increase of values D from 2500 to 3600 m/s with full acceleration of the flyer plate (test series 5) causes decrease of τ_{i} from 8.7 to 4.6 μs. The same change in the detonation velocity when the flyer plate is considerably affected by residual pressures (h_1/H = 0.014, test series 6) regularly leads to a corresponding decrease of τ_{i} from about 4.0 to 1.8 μs.

Therefore, mass (thickness) of the elements to be welded and residual pressure of detonation products on the surface of the flyer plate are the main factors affecting duration and character of acceleration at the initial stage. In general, the experimental results may be reflected in the form of the dependence of the

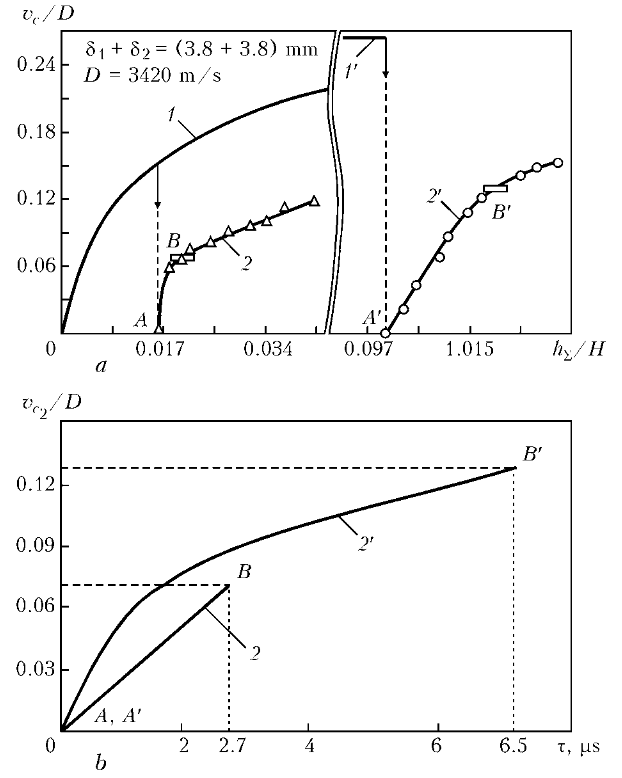

Figure 2. Curves of acceleration of the elements in three-layer stack of aluminium plates (*a*) and a character of changing of v_{c_2} at initial stage (*b*) at different acceleration stages of flyer plate (test series 2): *1, 2* — h_1 / H = 0.017; *1′, 2′* — h_1 / H = 1.000 (other designations see in Figure 1)

duration of the initial stage of stack plate acceleration τ_i on pressure of detonation products on the surface of the system being welded p / p_0 (Figure 4), which is a certain domain whose upper boundary corresponds to the greater mass of the elements welding by explosion and lower velocities of the contact points while the lower boundary corresponds to a smaller mass (thickness) of the stack elements with high velocities of the contact point. The left part of the domain belongs to the case of full acceleration of the flyer plate by the detonation products in explosion welding while the right one — to the incomplete acceleration ($p / p_0 >> 0$).

CONCLUSIONS

1. It is experimentally established that acceleration of the colliding stack plates at the second and subsequent boundaries in explosion welding of multilayer composites proceeds not instantly but during a certain time period τ_i whose duration may be 10 μs depending on the process parameters. Mass (thickness) of the plates, velocity of the contact point and acceleration phase of the flyer plate exert essential effect on τ_i.

2. It is shown that increase of a thickness (or mass) of the colliding elements as well as velocity of detonation and residual pressure of the detonation products lead to an essential increase of duration of acceleration of the colliding stack plates at the initial stage. This circumstance should be taken into account when presetting technological parameters of explosion welding of multilayer metallic composites.

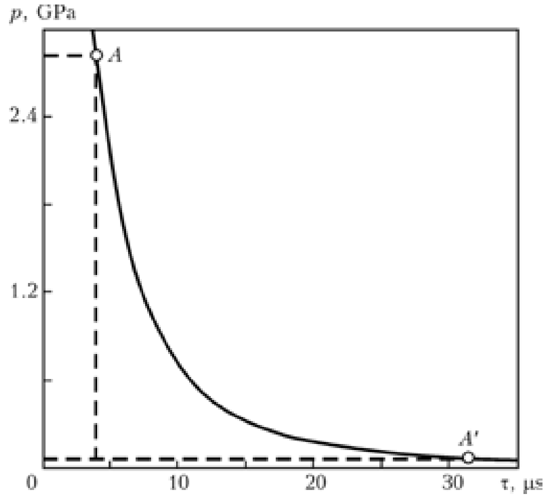

Figure 3. Change of pressure p on the surface of flyer plate by formula (1) (test series 2): A — collision of first and second plate at h_1 / H = 0.017; A' — same at h_1 / H = 1.000

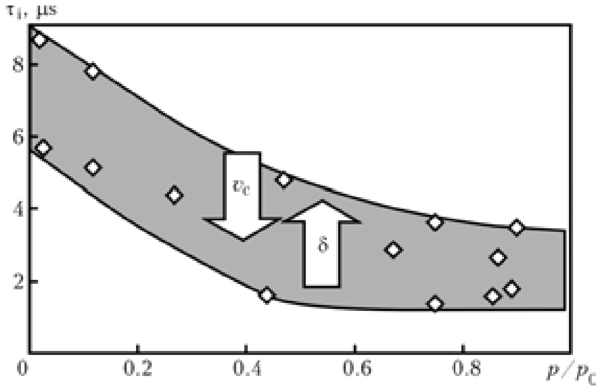

Figure 4. Dependence of duration of initial stage of acceleration of a stack τ_i of colliding plates at second interlayer boundary on relative pressure p / p_0 of detonation products; v_c — contact speed

1. Belyaev, V.I., Kovalevsky, V.N., Smirnov, G.V. et al. (1976) *High-speed deformation of metals*. Minsk: Nauka i Tekhnika.
2. Sonnov, A.P., Trykov, Yu.P. (1973) On calculation of explosion welding parameters of multilayer joints. *Fizika i Khimiya Obrab. Materialov*, **4**, 128–133.
3. (1984) *Shock waves and phenomena of high-speed deformation of metals*. Ed. by M.A. Mejers, L.E. Murr. Moscow: Metallurgiya.
4. Zhang Dengxia (1983) Research on movement of layer plate in explosive welding. *Transact. of China Welding Inst.*, 4(**3**), 109–118.
5. Shao, P.N., Zhou, Z.H., Li, G.H. (1985) Calculation on explosive bonding parameters of multilayer plates under glancing detonation. In: *Proc. of 6th Int. Symp. on Use Energy of Explosive* (Pradubise, CSSR, Sept. 22–24, 1985). Prague.
6. Shmorgun, V.G., Sonnov, A.P., Trykov, Yu.P. et al. (1997) Evaluation of collision parameters in explosion welding of multilayer compositions. In: *Transact. on Metals Science and Strength of Materials*. Volgograd: VolgGTU.
7. Lysak, V.I., Saparin, V.A., Kuzmin, S.V. et al. (1994) Computer model of calculation and optimization of technological parameters of explosion welding. In: *Abstr. of 1st Int. Sci.-Pract. Conf. on New Industrial Technique and Technology. Software and Computer Technologies* (Volgograd, Dec. 5–9, 1994). Volgograd.
8. Kuzmin, S.V., Lysak, V.I., Starikov, D.V. (1994) Kinetics of collision of metallic plates in multilayer stack during explosion welding. *Prikladn. Mekhanika i Tekhn. Fizika*, **5**, 173–175.
9. Kuzmin, S.V., Lysak, V.I., Salomatin, I.A. (2001) Method for estimation of acceleration parameters of plates in a multilayer stack during explosion welding. *The Paton Welding J.*, **2**, 20–24.
10. (1975) *Physics of explosion*. Ed. by K.P. Stanyukovich. Moscow: Nauka.
11. Aleksandrov, E.V., Sokolinsky, V.B. (1969) *Applied theory and calculations of impact systems*. Moscow: Nauka.

CORROSION ELECTROCHEMICAL PROPERTIES OF Cr–Ni DEPOSITED METAL IN ALKALINE MEDIA (REVIEW)

P.P. LAZEBNOV
Zaporozhie National Technical University, Zaporozhie, Ukraine

Data are given on corrosion resistance of chromium-nickel deposited metal in alkali environments. Short information is given on the influence of alloying elements on the electrochemical corrosion processes running in the metal of chromium-neckel welds.

Keywords: arc welding, coating, electrodes, chromium-nickel steels, welds, alkaline media, corrosion, corrosion potential, alloying, deposited metal

Soda, pulp and paper and other branches of industry employ high-temperature alkaline technological media. Cr–Ni steels of 18-10 grade [1, 2] are the main materials for welded structures (apparatuses, steam-curing chambers, cooking pipes and others). Examination of the Kamur and Pandia units for continuous cooking of sulphate cellulose allows concluding about a selective general-corrosion-type destruction of welds in structures [3, 4], which is specified by heterogeneity of chemical composition and structure of the deposited metal [5, 6].

Articles devoted to studies of the effect of chemical composition on corrosion electrochemical properties of Cr–Ni deposited metal in the alkaline media are reviewed.

High-alloyed metals (approaching in their chemical composition steel 12Kh18N10T and different from it by a level of alloying) deposited by commercial and test electrodes (Table) were studied. It is seen from the Table that corrosion resistance of the welds of welding consumables is specified by their chemical composition and structure. Austenite-ferrite metals deposited by electrodes OZL-8, TsL-11, TsT-15, ZIO-3 and others destroy in alkaline solutions more intensively than austenite ones. The best resistance is obtained in the deposited specimens with high nickel content (11Kh15N25M6G2, 09Kh15N25M6G2F) and in low-alloyed specimens (OZL-20 and 832MWR). A decrease of the content of nickel (by 15 %), molybdenum (6–7 %) and vanadium (down to 1 %) is

Corrosion resistance of Cr–Ni metals in alkaline media

Electrode grade	*Type of deposited metal*	*Content of δ-ferrite in metal, wt.%*	*Average indices of corrosion rate, g/(m$_2$·h), during tests*	
			Large-scale	*Laboratory*
OZL-8	E-07Kh20N9	7.0	0.0217	0.0613
TsL-11	E-08Kh20N9G2B	6.4	0.0125	0.0572
TsT-15	E-08Kh19N10G2B	3.8	0.0134	0.0550
ZIO-3	E-07Kh19N10G2B	6.0	0.0152	0.0500
NIAT-1	E-08Kh17N8M2	5.8	0.0203	0.0884
EA-400 / 10u	E-07Kh19N11M3G2F	5.0	0.0128	0.0738
EA-395 / 9	E-11Kh15N25M6G2	–	0.0057	0.0127
EA-981 / 15	E-09Kh15N25M6G2F	–	0.0061	0.0134
OZL-6	E-10Kh25N13G2	4.1	0.0094	0.0605
TsL-9	E-10Kh25N13G2B	8.0	0.0093	0.0597
OZL-20	E-02Kh20N14G2M2	1.8	0.0106	0.0541
OZL-5	E-12Kh24N14S2	5.6	0.0119	0.0620
832MWR (Sweden)	E-04Kh21N10G2	2.1	0.0099	0.0533
Test	E-08Kh20N10B (0.025% Y)	2.0	0.0255	0.0076

Notes. 1. Laboratory tests are carried out in the autoclave (P = 0.2 MPa, T = 130 °C, 30 % NaOH, 144 h duration). 2. Large-scale tests were carried out in the welding zone of the chip steaming of the Kamur boiler (P = 1.2 MPa, T = 160–170 °C, white liquor, 2150 h duration).

achieved in test electrodes along with increased corrosion properties of welds as compared to electrodes EA-395 / 9 and EA-981 / 15.

The base of steels and alloys determines a stationary potential of corrosion in solutions while alloying elements with their electrochemical parameters shift it towards positive or negative values. Studying the processes of metal corrosion in aggressive media it is efficient to attract the Purbe state diagrams [2, 7, 8] disclosing kinetics of corrosion resistance of alloying elements (Cr, Ni, Mn, Nb, Ti, Mo, W, Cu, V) of Cr–Ni steels in alkaline solutions (pH 10–16). In the analyzed area of diagrams a change of the potentials of the redox reactions of a number of metals from pH is described by linear laws [4, 9].

Standard electrode potentials of alloying elements used in welding consumables for steels Fe–Cr–Ni (Figure 1) are shown on diagram φ–pH for water. Main curves correspond to electrochemical equilibriums for H_2O with products of its reduction by hydrogen (curve *1*) or oxidation by oxygen (curve *2*). Area *1–2* corresponds to thermodynamical stability of water. With electrode potentials located outside area *1–2* the water components oxidize or reduce releasing gaseous oxygen or hydrogen.

Interval pH 12–14, i.e. the area of technologically white liquor in the Kamur sulfate-cooking boilers, is of practical interest. Elements whose potentials are located above the line of equilibrium hydrogen (oxygen) electrode destroy with hydrogen (oxygen) depolarization. On the contrary, metals with potentials below equilibrium oxygen electrode (Cr, Nb, V, Mn, Zn, Ti, Al, Y) are corrosion-resistant. They destroy only if there is a depolarizer in the solution (aside from H^+ and O_2) with reduction potentials more positive than standard with the given metals [7, 10]. The diagram allows projecting a probability of corrosion of alloying elements, which proceeds with certain depolarization. Metals (silver and tellurium are given for comparison) whose potentials are above curve *2* do not corrode in the alkaline media. In the area *1–2* and below curve *1* the studied elements (Cu, Mo, Fe, Al, Y) destroy with oxygen, hydrogen and mixed depolarization.

Iron in the lower part of the Fe–H_2O diagram is corrosion-resistant since it is thermodynamically stable (Figure 2, *a*). At pH 1.0–9.5 and potentials above –0.4 V stability of metal decreases, and ions Fe^{2+} isolate in solutions. In the middle area of the diagram at pH 10.0–12.5 φ = –(0.6–0.8) V, and surface of iron is covered with a film of lower oxide hydrate $Fe(OH)_2$. Above this boundary iron hydroxide $Fe(OH)_3$ is separated. In both reactions the metal correlates with formation of protection films of hydrates preventing metal corrosion. In alkaline area (pH 14.5–16.0) iron correlates with release of anions $HFeO_2^-$ in solution [1, 7, 9].

In the work [11] a tendency of the element to general corrosion in alkaline solutions is established, maximal corrosion rate is noted at the potential of –0.53 V. Passive state occurs at more positive potentials due to formation of $Fe(OH)_2$ and $Fe(OH)_3$ films.

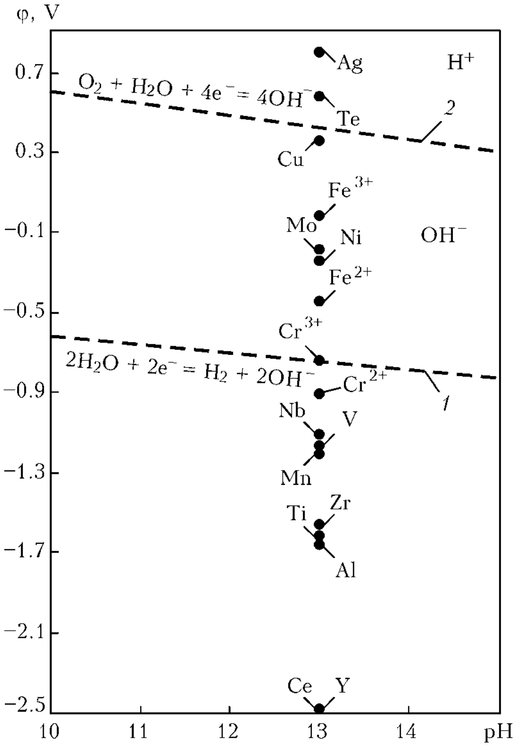

Figure 1. Standard electrode potentials of metals at pH 13

Chromium in alkaline solutions is corrosion-resistant at φ = –(1.25–1.60) V (Figure 2, *b*). Above this boundary a passive state occurs (-0.2 V ≤ φ ≤ 0.2 V) since chemically resistant chromium hydroxide $Cr(OH)_3$ forms on the metal surface.

Passivating ability of chromium is attributed to the availability of protection oxide of three-valency chromium on the metal surface [12, 13]. Its reduction to two-valency leads to cathode activity of chromium, while oxidation to six-valency — to anode activity. With more positive potentials metal dissolves in alkaline media with pH 10–15, ions CrO_4^{2-} forming in the solution. In the area of negative potentials with pH > 15, chromium oxidizes with separation of CrO_3^{3-} ions.

Chromium increases corrosion-resistance of alloy Fe–Cr–Ni in boiling solutions of sodium hydroxide [14, 15]. In these conditions without active dissolution it transfers to a passive state. Density of current of active dissolution and passivation decreases with increase of chromium concentration in the alloy up to 26 % [15].

Nickel has the highest resistance against general corrosion [1, 16] and corrosion cracking [17] in alkaline solutions. According to the authors of [12, 16–18] it increases a passivating ability of the weld metal in concentrated alkaline solutions. With increase of the nickel content in alloys Fe–Ni one observes a decrease of a critical density of the anode current in the active area and a separation of ions Ni^{2+} in the solution. For example, steels Fe–5% Ni, Fe–12 % Ni and Fe–30 % Ni in sodium hydroxide (48 % NaOH) at 140 °C have current density of 150, 110 and 90 A / m^2, respectively

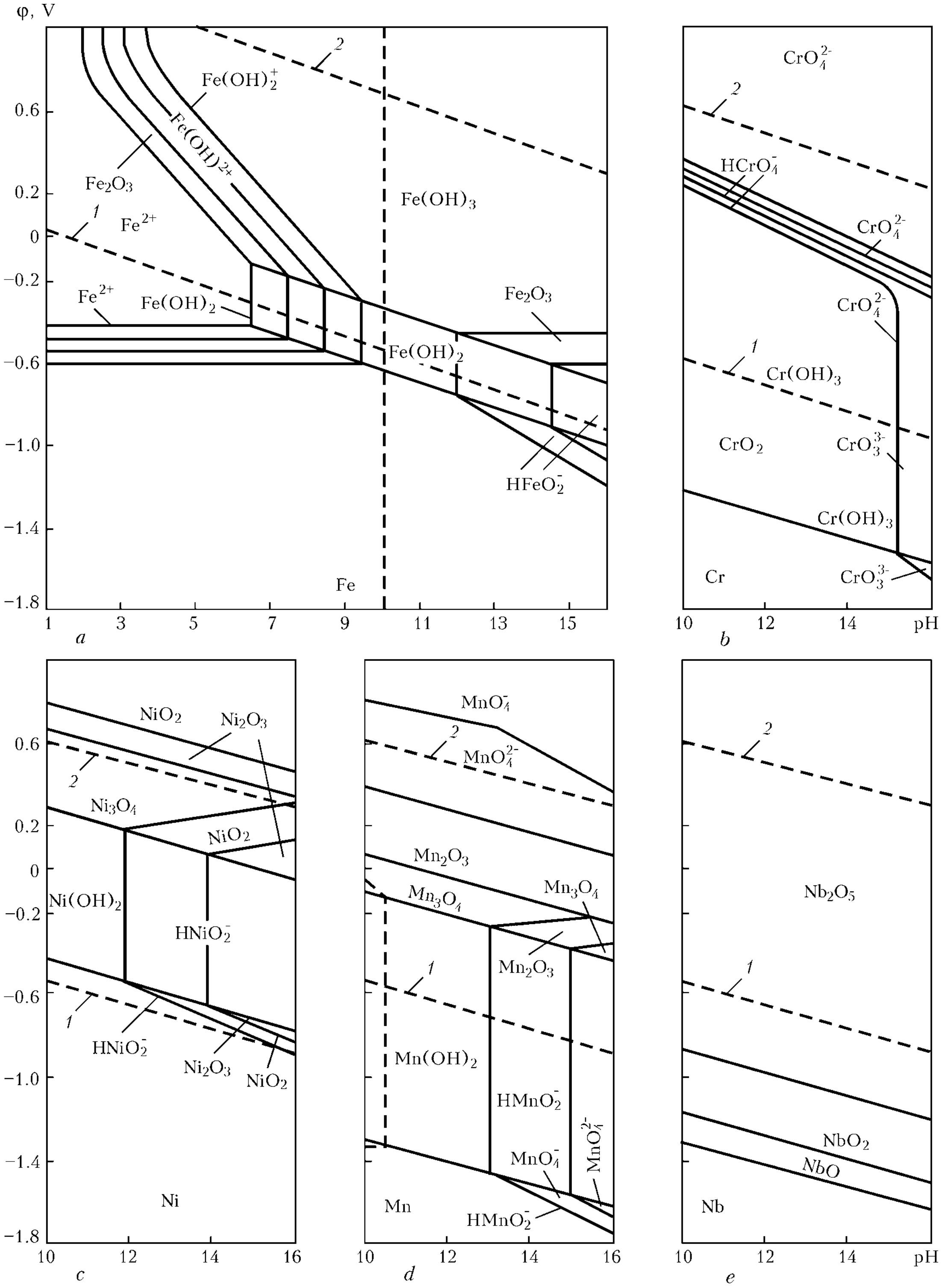

[19]. Similar effect is established for Cr–Ni steels. Passive state occurs under formation of nickel hydroxide $Ni(OH)_2$, $\varphi = -(0.5\text{–}0.6)$ V (Figure 2, *c*). Corrosion resistance of steels and alloys in alkaline media increases proportionally to concentration of nickel [20], its limit content achieving 26 %. Introduction of the element in larger quantities does not practically change the resistance of alloys [3, 6, 21].

Effect of silicon on corrosion resistance of Cr–Ni alloys is not definite. If steel contains 2 % Si its corrosion resistance increases in alkaline media [22]. In neutral solutions silicon decreases metal resistance against corrosion [23]. Welded joints of steel alloyed with 6 % Si are exposed to selective destruction in the near-weld zone due to precipitation of redundant phases on grain boundaries [22–24]. In work [24] silicon was introduced into stainless austenite steels for partial replacement of chromium. It is established that steel containing (%) 15Cr, 9Ni, 3Si as to its corrosion resistance in acidic media approach Cr–Ni steel (%): 0.025C; 0.45Si; 1.75Mn; 9Ni; 18.2Cr; 0.15Mo; 0.003S; 0.007P.

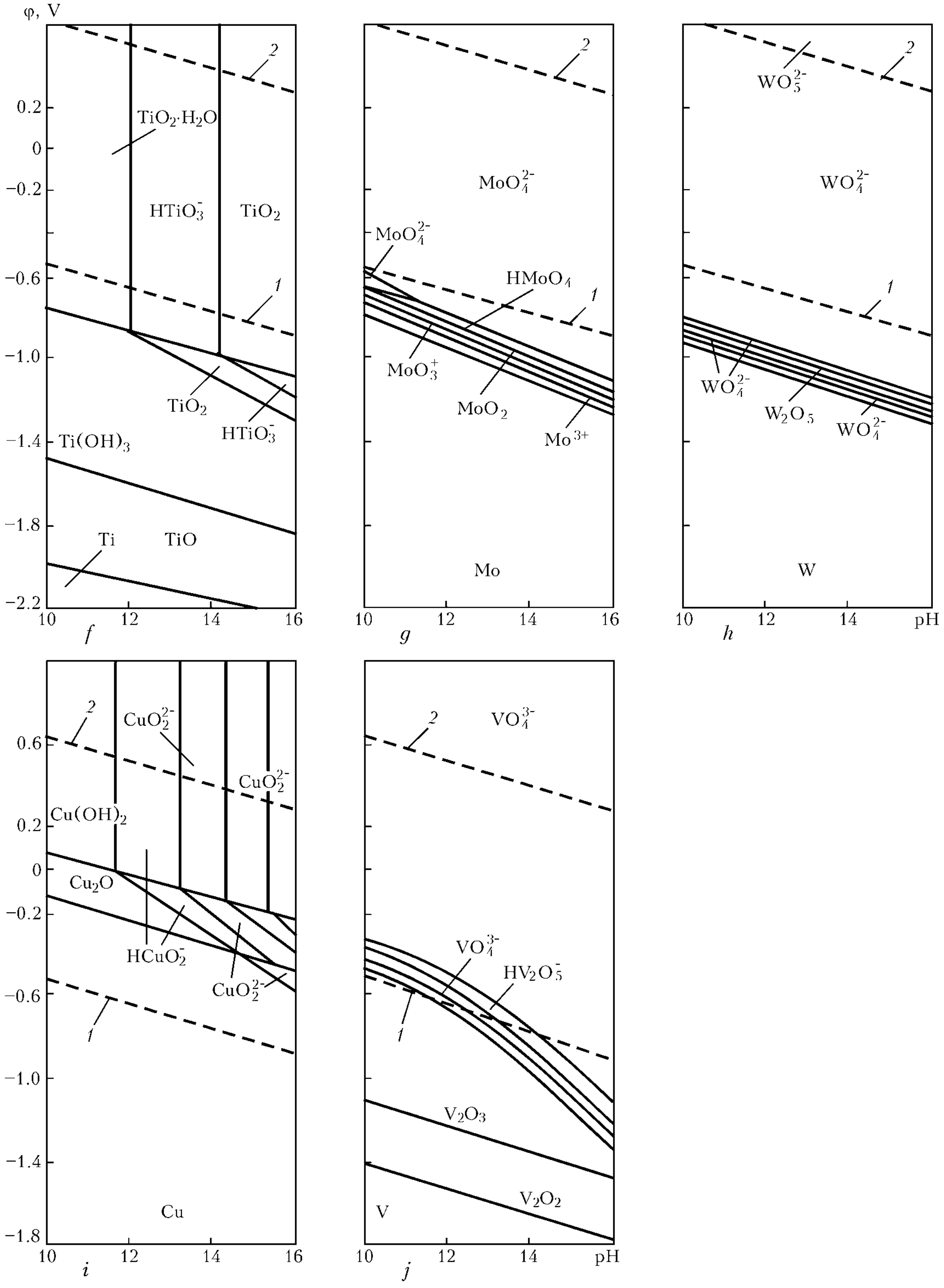

Figure 2. Alkaline area of the Purbe diagram of φ–pH row of the systems: *a*–*j* — Fe, Cr, Ni, Mn, Nb, Ti, Mo, W, Cu, V–H_2O, respectively

There are little data on chemical stability of silicon in alkaline media. Considering negative effect of silicon on resistance of austenite welds against hot cracks, toughness and plasticity, as well as on corrosion resistance of metals [23, 25–27], it seems necessary to restrict its content in the welds.

Manganese decreases corrosion resistance of high-alloy steel welds in oxidizing and reduction media [12, 26]. So, this index decreases by 10–15 % in Cr–Ni deposited metal alloyed with 6–8 % Mn [26]. Passivation of Cr–Ni–Mn steels deteriorates if manganese is introduced shifting the passivation potential towards positive values and increasing the anode current of metal dissolution in the passive area [11].

Area of chemical stability of the element in alkaline solutions (Figure 2, *d*) is located lower, φ = = –(1.4–1.8) V. Above this boundary a transition to a passive state is possible (pH 10.5–13.0) and active dissolution of the metal. Manganese distinguished by rather negative standard potential (–1.3 V) in alkaline media decreases corrosion resistance of Cr–Ni steels [7, 28]. Potential of its anode dissolution is located in the active area [28] exceeding such for Cr–Ni steel, thus impeding passivation of the metal and encouraging corrosion of the welds in solutions of sodium hydroxide.

Niobium is introduced into stainless steels for decreasing metal susceptibility to intercrystalline corrosion (ICC) as a result of fixing of carbon into independent carbides of NbC type. Alongside it facilitates expansion of the ferrite area. This element decreases ductility of the weld metal but as molybdenum decreases harmful effect of silicon on crack resistance of Cr–Ni steels. Analysis of the Purbe diagram for the system Nb–H_2O (Figure 2, *e*) shows that the area of niobium corrosion resistance is limited by the values of potential $\varphi = -(1.32–1.67)$ V. With shifting towards positive values of the potential it passivates with formation of a film of higher oxides NbO, $\varphi = -(1.20–1.57)$ V, dioxide NbO_2 and pentaoxide Nb2O5 chemically resistant in alkaline solutions [7]. Preventing susceptibility of Cr–Ni metal to ICC, niobium decreases resistance to general corrosion in aggressive media [26, 29].

As it follows from [30], niobium self-passivates in dissolved solutions of alkali and at optimal additives increases corrosion resistance of the welds of steels 08Kh18N10T and 08Kh22N6T in concentrated solutions of caustic soda. Introduction of the element above the quantity necessary for fixing carbon facilitates precipitation of redundant phases. As a result, passivation of the welded joints of steel Kh18N10 in aggressive media is impeded, thus leading to a selective corrosion by δ-ferrite [31].

Titanium stabilizes carbon in the welds of Cr–Ni steels and is characterized with passivating ability in alkaline solutions [32–33]. So, it is folowed from the Purbe diagram (Figure 2, *f*) that in alkaline media it is chemically resistant in the area of negative potentials up to –(1.89–2.25) V. A passive TiO film is formed on the metal surface above this boundary.

Molybdenum increases corrosion resistance of Cr–Ni steels in reduction acidic media [16, 22, 26, 34]. This element is distinguished for its resistance in Cl-containing media due to formation of protection films of $MoOCl_2$ composition [35, 36]. It prevents corrosion cracking of steels in alkaline solutions [35, 37]. Introduction of molybdenum into the welds of these material shows selective corrosion of the deposited metal by δ-ferrite in nitric acid and in non-oxidizing solutions [3, 27, 33, 38]. Stainless steels alloyed with molybdenum are established to dissolve in alkaline media [3, 34, 39].

According to the Purbe diagram (Figure 2, *g*) the area of corrosion resistance of the element in solutions pH 10–15 is limited to the values of $\varphi = -(0.7–1.8)$ V, a MoO_2 film is formed on the metal surface. With more positive potentials it dissolves with formation of MoO_4^{-2} ions. Electrochemical studies of high-chromium steels [7] showed that molybdenum in 65 % NaOH at 110 °C dissolve by the mechanism of repassivation and exists in the solution in the form of MoO_4^{-2} ions. The corrosion potential established in this medium is –0.63 V.

Additions of molybdenum in steel accelerate the cathode process of oxygen release and transfer of the metal into a passive state. It is proved [34] that in weal solutions KOH the lower oxides are unstable in the area of potentials where dissolution of molybdenum is possible. Oxides of β- and β′-phases also have high corrosion rate in alkali impeding passivation of molybdenum by these phases. Therefore, it is not passivating in KOH solutions, which is caused by instability of lower oxides (MoO_2 and Mo_2O_5) and intensive dissolution of molybdenum higher oxides in alkaline medium [34].

Tungsten in water solutions at pH 10–16 is characterized by corrosion resistance in the area of $\varphi = -(0.8–1.2)$ V [7]. Below this boundary it is passive, above — dissolves with release of WO_4^{-2} ions (Figure 2, *h*). Passive state of the element is conditioned by formation of chemically resistant WO_2 film. Refractory metals (W, Mo, Nb etc.) are distinguished with corrosion resistance in inorganic acids exceeding stainless steels and Hastelloys [39]. Most likely these metals facilitate improvement of corrosion properties of steels and alloys in alkaline solutions.

Copper from thermodynamical positions is characterized with corrosion resistance since its standard electrode potential is 0.153 or 0.520 V. Copper is rather stable in non-oxidizing acids, solutions of a number of salts, many organic and alkaline media [40]. According to [7] this metal is corrosion-resistant in alkaline solutions at pH 10–15 and $\varphi = -(0.12–0.42)$ V (Figure 2, *i*). Passive area corresponds to more positive potentials, the metal surface is covered with oxide Cu_2O film at $\varphi = 0.156–0.038$ V. Hydroxide $Cu(OH)_2$ forms at pH 10–12 and $\varphi = 0.16–0.04$ V. With shift of the hydrogen index towards area of pH 11.50–13.15 ($0.17 \text{ V} \geq \varphi \geq 0.04$ V) ions $HCuO_2^-$ separate in the solution, and at pH ≥ 13.15, $\varphi = -(0.04–0.20)$ V — ions CuO_2^{2-}. Analysis of the processes proceeding in alkaline solutions suggests that copper alloying increase corrosion resistance of Cr–Ni steels. It is shown in works [41, 42] that these steels in the alkaline and Cl-containing media exceed stainless steels in their resistance.

Vanadium improves corrosion resistance of deposited metal of Fe–Cr–Ni system in boiling alkaline solutions [43] as well as prevents ICC of stainless steels. As it is followed from [26] isolation of chromium carbides on the grain boundaries increases electrochemical heterogeneity of metal surface in aggressive media provoking ICC. To prevent ICC stainless steels are alloyed with stabilizing elements (Nb, Ti, V etc.), which form independent carbides excluding depletion of grain boundaries and adjacent surface of steel with Cr, Mn and Fe [12, 22]. Probability of obtaining carbides is illustrated by a number of standard isobaric-isothermal potentials [44]: Gibbs energy of Nb_2C, TiC, V_2C and Cr_3C_2 is –(190.2, 179.8, 145.5, 28.12) kJ / mol, respectively. This gives the basis to state that vanadium is rather effective in preventing ICC of Fe–Cr–Ni steels.

At $\varphi = -(1.4–1.8)$ V, vanadium is corrosion resistant in alkaline media (Figure 2, *j*). Above this boundary the metal oxidizes to dioxide V_2O_2, which when shifting of potential towards positive area of values form V_2O_3 ($\varphi = -(1.15–1.42)$ V). With potential below –1.187 V, V_2O_4 and ions HVO_4^{2-} are separated in the solution. The process of metal oxidation is completed on the boundary of $\varphi = -(0.47-1.37)$ V. Ions VO_4^{3-} are detected in the positive area (0.25–1 V) in alkaline media.

By regulation of chemical composition of metal by harmful impurities it is possible to change the nature of corrosion processes. Segregation of sulfur and phosphorus on grain boundaries and crystallites intensifies corrosion of stainless steels in oxidizing media [22, 45]. It is established [46–48] that these impurities accelerate ICC, pitting and pointed corrosion of steels of 08Kh18N10 grade in acidic medium as well as corrosion cracking in boiling solutions of sodium hydroxide. Information on the role of additives on corrosion properties on Cr–Ni steels is almost unavailable.

Therefore, analysis of the effect of chemical composition on corrosion resistance of welded joints of Cr–Ni steels and the Purbe state diagrams make it possible to state that chemical resistance of metal in alkaline medium may be achieved by a rational alloying of welds with Cr, Ni, Cu, Nb, V and by restricting the content of Mn, Si, Mo, S and P.

1. Hine, F. (1974) Corrosion of metallic materials in caustic soda concentrated solutions. *Soda-to-enso*, 25(**4**), 109–136.
2. Yonsson, K.E. (1980) The use of stainless steel in the pulp and paper industry. In: *Proc. of 3rd Int. Symp. on Pulp and Paper Industry Corrosion Problems* (Atlanta, May 5–8, 1980). Atlanta.
3. Aleksandrov, A.G., Pinkovsky, I.V., Tsentsiper, B.M. (1978) *Repair of pipelines of continuous pulping units*. Moscow: Lesn. Promyshlennost.
4. Lazebnov, P.P., Tsentsiper, B.M. (1990) Effect of alloying on corrosion resistance of chrome-nickel deposited metal. *Bum. Promyshlennost*, **3**, 23–25.
5. Backman, A., Lyngvist, B. (1977) Properties of a fully austenitic stainless weld metal for severe corrosion environments. In: *Proc. of Int. Conf. on Fabr. and Rel. Welding Process Plan* (London, 1976). Abington.
6. Lazebnov, P.P., Aleksandrov, A.G., Kibalchich, A.A. (1983) Study of corrosion resistance of weld metal in caustic soda. *Khim. i Neft. Mashinostroenie*, **2**, 31–32.
7. (1965) *Reference book of chemist*. Ed. by B.P. Nikolsky et al. Leningrad: Khimiya.
8. Fokin, M.N., Zhuravlyov, V.K., Mosolov, A.V. (1978) About some peculiarities of electrochemical behavior of stainless steels in NaOH solutions. *Zashchita Metallov*, 14(**6**), 690–693.
9. Mattsson, E. (1991) *Electrochemical corrosion*. Ed. by Ya.M. Kolotyrkin. Moscow: Metallurgiya.
10. Shluger, M.A., Azhogin, F.F., Efimov, E.A. (1988) *Corrosion and protection of metals*. Moscow: Metallurgiya.
11. Fontana, M.G. (1971) Perspectives on corrosion of materials. *Corrosion*, 27(**4**), 129–145.
12. Tomashov, N.D., Chernova, G.P. (1986) *Theory of corrosion and corrosion-resistant structural alloys*. Moscow: Metallurgiya.
13. Fajzulin, F.F., Levina, V.K. (1966) Anodic passivation of chrome in alkaline solutions. *Zashchita Metallov*, 2(**6**), 623–627.
14. Mesamichi, K., Takeo, K. (1979) Stress corrosion cracking of ferritic and duplex stainless in 30 % NaOH. *Corros. Eng.*, 26(**6**), 336–342.
15. Sakaki, T., Sakiyama, K. (1979) Corrosion of Fe–Cr alloys in hot concentrated NaOH solution. *Jap. J. Metals*, 43(**6**), 527–533.
16. Kanevsky, L.S., Kolesnikova, N.N., Mosolov, A.V. et al. (1985) Effect of chrome and molybdenum content on corrosion resistance of chrome-nickel steels in alkaline medium. In: *Anticorrosive protection in chemical industry*.
17. Kanevsky, L.S., Kolesnikova, N.N., Shirokova, N.V. et al. (1985) Effect of alloy elements on corrosion resistance of chrome-nickel steels in alkaline medium. *Zashchita Metallov*, 21(**5**), 781–789.
18. Garat, A., Gras, I.M. (1983) Corrosion study of nickel for alkaline water electrolysis. *Int. J. Hydrogen Energy*, 8(**9**), 681–688.
19. Sakai, T. (1980) Corrosion of alloys Fe–Cr–Ni in caustic soda concentrated solution at high temperature. *Nippon Kinzoku Gakkaishi*, 44(**5**), 582–587.
20. Borshchevsky, A.M., Sukhotin, A.M. (1992) Study of passive state of nickel in acid and alkaline media by microcoulometric method. *Zhurnal Prikladn. Khimii*, 65(**9**), 1942–1946.
21. Aleksandrov, A.G. (1970) Corrosion resistance and resistance to corrosion cracking of iron-nickel alloys in concentrated alkaline solutions. *Fiziko-Khim. Mekhanika Materialov*, **2**, 45–48.
22. Kolotyrkin, Ya.M. (1985) *Metal and corrosion*. Moscow: Metallurgiya.
23. Kolotyrkin, Ya.M. (1960) Progress and purposes of development of corrosion theory. *Zashchita Metallov*, 16(**6**), 660–673.
24. Eugazier, P., Chatainier, G., Petit, I.A. (1983) Corrosion generalisee et caverneuse d'aciers inoxydables austenitiques de substitution. Influence du silicium et de l'aluminium. *Rev. Met.*, 80(**5**), 267–275.
25. Kakhovsky, N.I., Fartushny, V.G., Savchenko, V.S. (1971) Effect of silicon on weldability, structure and properties of austenitic steel joints. *Avtomatich. Svarka*, **4**, 9–13.
26. Kakhovsky, N.I. (1975) *Welding of high-alloy steels*. Kiev: Tekhnika.
27. Aleksandrov, A.G., Lazebnov, P.P., Langer, N.A. et al. (1980) Corrosion resistance and electrochemical properties of chrome-nickel steel welded joints in hydrochloric acid. *Svarochn. Proizvodstvo*, **11**, 27–29.
28. Knyazheva, V.M., Vedeneeva, M.A., Khamel, S.E. et al. (1965) Electrochemical examinations of effect of carbon, titanium and manganese on corrosion resistance of chrome-nickel-manganese steels. *Zashchita Metallov*, 1(**5**), 465–472.
29. Jurgen, K. (1980) Die Auswirkung von Ferrit und Seigerung auf das Korrosionsverhalten austenitischer Staehle. *Schweiz. Maschinenmarkt*, 80(**24**), 76–79.
30. Koshkin, B.V., Safonov, A.A., Sidlin, Z.A. et al. (1979) Effect of niobium on corrosion resistance of stainless steels welded joints in NaOH solutions. In: *Anticorrosive protection of metals in chemical industry*. Moscow: NIITEKhIM.
31. Lazebnov, P.P. (1990) Role of ferritic phase in change of properties of chrome-nickel steel welded joints. *Avtomatich. Svarka*, **8**, 28–32.
32. Fajzulin, F.F., Bajtalov, D.A. (1966) Electrochemical behavior of titanium in alkaline solutions. *Zashchita Metallov*, 11(**4**), 439–443.
33. Lazebnov, P.P., Pulina, N.N. (1995) General corrosion in alkaline medium of 08Kh18N10 type deposited metal with various alloying. *Avtomatich. Svarka*, **4**, 20–26.
34. Pozdeeva, A.A., Antonovskaya, E.I., Sukhotin, A.I. (1965) Passivity of molybdenum. *Zashchita Metallov*, 1(**1**), 20–28.
35. Pleva, J. (1983) Influence of molybdenum on stress corrosion cracking of austenitic stainless steel. *Anticorrosion Meth. and Mater.*, 30(**8**), 4–7, 9.
36. Wilson, J.L., Pement, F.W., Aspden, R.G. (1974) Effect of alloy structure, hydroxide concentration and temperature on the caustic stress corrosion cracking of austenitic stainless steels. *Corrosion*, 30(**4**), 139–149.
37. Baumel, A.B. (1967) Einfluss des Deltaferrits auf das Korrosionverhalten von Schweissungen aus austenitischen Zusatzwerkstoffen. *Schweissen und Schneiden*, 19(**6**), 264–269.
38. Plakseev, A.V., Knyazheva, V.M., Dergach, G.A. et al. (1978) Special features of corrosion behavior of chrome-nickel-molybdenum steels in nitric acid. *Zashchita Metallov*, 14(**4**), 393–399.
39. Gulyaev, A.P. (1982) *Corrosion-resistant alloys of refractory metals*. Moscow: Nauka.
40. Smiryagin, A.P. (1966) *Commercial non-ferrous metals and alloys*. Moscow: Metallurgizdat.
41. Ooka, T., Yukawa, K., Ogawa, H. (1980) Corrosion problems and the selection of stainless steel in corrosive environments in the PFP process. In: *Proc. of 3rd Int. Symp. on Pulp and Paper Industry. Corrosion Problems* (Atlanta, May 5–8, 1980). Atlanta.
42. Masuo, M. (1982) Austenitic stainless steel R304Cu, R304LCu, resistant to stress corrosion. *Tokushuko*, 31(**10**), 6–8.
43. Lazebnov, P.P., Savonov, Yu.N., Aleksandrov, A.G. (1981) Effect of titanium, cerium and vanadium nitrides on corrosion resistance of chrome-nickel deposited metal. *Avtomatich. Svarka*, **8**, 69–70.
44. Kulikov, I.S. (1988) *Thermodynamics of carbides and nitrides*. Chelyabinsk: Metallurgiya.
45. Knyazheva, V.M., Chigal, V., Kolotyrkin, Ya.M. (1975) Role of excess phases in corrosion resistance of stainless steels. *Zashchita Metallov*, 11(**5**), 531–552.
46. Pyun Sull, Kirn Jeongtae, Lee Seongmin (1991) Effects of phosphorus segregated at grain boundaries on stress corrosion crack initiation and propagation of rotor steel in boiling 40 % NaOH solution. *Mater. Sci. and Eng. A.*, 148(**1**), 93–99.
47. Edstrom, J., Carien, C., Kampinge, S. (1970) Anforderungen an Staehle fuer die chemische Industrie. *Werkstoffe und Korrosion*, **21**, 812–821.
48. Steklov, O.I. (1984) Increase of corrosion resistance of products by surfacing and spraying methods. In: *Increase of quality and efficiency of welding production in Moscow enterprises*. Moscow: MDNTI.

APPLICATION OF HYDROGEN AND ITS MIXTURES FOR ENVIRONMENTALLY CLEAN METAL JOINING PROCESSES

A.S. PISMENNY and **V.M. KISLITSYN**
E.O. Paton Electric Welding Institute, NASU, Kiev, Ukraine

Prospects for improving metal joining methods with a purpose of decreasing evolution of harmful materials polluting the environment are considered. One of the variants of improving the known welding, brazing and soldering methods is the use of hydrogen as a shielding-reducing atmosphere for highly concentrated and pulsed heating methods. Conditions for safe application of hydrogen and its mixtures with oxygen in welding, brazing and soldering processes have been evaluated.

Keywords: *welding, soldering, brazing, braze-welding, technology, improvement, environment, gas shielding, hydrogen*

In the context of the Kyoto agreements, which are approved by the majority of the industrialised countries all over the world, development of environmentally clean methods for metal joining, allowing a substantial (by an order of magnitude) decrease in the amount of harmful materials evolved in melting and evaporation of solders, brazing filler alloys and fluxes, becomes particularly topical.

Much consideration should be given currently to revision of the available technological processes in terms of their harmful effect on the environment, as well as to certification of the processes employed by each industrial enterprise. During the soldering and brazing processes, melting of solders and brazing filler alloys leads to the evolution of not less harmful vapours of metals and other compounds in the amounts that are tens or more times in excess of their maximum permissible concentrations near the work site. Fluxes applied to remove oxides films from the metals joined additionally evolve volatile compounds of chlorine, fluorine, boron, phosphorus and other elements, which are not less hazardous in biological terms.

It is apparent that the environmental problems in the case of the soldering and brazing processes can be addressed using the ideas realised in arc welding (formation of an increased-pressure shielding atmosphere around the heating zone — MIG and MAG processes, submerged-arc welding) or cutting of metals, e.g. plasma cutting under a thin water layer [1, 2]. Welding methods with pulsed heating, where the heating time is up to 1 s, are also characterised by a minimal evolution of metal vapours [3, 4]. Shortening of the welding time leads to increase in the efficiency of transformation of energy needed for heating, minimisation of the HAZ volume, and improvement of strength characteristics of a welded joint. From this standpoint, upgrading of the methods of flame welding (where metal is subjected to a lower treatment temperature than in heating with the arc or plasma discharge), friction welding, and some types of capacitor-discharge and magnetic-pulse welding holds promise [5–7].

As to the soldering and brazing processes, here we have the following possibilities of decreasing the evolution of harmful materials:

- reduction of the volume of metals evaporated, which are contained in a solder or brazing filler alloy (e.g. by minimising consumption of the solder or filler alloy and time during which they are is in a molten state, which is provided by a more accurate fit-up of the parts for joining and utilisation of pulses heating);
- avoidance of the use of fluxes in the soldering and brazing processes (e.g. by heating the workpieces in vacuum, neutral or reducing gas atmosphere);
- performance of the soldering or brazing process in special atmospheres containing deactivators or adsorbents of harmful materials.

Brazing with pulsed heating includes the following methods for contactless heating of the joining zone: using gas flame, free or constricted electric arc (plasma), high-frequency currents induced in the parts joined, laser or electron beam. Power density in the case of the electric-contact heating methods, where the electric current is passed through one or all the parts joined at their contact with the electrode [8–10], can be varied over wide ranges from 10^3 to 10^7 J / cm^2, i.e. it can correspond to the efficiency of the methods of both arc and plasma heating. Manufacture of electrodes from materials with different electrical resistance (from $1.7\cdot10^{-8}$ to $0.8\cdot10^{-5}$ Ohm·cm) provides some expansion of the technological capabilities of the electric-contact heating method both in brazing and in braze-welding of parts.

Proceeding from the fact that the rate of heating in electric-contact heating may amount to several hundreds of degrees per second, the question arises whether this heating method is applicable for the pulse brazing processes. Some investigators [11] are of the opinion that, as opposed to the accepted one-stage mechanism, the brazing process consists of several stages, such as melting of a brazing filler alloy, wetting of the mating surfaces with the brazing filler alloy, formation of chemical bonds, and dissolution or diffusion of the metals brazed in the molten brazing filler alloy. To occur, each of these stages requires some minimal time exceeding totally a few seconds.

The issue of accurate estimation of the minimal tolerable time required for formation of the seam (excluding the time required for melting of a brazing filler alloy and heating of the region of the parts brazed, adjoining the brazing zone, to a brazing temperature) has an insufficient coverage in technical literature. However, our experimental data show that the brazing processes can occur during a time of fraction of a millisecond [9].

Consider possible variants of fluxless brazing in vacuum, neutral or reducing atmosphere. Brazing in vacuum is applied rarely and only in special cases, which is attributable to a high cost of equipment, limitations of the process as to productivity and option of brazing filler alloys (metals with low vapour pressure are not used).

Gas atmosphere of the neutral character can prevent formation of oxide films on the mating surfaces during heating. However, it can be used only in a case of preliminary, prior to brazing, removal of oxides in a given atmosphere. Naturally, this imposes dramatic limitations on the application fields for this method.

Hydrogen and its compounds, as well as mixtures of hydrogen with other gases are most suitable for the use as a reducing gas atmosphere for high-temperature metal brazing in terms of technology and ecology. As activity of the processes of removal of oxide films and reactivity of any gas grow with growth of temperature, hydrogen can provide the highest brazing quality, compared with other gases.

The use of hydrogen in the processes of soldering realised in conveyer furnaces is not that effective as in brazing. Normally, hydrogen supplied in bottles is insufficiently reactive to reduce oxides, the thermal dissociation temperatures of which are much higher than melting temperature of a solder. However, results of our technological studies indicate that hydrogen can be efficiently used for soldering as well. For example, in a case of soldering of leads to sprayed copper coatings on ceramics, because of a high degree of oxidation of a porous metal layer, the required soldering quality was not achieved even with the use of high-reactivity acid fluxes, which was caused by the absence of wettability, not speaking of the rosin-alcohol fluxes recommended for the manufacture of radio engineering parts. But with the pulsed flame heating of the joining zone using the hydrogen-oxygen flame it is possible not only to achieve the high soldering quality and reduce the process time, but also to fully avoid the use of flux. In turn, this excludes the need to use an expensive operation of post-soldering washing of parts from flux remainders (Figure 1).

Reportedly, the application of hydrogen is limited by high technological (procurement, transportation and storage of hydrogen supplied in bottles) and capital costs, including the cost of equipment and re-tooling of the production area because of the necessity to perform explosion hazard prevention operations.

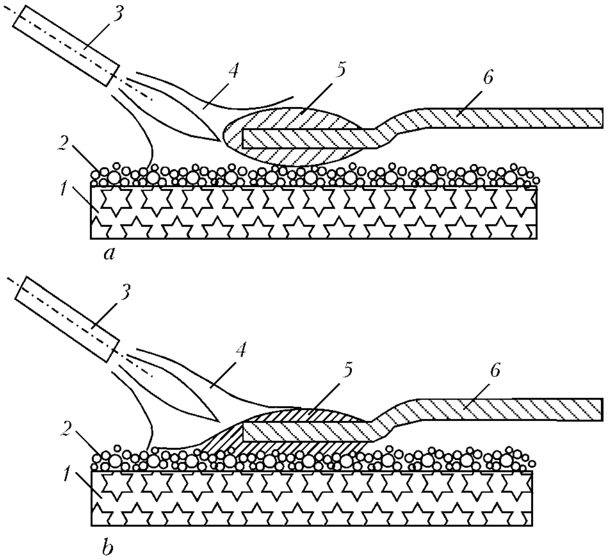

Figure 1. Flow diagram of fluxless soldering with pulse flame heating at the beginning of heating (*a*) and after heating to a melting point of a solder (*b*): *1* — ceramic substrate; *2* — sprayed layer; *3* — gas torch nozzle; *4* — reducing zone of the flame; *5* — solder; *6* — lead being soldered

Consider promising variants of fluxless soldering in hydrogen, which are free to some extent from such drawbacks as explosion hazard of its mixtures with air or oxygen, high cost of hydrogen supplied in bottles and its decreased reactivity in heating to a melting point of solders.

As far as the explosion hazard of a mixture of hydrogen with air or oxygen (at a hydrogen content of the mixture ranging from 4.0 to 74.2 %) is concerned, it should be noted that hydrogen has been applied already for several decades at the electronic enterprises for soldering semiconductor devices, where the use of fluxes is excluded because of high vacuum hygiene requirements. Soldering is performed in special conveyer furnaces equipped with lock devices for loading and unloading of assemblies to be soldered. In this case hydrogen fills up the internal cavity of the furnace and freely flows out via a hole in its upper part, where it is ignited at a stage of switching on of the furnace to the normal operating mode and burns up in a mixture with air in the form of a clear flame. Glow of a hot metal plate placed in the hydrogen flame is indicative of the fact of complete burning up of hydrogen flowing out from the furnace, i.e. it serves as an indicator of the absence of its accumulation in a production area.

In the case of an accidental extinction for the flame or leakage of hydrogen, the sensor for measurement of the indicator plate temperature and sensors warning of the presence of hydrogen in the production area generate a signal to switch off the feed of hydrogen into the conveyer furnace, switch on the alarm system and emergency ventilation. Nevertheless, explosions sometimes did take place as a result of mistakes of a conveyer furnace operator or an accidental failure of

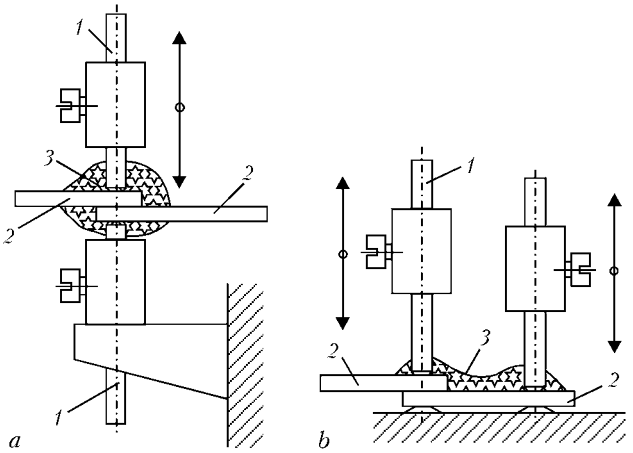

Figure 2. Schematic of gas shielding in resistance welding with two- (*a*) and one-sided (*b*) location of electrodes: *1* — electrodes; *2* — workpieces welded; *3* — gas-bearing interlayer

the automatic devices, and, as a rule, this was accompanied by breakdown of the furnaces.

However, we should not make a final conclusion of inevitability of explosion with hydrogen used in the welding or soldering processes on the basis of the facts of fixed breakdowns of hydrogen furnaces. There are quite tangible conditions that lead to initiation of explosion of hydrogen mixed with oxygen or its stable burning, and tangible conditions that give no way for this phenomenon to occur.

In contrast to the explosion of any other hydrocarbon-base gases mixed with oxygen, where the volume of the reaction products grows instantaneously hundreds of times, the explosion of the hydrogen-oxygen mixture occurs with an instantaneous decrease (more than thousands of times!) of the volume of the reaction products (water), i.e. the destruction occurs with no scatter of fragments from the explosion zone. The mechanism of this kind is similar to the explosion of a vacuum bomb.

The use of fluxes in the brazing and soldering processes, or formation of scale in the heating zone during the spot welding processes can be avoided in some cases by using a gas-bearing interlayer, which should be placed in the zone of heating of workpieces and impregnated with hydrogen, its mixtures with other gases or its compounds prior to heating (Figure 2). One of the variants of using hydrogen during welding or braze-welding of tubular parts is shown in Figure 3. Afterburning of hydrogen on the periphery of the heating zone, where it burns up in a mixture with air, provides protection of a heated metal from oxidation and excludes accumulation of hydrogen in the production area.

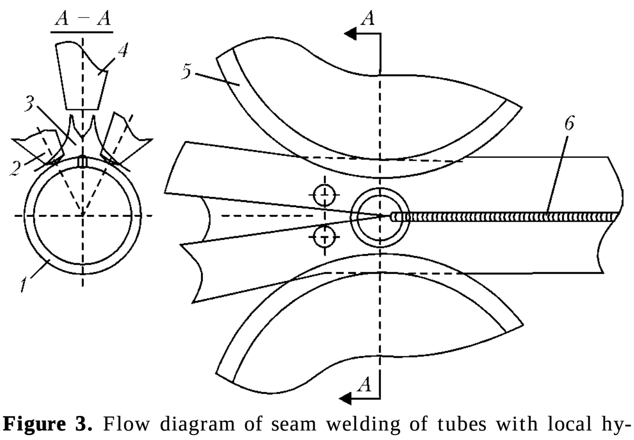

Figure 3. Flow diagram of seam welding of tubes with local hydrogen flame shielding of the heating zone: *1* — workpiece; *2* — current conductors; *3* — reduction flame zone; *4* — hydrogen feeding nozzle; *5* — forming rolls; *6* — weld

The process of stable burning of hydrogen in air is realised by igniting its jet or its mixture with oxygen flowing out at rate v_{f}, which is just slightly higher than its burning rate v_{b} under specific conditions. Here the boundary of the region of burning of the hydrogen flame is located in the zone where its flow rate is equal to the burning rate. In a case of decrease of the flow rate of hydrogen, the flame front will move at a rate of $v = v_{\mathrm{b}} - v_{\mathrm{f}}$ to the source of hydrogen or its mixture with other gases. And in a case of the flow rate exceeding the burning rate the flame-out will occur, which may cause increase in percentage of hydrogen in the production area atmosphere.

In addition to the above condition, elimination of the risk of formation of an explosive mixture in the production area can also be achieved by using an exhaust ventilation system, the capacity of which can be calculated with a sufficiently reliable result on the basis of the required consumption of hydrogen to ensure local shielding of the heating zone for a specific technological process, and on the basis of the ratio of the brazing or soldering process time to the cycle time.

Therefore, the use of hydrogen for brazing and soldering with pulsed heating can be considered absolutely safe in terms of the probability of its explosion in a mixture with air, providing that the conditions excluding the risk of an accident as a result of mistakes of an operator or probable failures of the automatic devices are kept to.

One of the factors that limit an extensive use of hydrogen supplied in bottles is its high cost. However, the possibility exists of producing this gas by the method of water electrolysis directly on site of its utilisation using small-size hydrogen generators. The majority of technological problems can be successfully handled by using hydrogen generators with a capacity of up to two cubic metres per hour, which are manufactured now in the European countries [12]. If necessary, their mass production can be arranged in Ukraine, based on the designs developed by the E.O. Paton Electric Welding Institute.

In addition to the economic benefits of producing hydrogen on site of its utilisation, other advantages include the absence of the need for its pressurised storage, which eliminates the risk of its leakage and formation of explosive mixtures with air.

Currently, there is a large amount of the experimental data that prove the probability of decrease in reactivity of hydrogen with time relative to its reactivity at the moment of production. It is a known fact that hydrogen is generated at the cathode in the ionised and atomic state characterised by a maximal reactivity during the processes of electrolysis of aqueous solutions. However, the processes of recombination of ions into atoms to form molecular hydrogen and combine molecules into associates are accompanied by a substantial decrease in the degree of reactivity of hydrogen. It is this fact that can account for a large scatter of reference data on the maximal burning temperature of hydrogen in oxygen (from 2100 [13] to 3400 °C [14, 15]). Higher values of the temperature apply particularly to the hydrogen-oxygen mixture produced during the electrolysis process and used within a minimum time period from the moment of its generation from water (e.g. not more than 0.2 s).

The more detailed analysis of advantages of different methods used for metal joining makes it possible to select the most optimal ones in terms of power saving and minimal impact on the environment. Of interest among them are the joining methods that were employed for welding of critical units even before the emergence of the specialised arc welding technologies and equipment. First of all, they include atomic-hydrogen and pressure-gas welding with flame heating.

The promising methods of metal joining include also arc-discharge welding in hydrocarbon atmosphere, as well as resistance brazing and welding with shielding of the heating zone with hydrogen or its compounds. Allowing for a chain character of the burning reaction, atomic or ionised hydrogen is indicated for the fluxless brazing and soldering processes, while the methods used to produce this hydrogen are not that difficult from the technical and power standpoints.

CONCLUSIONS

1. Highly concentrated and pulsed heating methods are most advisable from the economic and environmental standpoints to address the majority of practical problems arising in soldering, brazing and welding.

2. The promising trend in improvement of the known soldering, brazing and welding methods is to the use of gas mixtures based on hydrogen or its compounds as a reducing atmosphere.

3. Utilisation of special additions for generation of shielding atmosphere and adsorbents for the most harmful gases holds promise for the submerged-arc welding, soldering and brazing processes involving fluxes. To avoid formation of harmful substances, it is advisable to preliminarily fix filler materials within the joining zone using fluxes with subsequent removal of solid products (fused flux) together with the entire volume of the adsorbed gases generated in melting of metals.

1. Paton, B.E., Makara, A.M. (1944) *Experimental investigation of automatic submerged arc welding*. Kiev: AN Ukr. SSR.
2. Bach, Fr.-W., Versemann, R. (2001) Application of flame cutting under water. *Welding in the World*, 45(**1/2**), 27–31.
3. Moravsky, V.E. (1963) *Stored-energy welding*. Kiev: Gostekhizdat Ukr. SSR.
4. Mumrikov, P.V., Tarasov, S.I. (1956) Multiple-spot arc welding machine. *Tekhnologiya Avtomobilestroeniya*, **5**, 70–72.
5. Thomas, W., Fiedling, P., Threadgill, P. et al. (2001) «Skew-stir»™ variation on a theme. *TWI Connect*, **3**, 37.
6. Froehlich, F.F. (1970) Ueber das Perkussionschweissen und seine Anwendungen. *Schweisstechnik*, 20(**9**), 399–403.
7. Dudin, D.A. (1979) *Magnetic-pulse welding of metals*. Moscow: Metallurgiya.
8. Rossoshinsky, A.A., Lebiga, V.A., Kislitsyn, V.M. et al. (1968) Combined method for spot welding of miniature parts. *Svarochn. Proizvodstvo*, **9**, 38.
9. Kislitsyn, V.M. (1987) *Technology for resistance soldering of silicon diodes*. Syn. of Thesis for Cand. of Techn. Sci. Degree. Kiev: PWI.
10. Rossoshinsky, A.A., Pavlyuk, S.P., Kislitsyn, V.M. (1999) Application of silicon as a heating element of microsoldering irons. *Avtomatich. Svarka*, **2**, 41–44.
11. Petrunin, I.E. (1972) *Physical-chemical processes in soldering*. Moscow: Vysshaya Shkola.
12. Lashko, N.F., Lashko, S.V. (1969) Contact-reactive brazing. *Svarochn. Proizvodstvo*, **11**, 34.
13. (1952) *Reference book of mechanic*. Ed. by E.A. Matel. Vol. 2. Moscow: Mashgiz.
14. (1970) Sauerstoff-Wasserstoff-Mikroschweissgerat. *Elektrische Anzeiger*, 23(**9**), 204.
15. Lurie, H.H., Scherman, G.W. (1933) Flame temperatures of combustible gas-oxygen mixtures. *Industry and Eng. Chem.*, 25(**1**), 404–409.

MECHANIZED CUTTING OF METALS WITH APPLICATION OF PSh107R SEMI-AUTOMATIC MACHINE

V.A. LEBEDEV
E.O. Paton Electric Welding Institute, NASU, Kiev, Ukraine

The paper considers some features of practical use of the process of mechanized arc cutting of metals with application of a special semi-automatic machine of PSh107R type from the series of semi-automatic machines of a modular design. Several techniques and technologies are proposed that allow a significant increase of the speed of cutting and pulsed feed of the electrode wire.

Keywords: cutting, semi-automatic machine, flux-cored wire, hose holder, cutting technique, comparative characteristics

Mechanized arc cutting of metals is currently widely applied in different production sectors, where it is necessary to perform dismantling of constructions or reduce their dimensions, preparatory blanking operations, or technological cutting operations. In this case there are usually no special requirements on the purity of metal surface in the cut section and no need to prepare the cut up fragments for further technological operations. In these cases application of mechanized equipment is rational due to simplicity and universality of the arc cutting process.

References [1–3] deal with the issues of selection or development of semiautomatic machines for metal cutting, using flux-cored electrode wires; some theoretical prerequisites are given for calculation of welding equipment components, that are under special conditions at cutting, as well as technical solutions used in their development. This, in particular, is true for the current-conducting tip, roller feed mechanism, control and adjustment systems. Considering the special conditions in cutting (variation of electrode wire extension in a broad range requires adjustment of its feed parameters, protection of equipment elements, and the welder himself from the thermal impact of the arc and the molten cut metal, etc.) a semi-automatic machine for metal cutting with flux-cored electrode wires PSh107R was developed. It was developed around a basic model of semi-automatic machines of a block-modular design of PSh107V type [4]. A semi-automatic machine of this design has some special features, namely enhanced design of the hose holder as regards the current-conducting tip and protective element on the handle; use of feedback structure allowing the cutting mode to be maintained at considerable (40–90 mm) variations of the extension of 3 mm diameter flux-cored wire.

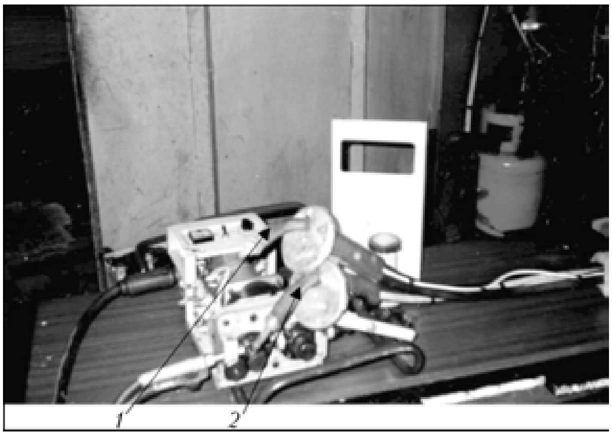

Figure 1. PSh107R semi-automatic machine with a regular (*1*) and reinforced (*2*) hose holder

The semi-automatic machine was developed in two variants, namely for cutting with a smooth wire feed (PSh107R) and for cutting with a pulsed feed (PSh107Ri). Both variants of the semi-automatic machine design were tested under the laboratory conditions. However, the industry is currently using just one variant with a smooth feed of an earlier design (Figure 1). The above semi-automatic machine includes a hose holder for cutting thin (10–20 mm) and thick (20–60 mm) metal. Figure 2 shows the results of cutting a steel sample 30 mm thick, performed at different angles of inclination to the downhand position. This shows the possibilities of changing the cutting direction and a relatively small in-flowing of molten metal during cutting.

Mastering of the technology and equipment for cutting metal of different thicknesses in different positions in space revealed certain features, which determine the process efficiency and consumption of electrode material; the main of them are the need to remove from the cut area the cut metal molten during the arc process and intensive start of cutting thick

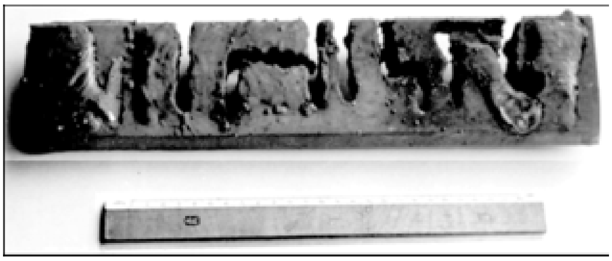

Figure 2. Typical cuts in cutting at different angles of steel sheet 30 mm thick using PSh107R semi-automatic machine

Parameter	*Cutting with special electrodes of ANR type of 4 mm diameter*	*Mechanized cutting with special flux-cored wires with PSh107R semi-automatic machine*	*Air-plasma cutting with AVPR type machines*
Speed of cutting a flat sheet of uniform cross-section, m / h	3.0–3.5	4.0--5.0	8.0--10.0
Cutting efficiency allowing for replacement of electrodes, current conduits, initial metal heating, change of cross-section and cut position, m / h	1.5–2.0	3.0--4.0	Not determined in view of the complexity of cutting across a variable cross-section and position of the cut area
Material consumption in cutting of a flat sheet of uniform cross-section, kg / m	2.0–3.0	1.0--1.2	3–4 inserts per shift
Cost of one kilogram of consumable material, UAN	1.6–1.7	3.5	–
Advantages	Simple equipment and materials, possibility of cutting variable cross-sections under different conditions, process safety	Simple equipment and materials, possibility of cutting variable cross-sections under different conditions, process safety. High efficiency	High efficiency, smooth edges
Disadvantages	Relatively low efficiency, rough edges	Rough edges	Complex supply lines, limited application
Main applications	Recycling and preparatory operations	Recycling and preparatory operations, not requiring the accuracy or smoothness of edges	Accurate cutting of blanks with relatively clean edges

metal (more than 25--30 mm thickness) under the conditions, when the metal is not yet heated. These drawbacks are eliminated using cutting flux-cored wires of PPR-EK4 type, providing the outflow gases that form during heating of the gaseous components of the charge, contained in the above wire, using special manipulations of the torch in the cut zone, performed without a risk of violation of arcing stability. As a rule, cutting is performed with the forward inclined torch, the angle being changed periodically, which allows avoiding the molten metal staying in the cut zone. If formation of the molten metal bridges proceeds in the already cut sections, the cutting technique is changed –– the cut width is somewhat increased due to torch oscillations, placing it across the cut with an inclination. Cutting thick metal (80 mm and more) is performed with compressed air, which is fed from the mains or a separate compressor into the cut zone.

Use of PSh107Ri semi-automatic machine with a pulsed feed of electrode wire yields an essential increase of the cut speed and improvement of the cut quality with less metal rolls. This is attributable to the increase of arc pressure (gas-dynamic impact) at pulsed motions of the above wire. At comparative testing of semi-automatic machines of grades PSh107Ri and PSh107R it was established that the cutting speed of the first one is 1.2 to 1.3 times higher than that of the second one.

Experience of application of semi-automatic machines when solving various problems (severing metal scrap, preparatory cutting mounting and construction, cutting during emergency operations) allowed determination of the actual technical capabilities of mechanized arc cutting with semi-automatic machine PSh107R. The Table gives a comparative characteristic of various widely-accepted processes of arc cutting of metals, based on experimental data, as well as data of the equipment certificates and publications [5]. Tabulated data are given for cutting a sample of steel St3 20 mm thick in the downhand position. Data of [3] can be used to evaluate the technical capabilities of semi-automatic machines of PSh107R type in comparison with other cutting processes.

Let us dwell on the problem of increasing the cutting speed in the initial period at a large thickness of the cut metal. In this case several processes can be used, namely cutting mode parameters can be changed for large values or the shape of the initial section of the cut zone can be modified.

We have analyzed both the processes. Use of the first one requires a certain change of the semi-automatic machine schematic. The semi-automatic machine should be a two-mode one with the controllable moment of mode switching, which is rather complicated from the engineering viewpoint and is not always convenient for the operator. The second process is more practicable. It consists in a certain thinning (angle grinding) of the initial section of the cut zone, which is provided using regular manual grinder. As shown by practical experience, when cutting more than 40 mm thick metal this technique is effective both in engineering and in technological respect, and for large metal volumes –– also in the economic respect.

It should be noted that higher capacity hose holders are required, when cutting up to 50 and 60 mm and thicker metal at currents above 500 A. A holder

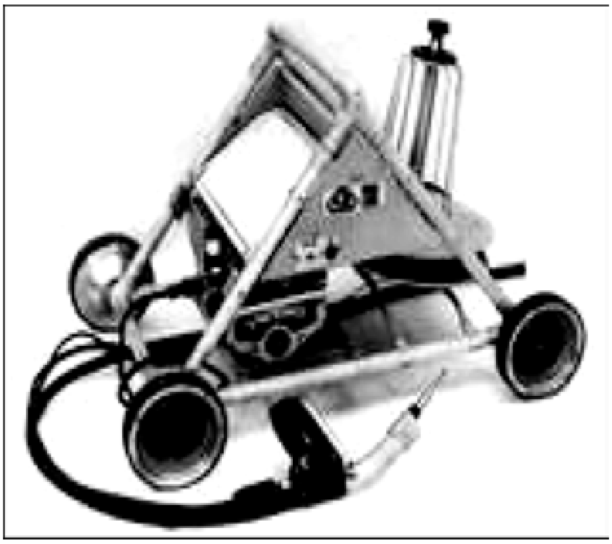

Figure 3. Semi-automatic machine with a reinforced holder for cutting thick metal

of such a type in a set with a semi-automatic machine in the form of a carriage with fixed wheels, that moves easily along the material being cut, is shown in Figure 3.

Quite extensive experience of application of mechanized arc cutting of steels under different conditions and in different modes allows generalizing the values of cutting speed v_c of flat steel sheets as the following dependence $v_c = f(\delta, I_a)$, where δ — thickness of steel being cut and I_a — arc current. This dependence is shown in Figure 4. From the Figure it follows that the relative cutting speed is essentially reduced with the increase of arc current, this being, probably, attributable to the difficulties arising in connection with the need to remove liquid metal from the cut zone.

Semi-automatic machines of PSh107R type have so far been successfully applied at:

- cutting of wheels of obsolete armour vehicles and tanks with the variable cross-section and 3 to 5 fold change of the cut material thickness, that requires special adjustment of feedbacks in the system of the semi-automatic machine regulation;
- severing the ship hull directly on the shore, where the metal already has considerable local corrosion and constant impact of sea water in the form of spatter and moisture is in place. In this case the semi-automatic machine was placed into the container, and a self-sufficient welding plant (generator with a driven internal combustion engine) was used as a welding current source;

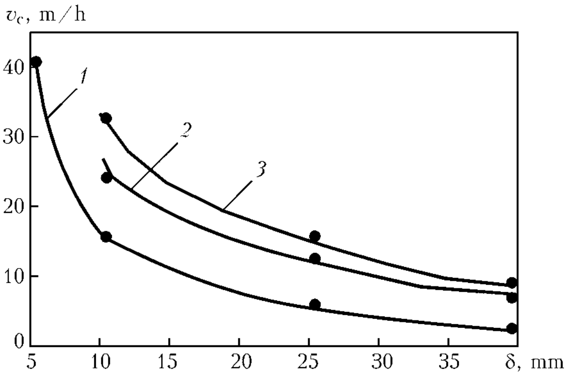

Figure 4. Dependence of the speed of cutting a steel sheet made with application of special flux-cored wire of 3 mm diameter, on its thickness at different currents: 250 (*1*), 350 (*2*) and 450 (*3*) A

- cutting-up the tanks, earlier used for fuel storage. In order to avoid an explosive situation the tanks were filled with water and cutting was performed in such a condition, lowering the cutting speed in places, close to the water. Such an approach was used, for instance, when severing aircraft wings, repair of tank cars, etc.;
- cutting out process holes in repair and mounting of steel tanks of anode blocks of aluminium electrolyzers, and cathode blocks of magnesium electrolyzers;
- cutting elements of busbars, made in the form of a multilayer structure of different metals (cast iron, steel, aluminium). Similar problems on cutting structures of various metals were solved at recycling ship engines.

In a number of cases we performed metal cutting with other types of semi-automatic machines (A765, A1197, etc.). Practical experience suggests that cutting is the most effective, if a special semi-automatic machine and special electrode wire are used as a package.

1. Danchenko, M.E., Nefyodov, Yu.N., Ponomaryov, V.E. (1993) Specifics of underwater flux-cored wire cutting process. *Avtomatich. Svarka*, **10**, 15–19.
2. Lebedev, V.A. (1999) Mechanized consumable electrode arc cutting. In: *Abstr. of 1st Ukrainian Sci.-Techn. Conf. on Modern Technologies and Equipment in Gas-Thermal Processes of Restoration and Recycling of Machines and Structures* (Kyiv, Oct. 27–29, 1999). Kyiv: KPI.
3. Lebedev, V.A., Moshkin, V.F., Pichak, V.G. (1995) Selection of equipment for mechanized flux-cored wire cutting. *Avtomatich. Svarka*, **6**, 53–58.
4. (1998) Semi-automatic machines for welding and surfacing of PSh107 type. *Ibid.*, **7**, 38–42.
5. Khrenov, K.K. (1973) *Welding, cutting and brazing of metals*. Moscow: Mashinostroenie.

TECHNOLOGICAL PECULIARITIES OF LOCAL STRENGTHENING OF HIGH-STRENGTH CAST IRON

Yu.S. SAMOTUGINA
Priazovsky State Technical University, Mariupol, Ukraine

A possibility is shown of a considerable increase of abrasive wear resistance of high-strength cast iron in plasma surface treatment with deposition of a strengthened layer of a discrete structure. The extent of increase of the wear resistance depends on the treatment mode, direction of plasmatron displacement and relative area of the strengthened surface.

Keywords: plasma surface treatment, high-strength cast iron, strengthened layer, discrete structure, wear resistance

Surface treatment with high-concentrated plasma jet is one of the most promising methods for surface strengthening of parts and tools of cast iron (rolls, guide bars of metal-cutting machine tools, crankshafts, camshafts and others) [1]. Due to considerable (up to 3 and more times) increase of the strength of a surface layer this treatment allows achieving a proportional increase of wear resistance of strengthened parts [2]. At the same time formation of brittle metastable structures under accelerated hardening of cast iron (especially in plasma treatment with surface fusion) leads to a considerable decrease of its fracture toughness [2, 3].

The use of the concentrated heating source as against conventional methods of surface treatment (chemical-thermal treatment, induction hardening) allows producing a surface strengthened layer of both continuous and discrete structure with alternating of strengthened zones with high hardness and wear resistance and non-strengthened ones with decreased hardness. The presence of locally non-strengthened sites with relatively higher ductility and toughness on the hard surface of the part allows considerably increasing crack resistance of strengthened parts in the process of operation without decreasing their wear resistance. Local non-strengthened sites of the surface wear by the mechanism of plastic edging while adjacent hard sites — mainly by the mechanism of ductile flaking [2]. Besides, formation of surface micropits on the non-strengthened sites in the process of friction facilitates improvement of lubrication conditions, increase of setting and corrosion resistance, shortening of run-in period. On the whole, under complex conditions of external loading (joint action of high temperatures, mechanical loads and corrosive media) strengthened layers of discrete structure may possess higher operational reliability than coatings of continuous structure [4].

In the process of surface treatment with concentrated heating sources a discrete structure of the strengthened layer may be obtained not only by application of alternating hard and soft sites but also by treatment of surface in the direction perpendicular or located at a certain angle to the direction of wear.

A number of technological techniques for producing a discrete structure of the strengthened layer are known as applied to laser and EB surface treatment of steels and alloys. Experience on application of differentiated laser and EB treatment (by application of alternating hard and soft sites) of steels of different structural classes — structural, chromium-manganese, martensite-aging, low-carbon is generalized in the work [5]. Depending on specific conditions of operation of the part the differentiated treatment facilitates additional increase of characteristics of strength, endurance and wear resistance. It is established on the example of laser hardening with fusion of the surface of parts of grey cast iron machines [6] that optimal scheme for application of hardened tracks is their location at an angle 45° to the direction of sliding friction. The wear resistance decreases with increase of a distance between the strengthened tracks (treatment step) within 4–16 mm (beam diameter is 3 mm). It is also established [7] that in laser treatment of cylindrical specimens of cast iron SChKhNMD by application of tracks 2–3 mm wide with 10 mm step a higher wear resistance is achieved when the tracks are located at an angle of 45° to longitudinal axis as against their location at an angle of 90°. Treatment of plane and cylindrical guides of grey cast iron machines with fusion of the surface and application of different strengthening «patterns» (as spiral, loop, wave etc.) with different relative area of the strengthened sites was carried out in [8]. It is established that increase of the area of the strengthened surface within 20–50 % considerably (2–3 times) enhances the wear resistance of specimens. An increase of the track area by more than 50 % does not cause essential improvement of wear resistance. Alongside, the accepted in [6–8] limits of variations of geometrical and technological parameters of laser treatment does not allow making a scientifically justified conclusion on preference of this or other technology for a wide range of cast iron parts and conditions of their operation. There is no data in literature on the efficiency of obtaining a discrete structure of the strengthened layer under plasma treatment, which differs from the laser one by a much bigger size of the strengthened zone (width

Modes of plasma strengthening and characteristics of strengthened zone of cast iron specimens

Variant of surface treatment	Current of plasma jet *I*, A	Speed of plasmatron displacement *v*, m/h	Thickness of the hardened zone, mm	Surface hardness *HV*
Without fusion	400	27	2.7	800
With fusion	400	18	3.4	790

is not more than 15 mm and depth is not more than 5 mm [1]) and a more developed structural heterogeneity. Besides, the preliminary studies established [2] that the highest abrasive wear resistance is achieved under plasma treatment of high-strength cast iron without fusion of the surface, which is specified by a high brittleness of quasiledeburite of the plasma fusion zone and brittle microfailures of the fusion layer surface under the action of abrasive particles.

This work presents a development of technological principles for plasma strengthening of parts of high-strength cast iron to produce strengthened layer of a discrete structure with high serviceability under conditions of abrasive wear. Plasma treatment of 50 × 60 × 15 mm plane specimens of cast iron VCh-80 was carried out by plasmatron of indirect action with sectioned interelectrode insert [1] in modes presented in Table.

It is seen from the Table that plasma treatment of high-strength cast iron with fusion of the surface with practically similar surface hardness provides increase of the strengthened zone thickness as compared to treatment without fusion. Microstructure of the hardened zone (zone of plasma action) under treatment without fusion consists of high-dispersed martensite, residual austenite (not more than 15 %) and fully preserved graphite [1]. With fusion a dissolution of the graphite phase occurs in the molten matrix (considering a high rate of cooling down) and hardening from the liquid state with formation of a surface layer of white cast iron with the structure of quasiledeburite, i.e. high-dispersed austenite-cementite eutectic (the content of residual austenite is not more than 50 %).

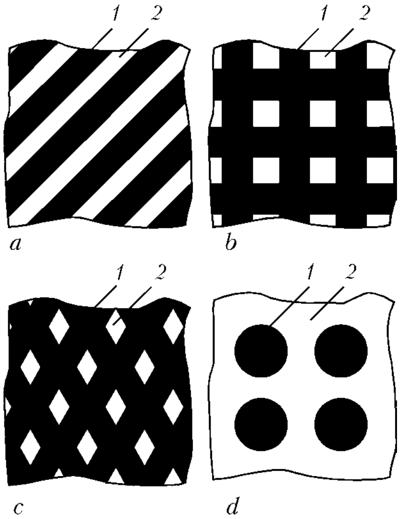

Figure 1. Discrete structure of working surface of the part with application of strengthened zones as parallel strips (*a*), cross cutting (*b, c*), circle (*d*): *1, 2* — hard and soft sites, respectively

Selection of the technology for plasma treatment in application of the strengthened layer of a discrete structure depends on the shape of the part to be strengthened. When strengthening parts of plane shape a formation of hard and soft sites is possible under reciprocating motion of plasmatron along and across the working surface (depending on the selected orientation of the strengthening direction relative to the wear direction) with a discrete shift of the motion axis by a size of the step exceeding the width of a single strengthened zone. The similar principle is used under plasma treatment of cylindrical parts in case of the plasmatron displacement along the generatrix. Plasma treatment of cylindrical parts is also possible when a plasmatron moves by a spiral. In this case a size of the clearance (soft site) between strengthened tracks is regulated by selecting a speed of the part rotation and a speed of the plasmatron displacement. Discrete strengthening of the working surface of the part when strengthening both plane and cylindrical parts may be obtained with application of hard and soft part as parallel strips (Figure 1, *a*), cross cutting (Figure 1, *b, c*) when local soft sites have a limited configuration of the square (under perpendicular cross displacement of the plasmatron) or rhomb (under non-perpendicular cross displacement). It is also possible to obtain a discrete structure of the strengthened layer with application of the strengthening zones in the form of circle (Figure 1, *d*), ellipse, triangle etc. In this case between the surface of the part and the plasmatron there is a protection shield of refractory materials with the holes of preset shape.

Tests of four groups of specimens were carried out for simulation of the wear of the discretely strengthened layers obtained by the above-described methods (Figure 2):

a) plasma treatment without fusion of the surface is carried out in the direction coinciding with the wear direction; specimens are without a clearance between strengthened zones (No.1) and with a clearance, whose value is 1 / 4 (No.2) and 1 / 2 (No.3) of the strengthened zone width;

b) plasma treatment without fusion of the surface is carried out in the direction perpendicular to the direction of the wear; specimens are without clearance (No.4) and with them, whose value being 1 / 4 (No.5) and 1 / 2 (No.6) of the strengthened zone width;

c) plasma treatment with fusion of the surface is carried out in the direction perpendicular (Nos. 7, 8) and coinciding (No.9) with direction of the wear; specimens are without clearance (No.7) and with clearance (Nos. 8, 9) whose value is equal to 1 / 2 of the strengthened zone;

d) plasma treatment is carried out with cross displacement of the plasmatron in the perpendicular direction (No.10) and in the direction making up an angle of 45° with the direction of the wear (No.11);

in both cases the value of the clearance is 1 / 2 of the strengthened zone.

Wear tests of the specimens were carried out by the Hawort--Brinell method, the wet sand being used as an abrasive. Tests of each type of specimens lasted 1.5 h with intermediate weighing of the specimens every half an hour. As a result of the tests the kinetic wear diagrams were plotted and wear resistant coefficient was calculated by the formula $K_w = \Delta m_{st} / \Delta m_{ref}$, where Δm_{st} and Δm_{ref} are the losses of mass of the studied specimen and the reference specimen, respectively, under friction in preset conditions during the preset time period. Specimens of cast iron VCh-80 in the initial (non-strengthened) state of similar sizes were used as standard. Depending on the number of the specimen the coefficient of abrasive resistance of the specimens of cast iron VCh-80 after plasma treatment was calculated: 1 — 2.35; 2 — 1.95; 3 — 1.75; 4 — 2.57; 5 — 2.40; 6 — 2.08; 7 — 1.38; 8 — 1.62; 9 — 1.44; 10 — 2.87; 11 — 3.15.

The tests have shown that under strengthening in the direction perpendicular to the direction of wear the wear resistance of the specimens after plasma treatment without fusion is higher than under strengthening in the direction of the wear. In both cases the wear resistance coefficient increases together with the relative area of the strengthened surface, i.e. with decrease of the value of clearance between the tracks (Figure 3). A reverse dependence is established under strengthening with fusion. In this case under treatment without clearance between tracks and across direction of the wear the lowerest wear resistance in this experiment is established, which may be explained by the embrittlement of the surface, formation of microcracks in the sites of stress concentration near microprotrusions on the surface of the fused zone and separation of the cast iron particles under the action of the abrasive particles [2]. The presence of intermediate soft sites under treatment with clearance between fused tracks somewhat decreases microcracking and inconsiderably increases wear resistance (see Figure 3). The highest wear resistance coefficient is observed in specimens treated without fusion under cross displacement of the plasmatron, especially in the case when direction of the treatment makes up an angle of 45° with direction of the wear.

The performed studies have shown that by changing a relative area of the strengthened surface, varying treatment direction relative to the direction of the wear, selection of optimal modes of plasma treatment with application of the strengthened layer of a discrete structure it is possible to change within a wide range operational properties, and depending on specific conditions of loading to attain the most favourable combination of wear- and crack resistance of the working surface of high-strength cast iron parts.

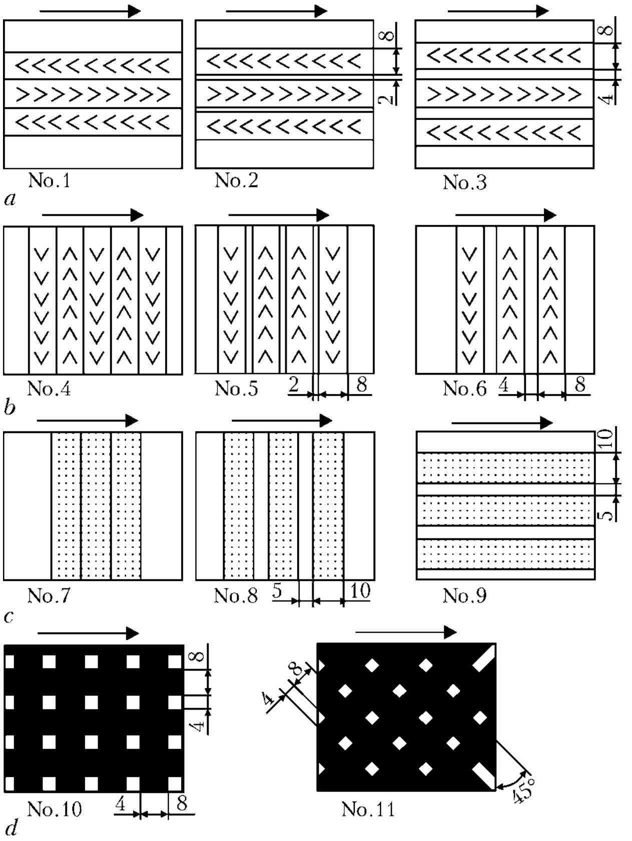

Figure 2. Scheme of plasma treatment (*a*–*d*) of specimens (Nos. 1–11) for abrasive wear tests (arrow shows the wear direction)

The established principles of plasma treatment of parts of high-strength cast iron with application of the strengthened layer of a discrete structure are implemented in practice for strengthening the guide bars of metal-cutting machine tools and rolls for grinding grain [9]. In the former case treatment is carried out with application of parallel strengthened tracks (see Figure 1, *a*). With optimal correlation of the area of non-strengthened and strengthened sites (1 / 3--1 / 4) one achieves at least 3 times increase of the wear resistance of the bars. When strengthening rolls 200–250 mm in diameter a cross displacement of the plasmatron at an angle of 45° to the axial line (see Figure 1, *c* and Figure 2, No.11) obtaining limited soft sites whose size is equal to a size of a single grain (wheat, barley, corn) is more preferable. In this case

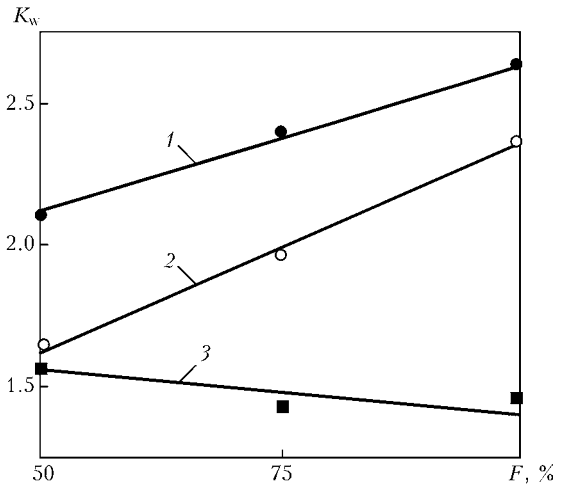

Figure 3. Effect of the relative area of the strengthened surface F on wear resistance coefficient K_w: *1*, *2* — treatment without fusion perpendicular and along wear direction, respectively; *3* — treatment with fusion perpendicular to wear direction

along with increase of wear resistance of rolls 2--2.5 times the seizure of the grain is improved and efficiency of its grinding is increased.

CONCLUSIONS

1. Plasma treatment of parts and tools of high-strength cast iron with application of a strengthened layer of a discrete structure facilitates considerable increase of abrasive wear resistance. In this case the wear resistance coefficient depends on the relative area of the strengthened surface, treatment technology (with fusion of the surface or without it), correlation of the treatment direction to the direction of wear.

2. Coefficient of abrasive wear resistance under plasma treatment without fusion increases with the relative area of the strengthened surface and decreases under treatment with fusion. This can be explained by a high brittleness of the fused layer with quasiledeburite structure and microcracking under the action of abrasive particles.

3. Higher wear resistance of the strengthened layer of a discrete structure is achieved under displacement of the plasmatron in the direction perpendicular to the direction of the wear as against treatment along the wear direction. The highest wear resistance is achieved under cross displacement of the plasmatron when treatment direction makes up an angle of 45° with the direction of the wear.

1. Samotugin, S.S., Leshchinsky, L.K. (2002) *Plasma hardening of tool materials*. Donetsk: Novy Mir.
2. Samotugin, S.S., Malinov, L.S., Samotugina, Yu.S. (2004) Increase of wear resistance of high-strength cast iron by plasma surface hardening. *Vestnik PGTU*. Issue 14.
3. Samotugin, S.S., Malinov, L.S., Samotugina, Yu.S. (2002) Effect of hardening method on hardness and crack resistance of high-strength cast iron. *Ibid*. Issue 12.
4. Lyashenko, B.A., Kuzema, Yu.S., Digam, M.S. (1984) *Hardening of metal surface by discrete structure coatings with increased adhesion and cohesion resistance*. Kiev: IPP.
5. Malinov, L.S. (1997) Production of microheterogeneous regular structure in steels by differentiated treatment methods. *Metallovedenie i Term. Obrab. Metallov*, **4**, 7–11.
6. Samsonov, V.I., An, V.S., Shnypkin, A.G. et al. (1989) Laser quenching of cast iron parts of machine-tools. *Ibid.*, **11**, 6–9.
7. Astashkevich, B.M., Voinov, S.S., Shur, E.A. (1985) Laser hardening of cylinder liners of locomotive diesels. *Ibid.*, **4**, 12--15.
8. Yakshtas, E.V., Sipavichyus, Ch.Yu., Kanapenas, R.V. (1989) Study of laser thermal hardening of cast iron guide machine-tools. *Lazernaya Tekhnologiya*, **7**, 21–31.
9. Samotugin, S.S., Malinov, L.S., Samotugina, Yu.S. et al. (2002) Increase of wear resistance of cast iron parts by differentiated (discrete) plasma treatment. In: *Proc. of Int. Sci.-Techn. Conf. on Surface Engineering and Product Renovation*. Kiev: ATM Ukr.

INFORMATION BANK OF STRUCTURAL MATERIALS AND WELDING CONSUMABLES*

Yu.V. KASHIRSKY and **A.S. ZUBCHENKO**
Federal State Unitary Company TSNIITMASh, Moscow, Russia

The bank provides information on 2,000 Russian (ex-USSR) and more than 21,000 foreign grades of materials, which include steels, cast irons, alloys and plastics, used in power engineering, metallurgy, transportation and heavy mechanical engineering. It contains knowledge on different weldability properties of these materials, their manufacture and supply, as well as their analogs.

Keywords: information bank, structural materials, grades, technological and service properties, manufacturing plants, welding consumables, weldability, welding processes

An automatic data bank (ADB) on materials used in mechanical engineering and power generation has been functioning at FSUC TsNIITMASh for more than 10 years now, being continuously improved and upgraded. The bank consists of three main parts, namely sections including general information on material grades; information on the technological and service properties of the studied materials and data on the companies, and manufacturing plants. In addition, a data base on currently manufactured plastics and polymer materials has been developed, which is compatible with the main data bank, but is practically completely self-sufficient.

The system is an information complex of factrographic type. To reach the above goals, the data bank control system fulfills the functions of forming the data base, its entering, enquiry processing and replying to them.

A promotional-teaching system in Russian and in English was additionally developed, which demonstrates the functioning of the metal data bank and user actions on a concrete example.

The bank structure incorporates the data given in the metal and polymer material certificates. Certificate requisites are used as explanation of the kind of entered parameter.

A lot of attention was given to the degree of data validity for all the information entered into the bank,

---

[*] Based on the paper delivered at the 2nd International Conference «Mathematical Modelling and Information Technologies in Welding and Related Processes» (Katsiveli, Ukraine, Sept. 13--17, 2004).

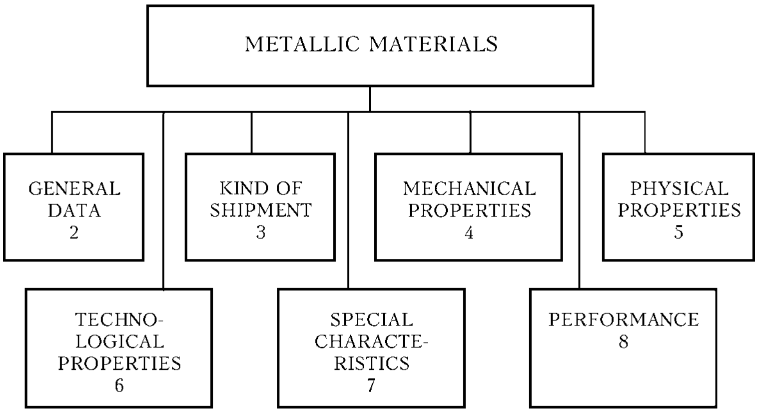

Figure 1. Block diagram

and there are references to the respective sources (GOSTs, RTM, TU, reports, technical and reference literature). The list of references used consists of more than 800 items.

The metal data base contains sufficiently complete information on approximately 2,000 local materials, including more than 100 cast irons and 500 alloys (high-temperature, heat- and corrosion-resistant, nickel-base, aluminium, titanium, magnesium and copper). The data describes their condition by approximately 300 parameters. It is natural that not all the indices are determined and are present in the information sources for each material grade. Lacking data are added after studying new scientific-technical information and involving TsNIITMASh specialists-technologists and metallurgists in development of the bank. User manual and description of the steel grading system in the main industrialized countries are appended as reference material.

Information on manufacturing plants in CIS countries is taken from the information leaflets of the plants proper [1, 2] and some journals. The same certificate was used in processing foreign materials as that for the local materials. Data on foreign analogs of the local grades were the first to be entered into the data base. In addition, the composition and purpose were entered, and for other materials also the data helping to perform material replacement in practice and evaluating its effectiveness.

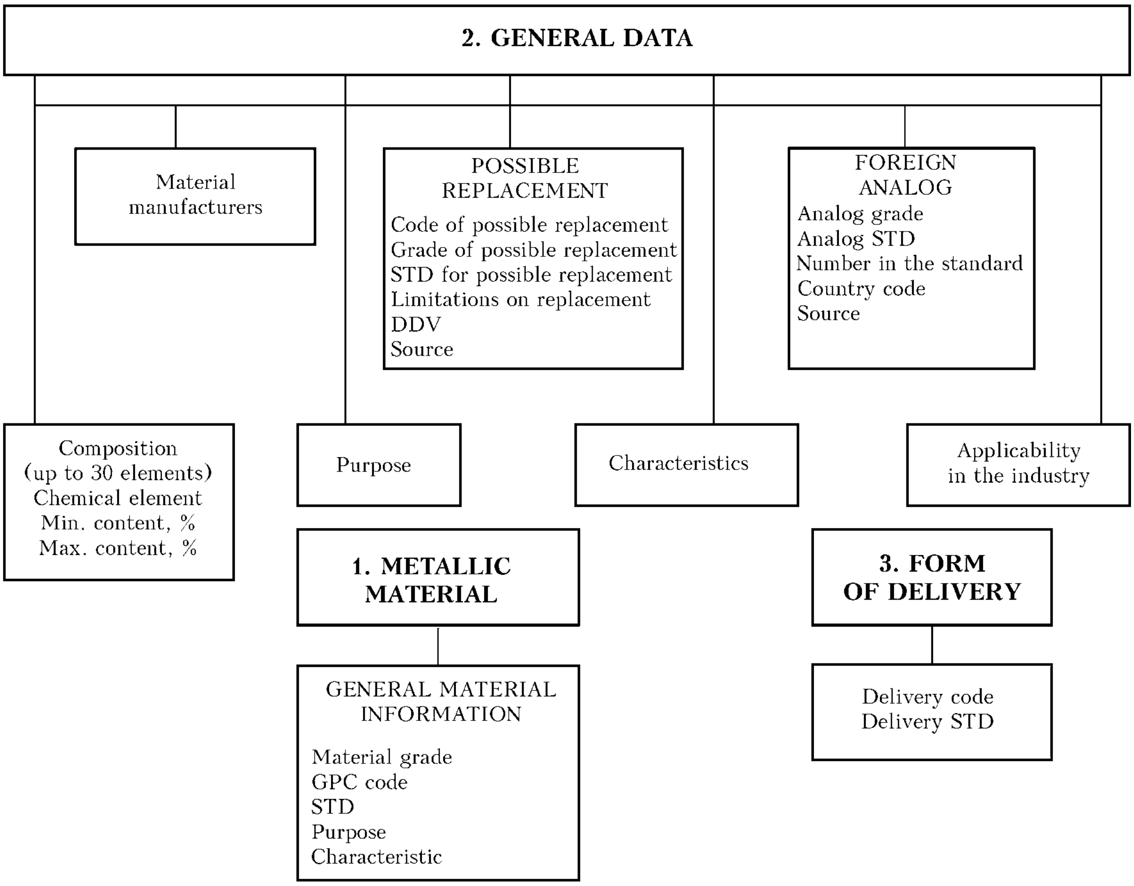

Figure 2. General information: STD — science-technology document, namely GOST, OST, TU; DDV — degree of data validity; APC — All-Union Product Classifier

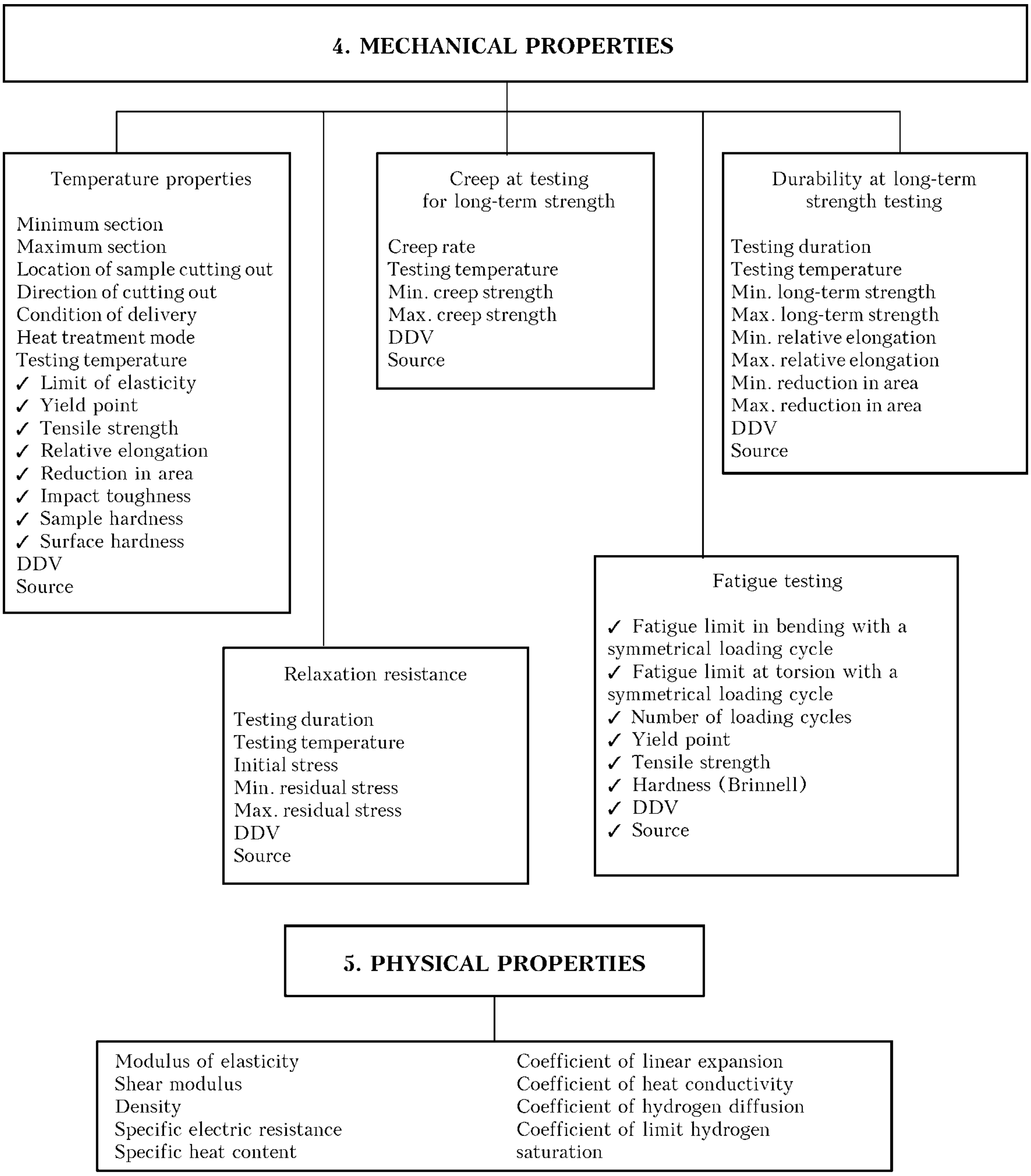

Figure 3. Mechanical and physical properties. Ticked off parameters are assigned by their minimum and maximum values. The following information is given for each physical parameter: its value at different testing temperatures, degree of data validity (DDV), source

Altogether the data on more than 21,000 foreign grades were entered.

The main data on foreign steels and alloys was taken from [3–5].

The main blocks of the metal data system and detailed interpretation of the subsystems on the technological properties are given in Figures 1–6.

As regards welding properties, special programs were developed allowing the steel grade, welding processes and need for preheating to be determined by the composition data. Similar programs were made for determination of such physical properties as hydrogen diffusion coefficient and coefficient of limit hydrogen saturation at different testing temperatures proceeding from the composition data. A subsystem has been developed on mutual weldability of materials.

A schematic of combination variants of different steels and alloys was proposed to develop a procedure for automatic analysis and issuing recommendations on their weldability.

All the materials were divided into 7 classes and 11 subclasses. The welding process and required electrodes, fluxes and welding wire are given for each variant, and there are references to the respective standards and reference books. The data covers almost all local (former Soviet) grades, included into the bank.

In the case of appearance of new materials, TsNIITMASh welding experts-specialists will determine

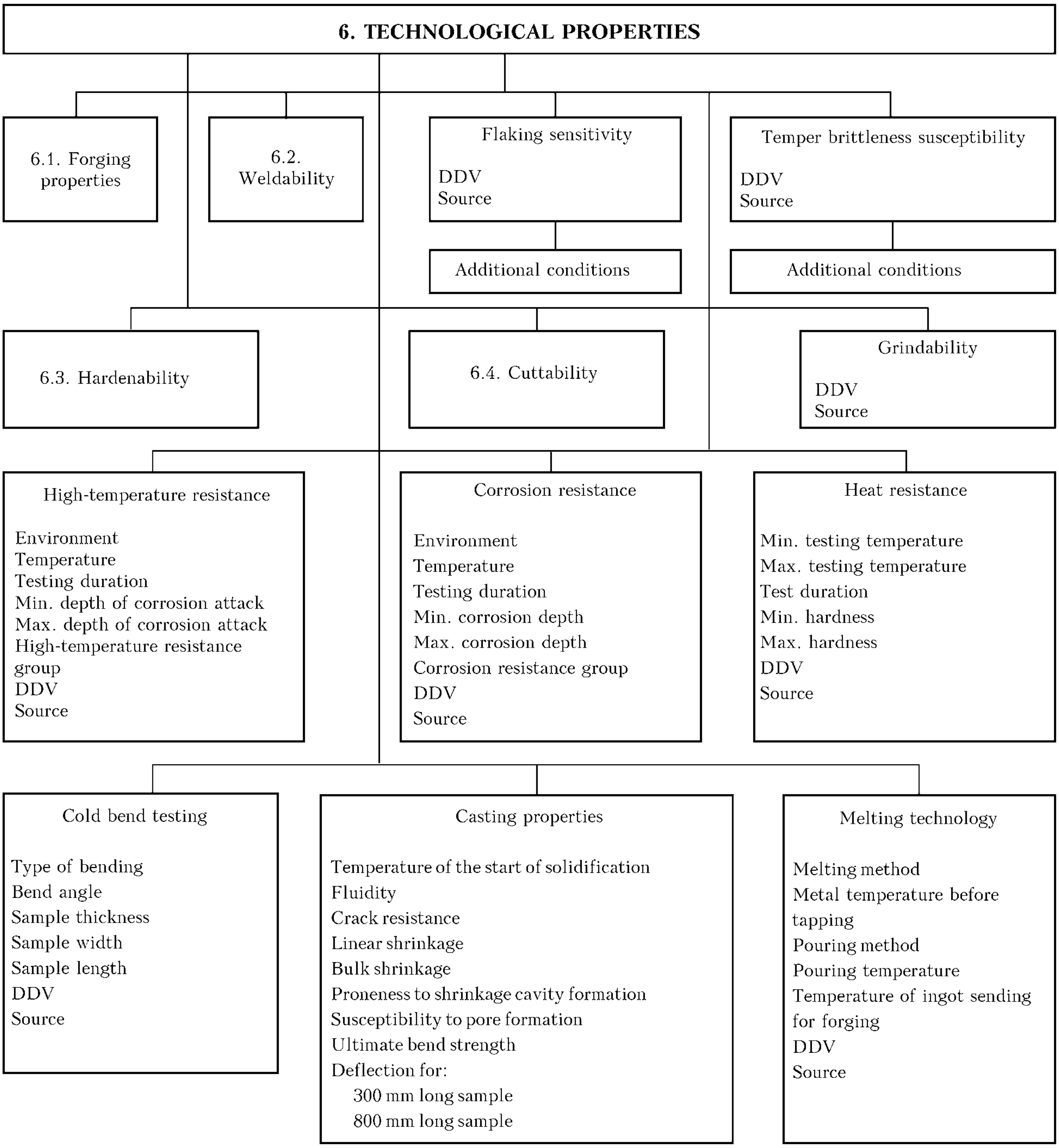

Figure 4. Technological properties (minimum and maximum values, degree of data validity (DDV), and source are given for the casting properties)

to which group these materials belong, and appropriate recommendations will be automatically issued for them.

As regards the plastics base, its structure is similar to that of the metal bank, but is somewhat simpler, namely the number of characteristics entered into it is about 100, it contains about 500 different polymers. The information for it was taken from [6], data of the Institute's departments and some other sources.

PC user interacts with the data bank as follows.

After entering the program, it is determined what part of the bank is to be used, namely the main (metal bank) or plastics base.

In the first case, the user goes over to the main menu of the metal bank:

1. Local materials.
2. Foreign materials.
3. Companies and manufacturing plants.
4. Using the dictionaries.
5. Using the system.
6. Exiting the system.

Selection of items 1–3 of the main menu leads to transition to the main menus of the respective sections.

Item 4 supports the use of dictionaries, which contain the lists of the types of system parameters with codes or abbreviations, used in ADB.

Item 5 includes the main procedures ensuring the system existence, its testing (checking the correctness and reliability of functioning), working with passwords (information protection from unauthorized user

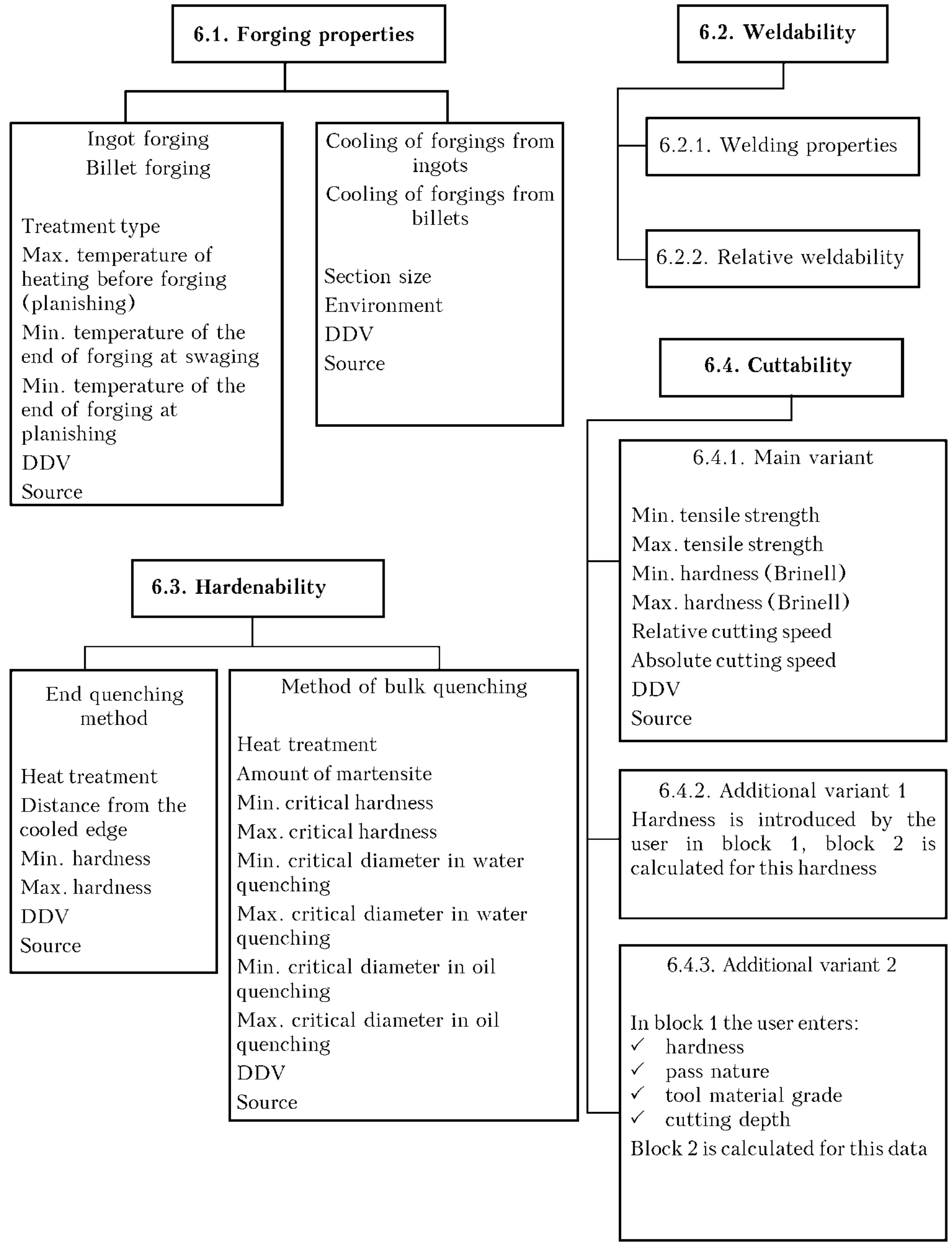

Figure 5. Technological properties. Individual blocks

intervention), base compression (for computer memory saving), system archiving and unarchiving, special functions, using a diskette.

The main menu for the local materials consists of the following items:

1. Viewing materials.
2. Entering and correction of materials.
3. Inquiries.
4. Using the bases.
5. Classifier.
6. Retro.
7. Exit.

Item 1 of the menu allows viewing the necessary properties of the selected material grade (direct inquiry).

Item 2 of the menu can be used to enter new or correct the available data on each material grade.

Item 3 of the menu enables the user to find those material grades in the base, which satisfy the conditions specified by him (inverse inquiry).

Results of inquiry processing can be viewed on the display screen or printed out.

Item 4 designed for the system programmer enables changing the structure of the bank and its sections, and it is not recommended to a regular user without special training to enter this section.

Item 5 enables choosing individual material classes, and, if required, working only with them, this increasing the speed of obtaining the information and facilitating its use.

Item 6 of the menu opens up an index, which allows identifying materials having different designations.

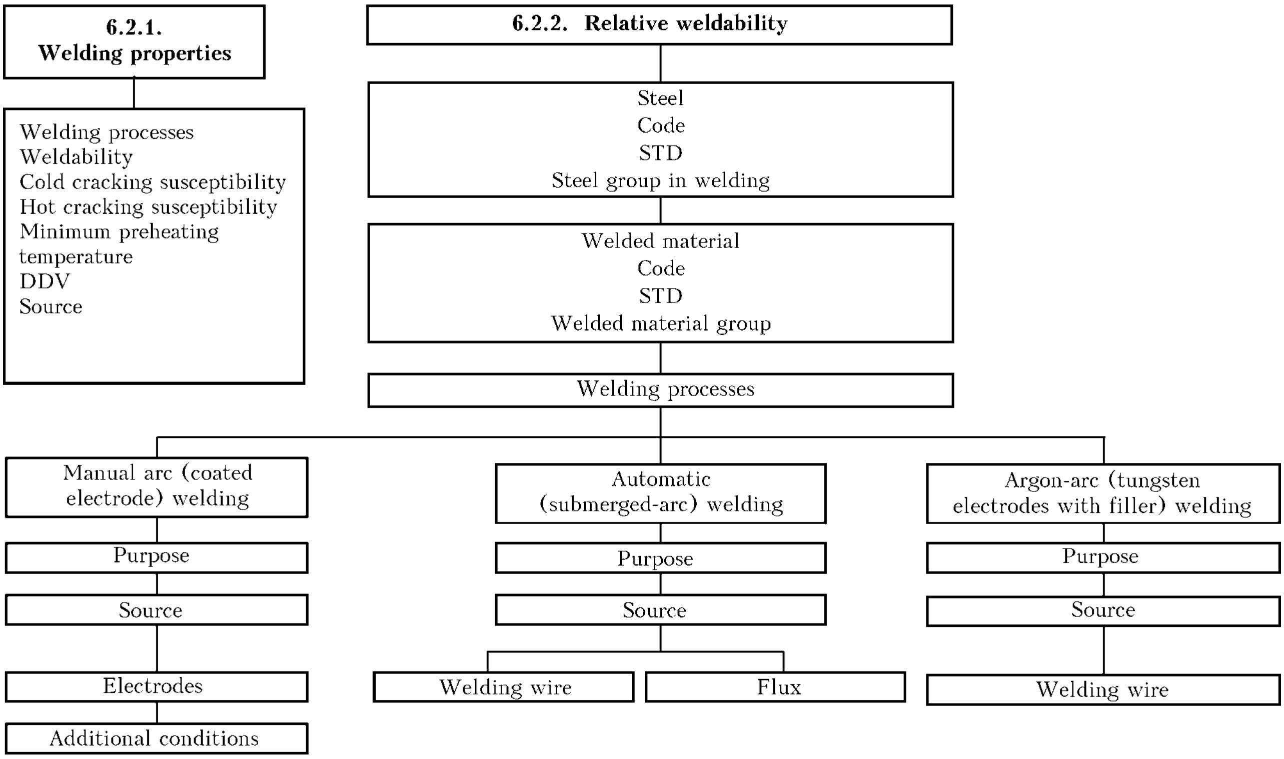

Figure 6. Weldability

The main menus for foreign materials and manufacturing companies are similar to the previous section, but they lack items 5 and 6.

These menus can be used to obtain information on steels, alloys and cast irons in industrially developed countries of the world, as well as companies, producing mechanical engineering materials, including the forms of their delivery, steel classes and (or) grades, manufactured in the plant, main characteristics of the grades, information about the products made of these materials.

As regards the plastics data base, its main menu coincides completely with that for ADB on metallic materials; compared to the earlier given main menu, the main menus on the local and foreign-made polymers lack «Retro» item, and the menu for manufacturing companies also lacks «Classifier» item.

Developed menu takes the user through all the stages of using the data bank, while allowing to cancel any earlier planned action at any moment.

The simplicity of using the data bank, not requiring any preliminary knowledge or PC skills should be particularly noted.

Information on this ADB and its capabilities is given in [7, 8].

The bank is already being used as an information-reference tool in mechanical engineering and power plants of Russia and Ukraine, and formed the basis for the second edition of «Grade List of Steels and Alloys» [9], published in 2003. This book contains information about approximately 600 material grades the most widely used in production.

Information bases on metal materials and plastics are included into the State Register of data bases and into the annual catalog «Data Bases of Russia».

Use of information accumulated in ADB allows simplifying and accelerating the research on development of individual information technologies. Using the data on service properties of materials, procedure of their properties prediction and the respective program package developed by FSUC TsNIITMASh, ADB enables studying and assessing the residual and fatigue life of the equipment, and issuing recommendations on extension of the service life of materials in critical structural elements.

1. (2003) *Metal A, B C. Works. Trading companies*. Refer. book. Dnepropetrovsk-Moscow: Metall-Kurier.
2. (2004) *Metal trading. Russia*. Refer. book. Moscow: IIS Metallosnabzh. i Sbyt.
3. Wegst, C.W. (1992) *Clue to steels*. Moscow: Giprokhim.
4. Wegst, C.W. (2001) *Stahlschluessel*. Marbach: Stahlschluessel Wegst.
5. (1992, 1993, 1995) *International translator of current steels and alloys*. Ed. by V.Ya. Kershenbaum. Vol. 1–4, Book 1, 2. Moscow: Intak.
6. (1993) *International translator of current plastics*. Ed. by V.Ya. Kershenbaum. Moscow: Intak.
7. Kashirsky, Yu.V., Koloskov, M.M. (2000) Information bank on mechanical engineering materials and treatment conditions. *Tyazh. Mashinostroenie*, **4**, 12–19.
8. Kashirsky, Yu.V., Koloskov, M.M. (2000) Information bank on mechanical and power engineering materials and treatment conditions. *Such. Mashynobuduvannya*, 3/4 (**1/2**), 81–87.
9. Zubchenko, A.S., Koloskov, M.M., Kashirsky, Yu.V. et al. (2003) *Grade list of steels and alloys*. Ed. by A.S. Zubchenko. Moscow: Mashinostroenie.

CALIBRATION OF TRIANGULAR OPTICAL SENSORS

F.N. KISELEVSKY and **V.A. KOLYADA**
E.O. Paton Electric Welding Institute, NASU, Kiev, Ukraine

Procedure of calibration of triangular optical sensors used in automation of welding processes has been offered. It allows calibration of sensors after their assembly into welding equipment under the industrial conditions.

Keywords: arc welding, welding units, triangular optical sensor, standard article, laser generator of line, radiation plane, mathematical model, transformation of coordinate systems, perspective transformation

An enhanced interest to optical sensor systems as means for automation of production welding processes is being observed in the recent time. Optical systems based on triangular sensors where the method of light section is employed are considered most functional. Such systems may be used both for tracking butt with groove preparation and for control of technological parameters of the welding conditions on the basis of the obtained data on groove preparation geometry. Requirements to the measurement accuracy for geometrical parameters of the butt are usually rather tough and the sensor should be properly calibrated for obtaining the desired accuracy.

Triangular optical sensor consists of two main components: video camera and laser generator of line (LGL). The third element is needed for calibration, which is a standard article of a certain type located to the working zone of the sensor. In the general case the task of the sensor calibration is reduced to unification of all three components into a system where parameters of one element (standard article) are known in advance.

In the work [1] it was proposed to use parallelepiped with a cut-out imitating a rectangular gap of the known height and width as a standard article. Mathematical model of the inner components of the sensor necessary for calibration is designed on the basis of the assembly drawing of the device. The main disadvantage is that the mathematical model of inner components is idealized.

Calibration procedure of the triangular optical sensor may be divided into two tasks: calibration of video camera and determination of a mutual arrangement of the video camera and a radiation plane of the laser generator of line.

Methods for calibration of video camera using a plane template as a standard article are proposed in the works [2, 3]. Several images of the template with different mutual arrangement of the video camera and the template are the input data. As applied to the task of calibration of the sensor assembled into the welding unit the main disadvantage of the methods proposed in [2, 3] is the necessity to change mutual arrangement of the video camera and the standard article.

The proposed method for calibration of video camera does not require changing of the mutual arrangement of the standard article (Figure 1) and the video camera for obtaining the initial data. Net consisting of similar cells of the same size is applied on the upper plane of the article. For calibration the standard article is placed into the working area of the sensor so that the central lines of the net coincide as full as possible with the central axes of the image on the screen and a distance from the sensor to the upper plane of the standard article is within the allowances for arrangement of the sensor relative to the surface of the object to be measured. A mathematical model is constructed describing a dependence of the image in the screen on the parameters of the video camera object as well as a mutual arrangement of the video camera and the standard article. Three coordinate systems are selected: for the standard article, video camera and the image.

Classical methods of transformation of the coordinate systems [4] by means of a consecutive multiplication of rotation and transfer matrices allow forming a matrix for transformation from the coordinate system of the camera into the coordinate system of the standard article A_c. Input parameters of the model are used in formation of the matrix A_c: rated values of the sensor components and peculiarities of the sensor design. Perspective transformation is used for construction of the transformation from the camera coordinate system into the coordinate system of the image [4]. Nodal points of the net are determined on the image of the standard article (Figure 2). Then under iteration change of the parameters α_c, β_c, γ_c, x_c, y_c, z_c determining a spatial arrangement of the camera relative to the standard article such values are found, under which a root mean square deviation be-

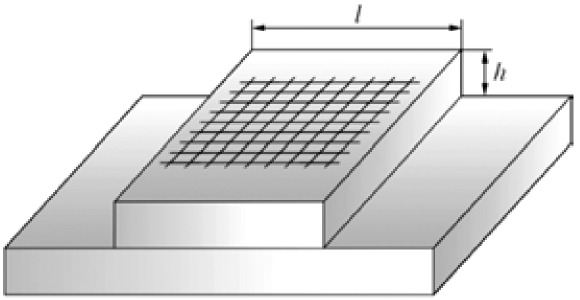

Figure 1. Appearance of standard article

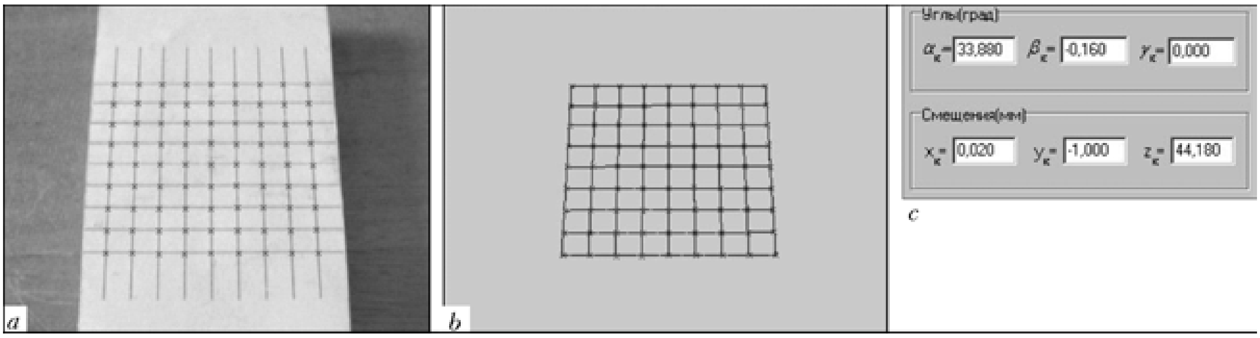

Углы(град)
$\alpha_{к}$= 33,880 $\beta_{к}$= -0,160 $\gamma_{к}$= 0,000

Смещения(мм)
$x_{к}$= 0,020 $y_{к}$= -1,000 $z_{к}$= 44,180

Figure 2. Visualization of camera calibration process: *a* — finding of nodal points of net on the image of standard article; *b* — application of net model on the found nodal points of real image net; *c* — numerical results of identification of the spatial camera arrangement

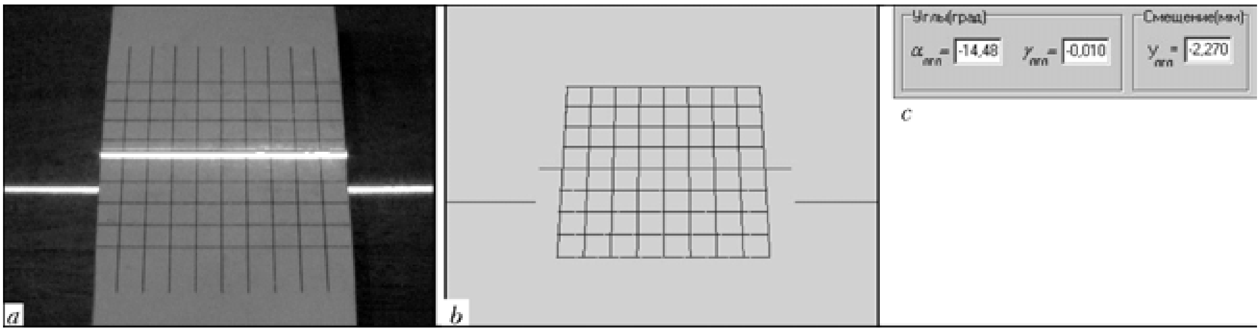

Углы(град)
$\alpha_{лгп}$ = -14,48 $\gamma_{лгп}$ = -0,010

Смещение(мм)
$y_{лгп}$ = -2.270

Figure 3. Visualization of process for determination of radiation plane arrangement: *a* — measured contour of light band; *b* — model of projection contour; *c* — numerical results for identification of radiation plane arrangement

tween coordinates of the nodal points of the simulated net and the found nodal points of the real image net are minimal.

At the next stage of the sensor calibration process it is necessary to determine a position of the LGL radiation plane relative to the standard article. A matrix for transformation from the LGL coordinate system into the coordinate system of the standard article A_{LGL} is formed. As in the case with the camera the iteration changes of the parameters α_{LGL}, γ_{LGL} and y_{LGL} determining a spatial arrangement of the radiation plane relative to the standard article allow finding such values of the parameters under which a root mean square deviation between coordinates of the points of the simulated projection contours and the measured coordinates of the contour points is minimal (Figure 3).

Therefore, spatial arrangement of the camera relative to the standard article, arrangement of the LGL radiation plane relative to the same standard article and transformation from the coordinate system of the camera into the coordinate system of the image on the screen are determined. The obtained parameters determining a spatial arrangement of the camera and the LGL plane relative to the standard article unite the video camera, the LGL radiation plane and the image into a single system. Thus, the coordinate points of the contour are transformed from 2D coordinate system of the screen image into the 3D coordinate system of the standard article, which permits measuring a real arrangement of any points of the contour relative to the center of the net on the surface of the standard article.

Correctness of the sensor calibration results was evaluated by comparison of the results of manual and programmed measurements of geometrical sizes of several different objects. The obtained experimental data allows a conclusion that accuracy of the programmed measurement of the object geometrical parameters is within the designed, i.e. this calibration method of triangular optical sensors yields the correct results.

The main advantages of the considered method for calibration of triangular optical sensors are as follows:

- mutual arrangement of the sensor and the standard article is not necessary in the process of calibration, consequently it is not difficult to carry out calibration in the production conditions after assembly of the sensor into the welding unit;
- the calibrated sensor is rather accurate measuring device (in this case with resolution power of the image 400 × 300 pixels the measurement error does not exceed ±0.2 mm).

The developed mathematical model and the tools constructed on its basis allow calibrating triangular optical sensors intended for operation in the composition of automated welding units, which is confirmed by the results of the experimental studies.

1. Powell, B.W., Kennedy, L.Z., Burroughsa, I.A. *Weld-bead profilometer*. Pat. 5264678 USA. Publ. 23.11.93.
2. Zhang, Z. (2000) A flexible new technique for camera calibration. *IEEE Transact. on Pattern Analysis and Machine Intelligence*, 22(**11**), 1330–1335.
3. Novikov, S.O., Lebedev, O.A., Zakharenko, G.V. (2003) Measurement and examination of 3D objects in conditions of incomplete information. *Inform. Tekhn. i Vych. Sistemy*, **2**, 61–63.
4. Ammeral, L. (1992) *Principles of programming in computer graphics*. Moscow: Sol Sistem.

INFORMATION SYSTEM FOR WELDING OF TITANIUM AND ITS ALLOYS*

A.B. LESNOJ, O.G. KASATKIN and **V.N. ZAMKOV**
E.O. Paton Electric Welding Institute, NASU, Kiev, Ukraine

Possibilities of using specialised software for welding titanium and titanium alloys are considered. The offered information system contains data on methods and parameters for welding butt, fillet, T- and overlap joints of different thickness, on welding consumables (electrodes, wires, fluxes), as well as reference data on titanium alloys, allowing selection of titanium alloys depending upon the service conditions of a welded structure.

Keywords: arc welding, titanium alloys, information systems, properties of alloys, welding consumables

Titanium is a promising structural material due to its high corrosion resistance, strength and small specific density. For ten more years it was mainly used in rocket-space and aviation engineering, military shipbuilding and other branches of war materiel. Today titanium occupies the third place as to the volume of its application in welded structures and is widely used in power machine-building, oil refining industry, medicine after steel and aluminium.

It is noteworthy that the volume of titanium used in welded structure is determined by technological possibilities of its welding. Main problem in fusion welding of titanium is related to its high chemical activity. When heated above 500–600 °C titanium starts to be saturated with hydrogen, oxygen, nitrogen and other impurities, which considerably decrease its ductility, toughness, fatigue resistance, facilitate retarded failure of titanium structures and decrease corrosion resistance. A possibility to obtain quality welded joints is determined by a correct selection of welding method and parameters. Solution of this problem may be essentially facilitated by the use of a specialized software «Information System for Welding Titanium and Its Alloys» developed at the E.O. Paton Electric Welding Institute of the National Academy of Sciences of Ukraine.

The proposed information system (IS) contains information on the methods and conditions of welding of titanium butt, fillet, tee and lap joints of 0.8–400 mm thick. The proposed IS contains data on EBW, eight methods of arc welding and three methods of electroslag welding. Depending on the type of joint and metal thickness the IS proposes one or two appropriate methods of welding to the user. For example, when selecting a butt joint (Figure) the IS presents information on the available range of thicknesses (0.8-400 mm) of the parts to be welded.

Once the thickness of the parts to be welded is preset (3 mm) the program presents a list of welding methods on which the database stores the information. In the case from the Figure, the welding may be carried out by the electron beam, submerged arc with consumable electrode or in inert gas in automatic mode, as well as using manual or mechanized TIG welding, immersed-arc TIG process or filler flux-cored wire.

For each method of welding the IS proposes one or several ways of groove preparation. For each variant of gap the program gives data on geometrical parameters and conditions of welding (for example, welding mode, diameter of the tungsten electrode and wire, the number of passes, kind and consumption of the shielding gas).

The IS also contains information on properties of commercial titanium and its welded α-, pseudo-α-, β- and $(\alpha + \beta)$-alloys. The data include chemical composition, physical properties, mechanical properties at normal and increased temperatures, corrosion resistance in natural conditions and corrosive media, mechanical properties of welded joints produced by different methods of welding, data on rolled stock sections and heat treatment parameters.

The system also contains information on welding consumables (flux-cored and solid wires, tungsten electrodes, fluxes) and rational spheres of their application.

The IS provides a possibility to select titanium alloy for welded parts regarding their operation. A necessary level of strength at preset operational temperature considering possible variants of the environment may be prescribed as parameters for selection of the alloys.

The IS also contains a section of general information on titanium alloys, their application and peculiarities of welding.

The IS is intended for designers and engineers working in project and construction organizations and dealing with welded structures of titanium alloys and

---

* From materials of the report presented at the Second International Conference «Mathematical Modelling and Information Technologies in Welding and Related Processes» (Katsiveli, Ukraine, Sept. 13–17, 2004).

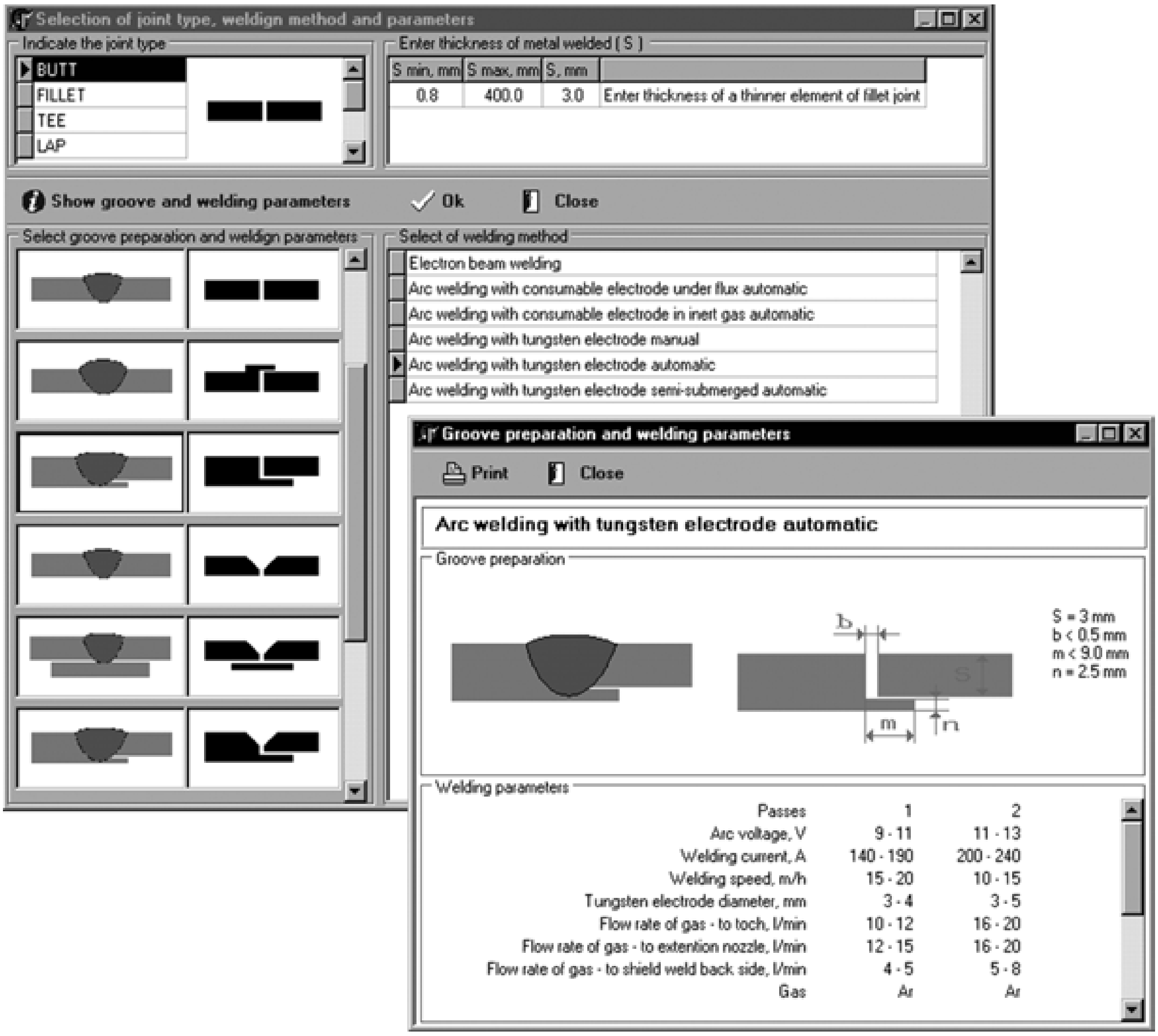

Indicate the joint type

- BUTT
- FILLET
- TEE
- LAP

Enter thickness of metal welded (S)

S min, mm	S max, mm	S, mm	
0.8	400.0	3.0	Enter thickness of a thinner element of fillet joint

Select groove preparation and weldign parameters

Select of welding method

- Electron beam welding
- Arc welding with consumable electrode under flux automatic
- Arc welding with consumable electrode in inert gas automatic
- Arc welding with tungsten electrode manual
- Arc welding with tungsten electrode automatic
- Arc welding with tungsten electrode semi-submerged automatic

Arc welding with tungsten electrode automatic

Groove preparation

S = 3 mm
b < 0.5 mm
m < 9.0 mm
n = 2.5 mm

Welding parameters

Passes	1	2
Arc voltage, V	9 - 11	11 - 13
Welding current, A	140 - 190	200 - 240
Welding speed, m/h	15 - 20	10 - 15
Tungsten electrode diameter, mm	3 - 4	3 - 5
Flow rate of gas - to toch, l/min	10 - 12	16 - 20
Flow rate of gas - to extention nozzle, l/min	12 - 15	16 - 20
Flow rate of gas - to shield weld back side, l/min	4 - 5	5 - 8
Gas	Ar	Ar

Selection of method and parameters for butt joint

technologies of their production. The program may also be useful for training of students.

The software is functioning in Windows 9x / Me / 2000, 15 Mb of disk space being needed for installation.

ELECTRODES FOR MANUAL ARC WELDING OF HEAT-RESISTANT STEELS WITH 9 % Cr*

L.S. ZAKHAROV and **A.R. GAVRIK**
E.O. Paton Electric Welding Institute, NASU, Kiev, Ukraine

Short information is given on development of coated electrodes for welding heat-resistant steels with 9 % Cr. The electrodes provide a lower content of diffusion hydrogen in the deposited metal and high physico-mechanical properties of the weld metal.

Keywords: arc welding, heat-resistant steels, coated electrodes, slag systems, diffusion hydrogen, welded joints, mechanical properties

Development of new designs of power units of increased capacity is caused by a necessity to increase working parameters of steam boilers. The use of super-critical parameters (steam pressure of up to 30 MPa, above 600 °C temperature of the overheated steam) provides a 10 % increase of productivity, decrease of fuel consumption, limited emissions of harmful gases into the atmosphere. On the whole it allows decreasing costs for electric energy production by 15--20 %.

However, the currently employed low-alloyed Cr--Mo steels of 12KhM, 15Kh1MF, 12KH2MFB type are characterized with heat resistance only to the temperature of 565 °C.

In the recent times steels with 8–12 % Cr additionally alloyed with Ni, Mo, Co, V, Nb gain a wider application in boiler manufacture abroad. The work on mastering production of steels of 10Kh9NMFB type for manufacturing pipes, pipelines, forged articles, castings of boiler parts has also been initiated in Ukraine. Increase of heat resistance in this case is provided by additional alloying of steel with niobium (about 0.05 %), vanadium and nitrogen (about 0.06 %) accompanied by a precipitation of fine-dispersed hardening vanadium and niobium carbonitrides. Electrodes of TsL-57 grade previously developed for welding of steel 10Kh9NMFB did not provide the required level of strength characteristics of the deposited metal, namely it is considerably lower than of steel 10Kh9NMFB (Table). Welded joins produced by the above electrodes need long-term heat treatment (760 °C, 10 h). In this connection the experts of the E.O. Paton Electric Welding Institute conducted studies on development of new electrodes.

Comparison of mechanical properties of steels and weld metal produced by electrodes TsL-57 and ANL-4

Object of study	*Tensile strength, MPa*	*Yield strength, MPa*	*Elongation, %*	*Impact toughnes KCV, J/cm^2*
Steel 10Kh9NMFB	580--640	415–520	14	41
Electrodes TsL-57	539	343	18	49
Electrodes ANL-4	789--814	669–693	12.8–16.0	42.6--53.3

In addition to traditional difficulties in welding of martensite steels because of their high tendency to formation of cold cracks, in this case there is also a necessity to provide a precision alloying of the metal deposited with niobium and nitrogen. Since currently there are problems with mastering of production of new grades of alloyed welding wires a scheme of allowing the weld metal through coating was chosen in development of new electrodes for welding steel 10Kh9NMFB.

Preliminary calculations have shown that to provide the required chemical composition of the deposited metal the electrode coating should contain about 50 % of the powders of alloying elements and respectively 50 % of gas- and slag-forming components.

One of the main requirements in welding of martensite steels is a tough restriction of the content of diffusion hydrogen in the deposited metal. For welding of chromium steels electrodes with the coating of two types are used: carbonate-fluorite (electrodes TsL-32, TsL-41, KTI-9A and others) and rutile-carbonate-fluorite (TsL-51, TsL-57). In both cases 30–50 % of fluor-spar with content of marble from 13 to 60 % are introduced into the coating. To check a possibility of using the well-known slag systems the test lots of electrodes with different correlation of the marble, fluorite and rutile content in the coating were produced. In this case their total quantity remained constant and made up 50 % of the mass of the dry charge. The conducted experiments have shown that due to a limited content of slag-forming components one failed to decrease the quantity of the diffusion hydrogen in the deposited metal below 2 cm^3 / 100 g of metal with any correlations of slag forming components.

---

* This material was presented at the 3rd International Conference on Welding Consumables in CIS Countries (Dnepropetrovsk, June 1--4, 2004).

At the same time welding with the ESAB electrodes of OK76.28 grade and Boehler electrodes FOXC9MV intended for welding of steel P91 (10Kh9NMFB type) resulted in that the content of diffusion hydrogen did not exceed 1 cm^3 / 100 g. Therefore, it was necessary to take additional measures for decreasing of the quantity of diffusion hydrogen in the deposited metal.

It is known that absorption of hydrogen by a molten metal decreases if hydrogen is fixed into fluoric hydrogen by the following reactions:

$$2CaF_2 + SiO_2 \rightleftarrows 2CaO + SiF,$$

$$SiF_4 + H_2O \rightleftarrows 2HF + SiO + F_2,$$

$$CaF_2 + H_2O \rightleftarrows CaO + 2HF.$$

Probability of these reactions is especially high within the temperature interval 1500--2500 °C. It would be interesting to use the raw material components providing formation of gaseous compounds of fluorine as early as at the stage of coating heating. Silicon-fluoric sodium and sodium fluorine aluminate whose dissociation proceeds at the temperature 800--900 °C may serve as such components.

$$Na_2SiF_6 \rightleftarrows 2NaF + SiF_4,$$

$$Na_3AlF_6 \rightleftarrows 3NaF + AlF_3.$$

This helps not only fixing hydrogen but also decreasing a partial pressure of the water steam.

The test lots of electrodes with different content of silicon-fluoric sodium and cryolite were produced to confirm the above. The tests have shown that with their content in the coating at the level of 25–30 % the quantity of the diffusion hydrogen in the deposited metal decreases down to 0.8–0.9 cm^3 / 100 g. Rutile-carbonate-cryolite system providing higher welding and technological characteristics of electrodes was chosen as the basis. The conducted studies underlay the development of electrodes of ANL-4 grade.

The above electrodes were used to weld butts of steel 10Kh9NMFB 20 mm thick for determining service characteristics of the welds. The welding was conducted with preliminary and accompanying heating to the temperature 220--230 °C. Under flaw detection of butts during metallographic studies neither cold cracks nor other defects were detected in the weld metal. Mechanical properties of the weld metal after heat treatment (720 °C, 2 h) are at the level of the parent metal (see the Table).

Therefore, the developed electrodes ANL-4 with rutile-carbonate-cryolite coating provide a decreased content of diffusion hydrogen in the deposited metal. Besides, they are distinguished with good welding and technological characteristics under welding in all spatial positions and provide satisfactory mechanical properties of the weld metal in welding of heat-resistant steel 10Kh9NMFB.

Prof. J. Norrish — winner of the E.O. Paton Prize of IIW

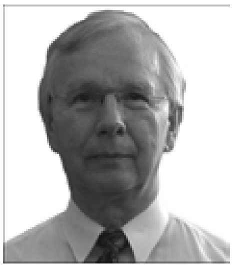

By the results of voting of IIW Technical Committee members with participation of the delegates of the National Welding Committee of Ukraine the E.O. Paton Prize for 2005 was awarded to Mr. J. Norrish, Professor of the Australian University of Wollongong, Chairperson of the Chair of Welding and Joining of Materials. The Prize and memorial token will be presented during the opening ceremony of IIW Annual Assembly in Prague on July 10, 2005. Given below is a short biography about the activity of Prof. J. Norrish in the welding field.

John Norrish commenced his career in welding technology as a student apprentice with Rubery Owen and Company in the UK where he worked on the development of electroslag welding, electroslag refining and high productivity GMA.

In 1969, after completing post graduate studies at the University of Aston in Birmingham he joined the BOC group in the UK as welding process research engineer. He originally worked on plasma welding research and the development of single phase GMAW welding equipment for the car repair industry. As a result of this work British Oxygen produced the first purpose designed «single knob» GMAW package (Autolynx) for the industry. He was instrumental in optimizing the short circuit transfer characteristics and design of this equipment to operate with 100 % CO_2 shielding. He later became Technical Manager of BOC Arc Equipment with responsibility for process and equipment research and development.

During this time he was responsible for the introduction of the first electronically regulated, computer controlled welding power supplies. In cooperation with TWI and Cranfield University practical control algorithms for synergic MIG welding were established and BOC produced a commercial power source which was employed in the fabrication of submarines and nuclear power plant. He was also involved in sponsoring early work on welding fume at Bradford University and developed and patented an on-torch fume extraction nozzle. He was involved in the early research into robotic welding, assisting Hall Automation to develop the first GMAW robot package in the UK. He also represented BOC-UK on a task force which rationalized the range of shielding gas compositions offered by its international partners.

He played an active role in the professional welding body (TWI) in the UK promoting process developments in arc processes, automation and computer control. In 1981 he joined BOC's associate company (CIG) in Australia and became Consultant Welding Engineer for CIG in Queensland. He spent three years assisting industry with the development of welding procedures, technology audits, consumable development, surfacing technology, introduction of robotics, and weld failure analysis.

Much of this time was spent in the mining industry in central Queensland. During this time he was an active member of the local WTIA branch committee and editor of the monthly newsletter.

He returned to the UK in 1985 to take up a position as senior lecturer at Cranfield University, where he later became Head of the Welding Group. In this role he was responsible for postgraduate education and research in welding processes and during his 10 years at Cranfield he was responsible for the supervision of more than 50 Masters and Doctoral research students. He continued his applied research activities and promotion of advanced welding developments.

The applied research which he was responsible for at Cranfield included shielding gas optimization, metal transfer control, welding power source design, weldability of HSLA steels, and mechanized welding of pipelines. His industrial clients included Rolls Royce, BOC Gases, ESAB, Migatronic, European Marine Contractors, and BP. He managed an EU research program on process monitoring for robotic welding and initiated two major UK projects on in process monitoring for the automotive industry and advanced joining techniques for the aerospace industry. During this time he was also technical editor of the journal «Welding & Metal Fabrication» and in this role he organized a conference on Synergic MIG Welding at Cranfield in 1987. He was active in the professional division of TWI and became chairman of the education committee as well as serving on the membership committee, and council.

He moved to the University of Wollongong in November 1995 to take up the newly established CRC Chair in Materials Welding and Joining. At Wollongong he is responsible for coordinating welding research and education activities, in particular those related to the Australian CRC in Welded Structures.

Current research activities include automation and mechanisation, robotic welding, pipeline girth welding, GMAW process and power source optimisation, weldability of HSLA and coated steels and welding fume control. The majority of this work is applied and is devoted to the improvement of the quality and productivity of welding processes for pipelines, power generation, defence and construction industries. Current projects include novel process investigations for the Alaska pipeline, intelligent control of inverter power supplies, in situ repair of hydroturbines, high-power diode-laser welding and on line quality control in continuous steel strip welding. He has recently been granted patents for two welding process control techniques which are now being commercialized by international manufacturers.

He is a Fellow of the Welding Institute (UK), a Chartered Engineer, a FEANI Eur. Eng., the Australian delegate on International Institute of Welding (IIW) commission XII and member of study group 212 (Physics of Welding). He is also a current member of the Technical Management Board and has served as a member of WG6a of the IAB on distance delivery guidelines. He also takes an active part in WTIA panels 7, 9 and 14.

As education program manager of CRCWS he has been responsible for developing an innovative flexible delivery program for post graduate welding engineers. This was the first flexible delivery program in the world to meet the syllabus requirements for IIW International Welding Engineer.

John Norrish has well over a hundred publications in refereed journals and international conferences. He is also the author of a Book «Advanced Welding Processes», originally published by TIPh in 1992.